

# **Determinants of the temperature adaptation of mRNA degradation**

Vincent Jaquet<sup>1</sup>, Sandrine Wallerich<sup>1</sup>, Sylvia Voegeli<sup>1</sup>, Demeter Túrós, Eduardo Calero Vilorio and Attila Becskei\*

Biozentrum, University of Basel, Klingelbergstrasse 50/70, 4056 Basel, Switzerland

\*E-Mail: attila.becskei@unibas.ch

<sup>1</sup>These authors contributed equally.

## **ABSTRACT**

The rate of chemical reactions increases proportionally with temperature but the interplay of biochemical reactions permits deviations from this relation, and adaptation. The degradation of individual mRNAs in yeast increased to varying degrees with temperature. We examined how these variations are influenced by the translation and codon composition of mRNAs. We developed a method that revealed the existence of a neutral half-life above which mRNAs are stabilized by translation, but below which they are destabilized. The proportion of these two mRNA subpopulations remained relatively constant under different conditions, even with slow cell growth due to nutrient limitation, but heat shock reduced the proportion of translationally stabilized mRNAs. At the same time, the degradation of these mRNAs was partially temperature-compensated through Upf1, the mediator of nonsense-mediated decay. Compensation was also promoted by some asparagine and serine codons, whereas tyrosine codons promote temperature sensitization. These codons play an important role in the degradation of mRNAs encoding key cell membrane and cell wall proteins, which promote cell integrity.

## **INTRODUCTION**

Heat increases the velocity of molecular motion, leading to more intense and frequent molecular collisions and consequently, faster reactions. Typically, the rate of enzymatically catalyzed biochemical reactions plateaus or even decreases at higher temperatures because the enzymes denature or their biophysical properties change (1). Biochemical processes can also cause deviations from the simple, linear relation between the temperature and reaction rate. Sensitization brings about larger than expected changes in reaction rates, whereas temperature compensation buffers the temperature-induced changes in a reaction. These two forms of temperature adaptation have been observed in various organisms. Sensitization can be

achieved for example with molecular thermometers, which allow the translation of bacterial heat shock and virulence factors to increase abruptly at a threshold temperature (2). Conversely, the response rate of a network with antagonistic reactions can remain constant (3). This temperature compensation is important to maintain constant biological rhythms, neurobiological behavior or animal development over a wide temperature range (3-6).

Little is known whether and how the mRNA degradation, a core process of molecular biology, is subject to temperature compensation, or sensitization. mRNA degradation is strongly affected by translation and it is therefore plausible that the two processes together determine the temperature-dependence of mRNA stability. The codon composition of mRNAs affects not only translation efficiency but also the mRNA degradation rate (7-9). Typically, codons recognized by abundant tRNAs stabilize mRNAs whereas codons recognized by scarce tRNAs destabilize mRNAs. Under standard environmental conditions, there is a positive correlation between the frequency of optimal codons in an mRNA and mRNA stability.

The degradation of mRNAs can also be controlled through sequestration or by other means. High temperature or heat-shock promotes the appearance of ribonucleoprotein aggregates, such as P-bodies and stress granules, which have been proposed to act as storage sites of translationally repressed mRNAs (10-12). The stabilization and storage of mRNA in such aggregates could compensate the degradation kinetics due to increases in temperature.

Despite the fact that codon optimality was recognized early on as a major determinant of mRNA stability (13), the confirmation of these initial studies was hindered for a long time by the variable, often inconsistent results of different methods and protocols for measuring half-lives (14-16).

The measurement of half-life under stressful conditions, such as heat-shock, is even more demanding, since the perturbations introduced by different methods imitate and amplify stress response (17,18). In the first part of our work, we were able to measure mRNA half-lives over a wide temperature range with minimal methodological interference. To study how translation affects the temperature response of mRNA degradation, we created mRNAs devoid of start codons to eliminate translation with minimal disruption of cell physiology. We found that heat shock is a special environmental condition in that it reduces the proportion of translationally stabilized mRNAs, a process that is mediated in part by Upf1. Simultaneously, the degradation of these mRNAs becomes temperature compensated, partly by Upf1. We then

turned our attention to the intrinsic mRNA determinants and uncovered how codon composition affects temperature compensation and sensitization in mRNA degradation.

## MATERIALS AND METHODS

### Construction of plasmids and yeast strains

The plasmids constructed in this study are listed in Table S1. Plasmids containing an RNA expression cassette include a promoter and a sequence that is identical to or creates the open reading frame (ORF) upon integration into the yeast chromosome. The promoter is a truncated *GAL1* promoter, where the four Gal4p binding sites were replaced by *tet* operators. The 5'UTR of the gene of interest was inserted 12 bp downstream of the TATA box of the *GAL1* promoter.

Two strategies were used to express the gene of interest in yeast: (1) promoter replacement, resulting in the expression of the gene at the endogenous chromosomal locus and (2) expression of the whole gene at an exogenous locus. In the first strategy, employing promoter replacement, a truncated ORF constituted the homologous sequence for integration to the endogenous locus, and the *URA3* was used as a selection marker (19). The plasmid was linearized typically with *SpeI* or with other restriction enzymes whose recognition sites were introduced by fusion PCR (as indicated in Table S1). In the second strategy, the whole gene along with the 5' and 3' UTR flanking the ORF was cloned downstream of the promoter in the pRS303 plasmid, to be integrated at the *his3* locus of yeast. The *his3* locus has a partial deletion in the BY4741/2 strains. The sequence downstream of the ORF contained the 3'UTR and a further 100 bp sequence in order to allow for transcriptional termination as it occurs at the endogenous locus. This second strategy was mainly used for genes that have a short ORF (600 bp or less), contain an intron, are essential or mutations were introduced into the whole coding sequence (see below), as well as for the synthetic genes. The linearization was performed primarily with *MscI*, but when this restriction site was also present in the gene sequence, *BssHII* was used. In order to permit the simultaneous measurement of multiple RNA, multiplexing was used with the help of synonymous codon substitution (19).

A second form of multiplexing was used for the genes encoding extreme  $\sum dtCSC$  values: multiple stop codons were inserted downstream of the endogenous stop codons instead of inserting the synonymous codons. These genes with 3'UTR modifications can be distinguished with qRT-PCR from the endogenous counterparts with repetitive sequences, which is common in serine-rich genes.

To construct the noATG versions of the endogenous genes, all ATGs were replaced by a TAG triplet in all three frames and also in the 3'UTRs in order to prevent translation. The noATG version of the *TSL1* used for the single molecule RNA FISH was additionally modified to avoid cross-hybridization, which was achieved by swapping the position of the *i* and *i*+1 codons and this construct was named as scrambled noATG *TSL1*. These noATG constructs were synthesized by General Biosystems (pGB series) or Biomatik (pBM series) and cloned into pRS303 and integrated according to the second strategy, which is pursued when the insert in the plasmid contains the entire ORF.

The plasmids were chromosomally integrated into *S. cerevisiae* BY4741 and BY4742 strains. Single copy integrands were screened with colony PCR and the haploid strains were mated resulting in diploid strains (Table S2). Integrated repetitive sequences were also verified by sequencing. The *tet* operators were recognized by the constitutively expressed tTA, driven by the *CLN3* promoter. The haploid strain containing the tTA (Ysv71.1) was mated with the strain containing the RNA expression cassettes.

Strains with gene deletions, including the  $\Delta xrn1$  (Y34540) and cell wall mutant strains were obtained from EUROSCARF. The genes are deleted with the kanMX cassette.

In summary, the following classes of strains expressing the RNA under TET control were obtained (Table S2): (1) RNAs with synthetic codon composition, (2) a set of representative mRNAs, the (3) set of stable and unstable mRNAs and (4) mRNAs with extreme  $\sum dtCSC$  values.

To obtain a representative set of mRNAs, genes in the segments of the YML and YBR chromosomes were selected. Such a selection provides a faithful estimation of the average half-life and correlations of the genome-wide measurements (19). To increase the power of the predictions, we combined all the YML and YBR genes mentioned in the previous study using multiplexed gene control (19) and the YML and YBR genes listed in Table S1. To obtain stable and unstable mRNAs, we selected mRNAs that had very short or long half-lives according to multiple measurements using different methodologies (16,20). The no-ATG counterparts were constructed for this set to estimate the neutral point half-life.

The codons of the synthetic versions of *MTL1* were replaced as shown in Figure 6A.

### **Yeast growth, and shut-off experiments**

Cells were grown in synthetic drop-out medium (Yeast nitrogen base, Formedium). We used either of the three following carbon sources: 2% raffinose (supplemented with 0.005% glucose, reference condition), 2% glucose and 3% Glycerol supplemented with 0.005%

glucose. Raffinose is the trisaccharide galactose  $\alpha(1\rightarrow6)$  glucose  $\beta(1\rightarrow2)$  fructose. The reference temperature was 30°C. We measured decay rates also at 20°C and 42°C. For the measurement at 42°C, cultures were grown overnight and initially after refreshment at 30°C. After reaching the mid-log phase (optical density at 600 nm, OD<sub>600</sub> ~ 0.5), the cells were filtered through a cellulose acetate membrane and then transferred into a new medium at 42°C. The culture was grown for 30 min before starting the decay measurement by adding the doxycycline.

The overnight cultures were refreshed at OD<sub>600</sub> = 0.1 and let further grown until they reached an OD<sub>600</sub> ~ 0.5 unless otherwise specified. For growth in glycerol, the OD<sub>600</sub> after refreshment was adjusted to 0.5 and the culture was grown for 4 h before starting the decay experiment. At this point, up to 20 cultures were pooled to measure the decay rate of multiple mRNAs simultaneously (19). Gene expression was shut off by adding doxycycline at a final concentration of 10  $\mu$ g/ml to dissociate tTA from the promoter. Samples were collected before and 2, 4, 6, 8, 12, 18, 24, 36, 48, and 64 min after the addition of doxycycline unless otherwise specified. The samples were fixed by pouring them into the same volume of methanol cooled in dry ice.

## RT-qPCR

Total RNA isolated from the cells was used to quantify mRNA. RT-qPCR was performed with gene specific primers (Table S3). The 15aa repetitive sequences containing 15 identical codons had a low efficiency amplification. For these constructs, we used RT-qPCR with barcoding, in a way that a barcode sequence incorporated into the reverse transcription primer was recognized by reverse primer in the qPCR instead of annealing directly to the repeat sequence.

## Calculation of mRNA half-lives

The half-lives were fitted as described earlier (19). The mean decay rate constant (or half-life) was calculated from at least two independently fitted decay rates obtained from biological replicates. Three replicates were performed always for the mRNAs with synthetic codon composition and extreme  $\sum dtCSC$  values. Otherwise, we performed more than two replicates if the determination of the half-lives was not satisfying either the criteria defined based on the dynamic range or experimental variability. The dynamic range of expression was defined as the ratio of maximal to the minimal value in the time series. If the dynamic range was less than 5, the time series was replaced by a new replicate experiment. If the dynamic range

remained below 5, the half-life was not measured for that construct. The experimental variability was quantified with the coefficient of variation (CV). If the CV of two replicates was above 0.5, additional replicates were performed. Outliers that were greater than twice the mean absolute difference (2 MAD) were removed from the representative mRNA data set (21) to achieve high precision in the input data. The 2 MAD criterion was not applied to data with error bars for which conclusions were drawn.

### **Splinted ligation RT-qPCR (qSL-RT-PCR)**

Total RNA isolated from exponentially growing cells was used for the splinted ligation, which was performed as described earlier (22) with a few modifications. Since the splint can promote the ligation of only one mRNA isoform with a given 5'UTR length, we selected the most frequent 5'UTR length, having 31bp, 16bp and 34bp, for the *YBR025C*, *YJL190C* and *YLR094C* 5'UTRs respectively (23). The primers were designed to avoid cross-reaction with the endogenous mRNA (Figure S4, Table S4). The increased specificity was achieved by having anchor forward primers that overlapped with the 5'UTR of the gene over a few base pairs and by using distinct primers annealing to different sequences in the reverse transcription and in the qPCR. The primers for RPL41A were the same as previously described (22) except for the design of anchor forward PCR primer which was designed as described above. The RNA ligation reaction was performed with T4 DNA ligase (Promega), and the RNA was purified with RNeasy MinElute Cleanup Kit (Qiagen) upon the completion of the ligation reaction. Reverse transcription and qPCR were performed as described in the RNA quantification section.

Decapping was performed with the 5' Pyrophosphohydrolase enzyme RppH (NEB) in the NEB2 buffer for 90 min at 37°C. The reaction was stopped by adding EDTA and heating it to 65°C for 5 minutes. The RNA was purified from the reaction mixture with RNeasy MinElute Cleanup Kit (Qiagen).

The percentage of the decapped RNA is calculated by dividing the amount of the mRNA ligated to the anchor RNA (mRNA – anchor RNA hybrid) by the total RNA amount. This raw value was normalized by the bulk ligation efficiency to obtain the final value of the decapped RNA percentage. The ligation efficiency is assessed by performing the SL-RT-qPCR on the mRNA decapped with RppH, and it is affected by the efficiency of ligation of a given mRNA isoform as well as by the proportion of the isoform in the RNA population to be measured with respect to the total RNA, which comprises all RNA isoforms.

$$\begin{aligned} \text{Decapped RNA [\%]} &= \frac{\text{mRNA-anchor hybrid}}{\text{Total RNA}} \bigg/ \frac{\text{In vitro decapped mRNA-anchor RNA hybrid}}{\text{In vitro decapped Total RNA}} = \\ &= \frac{\text{SL-RT-qPCR(RNA)}}{\text{RT-qPCR(RNA)}} \bigg/ \frac{\text{SL-RT-qPCR(decapped RNA)}}{\text{RT-qPCR(decapped RNA)}} \end{aligned}$$

The (SL)-RT-qPCR values were calculated from the Cp values and the amplification efficiency. The primers were designed to maximize the signal-to-noise ratio. This ratio was calculated by dividing the amount of the mRNA-anchor hybrid RNA molecule detected in a reaction containing a ligase by that detected in the mock reaction without ligase:

$$\text{Signal-to-noise Ratio} = \frac{\text{In vitro decapped mRNA-anchor RNA hybrid}}{\text{In vitro decapped mRNA-anchor RNA hybrid (without T4 ligase)}}$$

### Single molecule RNA FISH

The microscopic slides of the sample were prepared according to Stellaris® RNA protocol for yeast (24,25), with a few modifications. Following the fixation with formaldehyde, the cell wall was digested with zymolyase at 37°C for 15 minutes in spheroblast buffer. Following the hybridization, the cells were placed on slide using the ProLong™ Glass Antifade Mountant (ThermoFisher) mounting medium. The images were acquired as previously described (19). Two sets of probes were designed to bind either the WT or the scrambled noAUG sequence variants of the 5' region of the *TSL1* RNA. Both sets comprehended 35 probes labeled at their 3' end with Quasar® 670 (Stellaris probes). The probe length was adjusted between 18 and 22 bp to have a melting temperature of 55°C and a gap of at least 2 bp in the complementary sequences between each probe (Table S5). Microscopy data are stored as multichannel (Quasar 670 RNA probe, DAPI, autofluorescence at 523 nm) image stacks. Each stack consists of 20-25 slices and approximately 15 field of views have been imaged for each experimental condition.

### Mass spectrometric analysis of protein abundance

Cells were harvested 3 hours after shifting the culture to 42°C. Cells were processed as described earlier (26). Synthetic peptides (Data S2) were used for the quantification of relative changes in protein abundance by selective reaction monitoring.

## **Image analysis**

To segment cell bodies, the Cellpose Python Package (Python 3.8.5) was utilized in a cloud-based Python environment with GPU support provided by Google Colaboratory (27). Each image plane in a stack was segmented using the Cellpose 2D segmentation algorithm with the diameter parameter set to 70. After completion, the corresponding 2D segmentation masks were merged together forming a 3D binary mask for each individual cell in each image stack. Too small or too big cell bodies have been removed as well as cells touching the image boundaries. The DAPI labelled cell nuclei were segmented by separating the pixels into two classes using Otsu's method and creating a binary image by multiplying the threshold value by 1.9 with subsequent manual validation. Too small regions have been discarded. Next, we computed the Euclidean distance between the centroid of each cell and each nucleus and paired them according to the smallest distance value. Cells with no visible nuclei were omitted from further analysis.

In order to quantify the RNA spots, the binary cell body masks were applied and the mean cell volume intensity was calculated for each field of view on the previously deconvolved Quasar 670 image channels. Individual RNA spots were selected by employing a threshold value corresponding to the mean cell intensity multiplied by 5.0. This approach was consistent across strains since the mean cell intensity did not change more than 1.3 times upon subtracting the RNA spots. Next, the numbers of RNA spots in the cytoplasm and nucleus were counted for each cell.

## **Quantification of cell wall integrity**

The cell wall integrity was assessed by exposing the cells to a mixture of glucanases (zymolyase) that degrade the cell wall, yielding spheroblasts, cells devoid of cell wall. The susceptibility of cells to lysis was quantified according to the spheroblast rate assay (28), with a few modifications.

To obtain cells in exponential growth phase, overnight cell cultures were grown at 30°C in minimal medium containing 2% raffinose. The overnight culture was diluted to an OD<sub>600</sub> of 0.15 (0.25 for slow-growing strains), and incubated for 5 hours at 30°C. In this way, the culture did not exceed an OD<sub>600</sub> of 0.5, allowing the analysis of cells in a mid-exponential growth phase. The culture at 42°C was also incubated for 5 hours, which was preceded by a growth for 2 hours at 30°C following the dilution of the overnight culture grown at 30°C.



The cells in the mid-exponential growth-phase were pelleted and washed 3 times with 30°C Tris-EDTA (TE) buffer. The cells were then resuspended in 1ml of TE buffer to an OD600 of 0.6. The enzymatic reaction was started by adding 25 µg/ml zymolyase (Zymolyase 20T (Arthrobacter luteus) amsbio #120491-1) to 1 ml of cell suspension. The progress of spheroblast lysis was monitored by recording OD600 at intervals ranging from 3 to 8 minutes. The exponential phase of the lysis begins after a lag. The zymolyase rate index (zymolyase RI, ZRI) was calculated from the lag time (LT) and the maximal lysis rate (MLR).

$$ZRI = \frac{MLR}{LT}$$

The MLR was fitted in the interval starting from the latest time point at which the OD600 remained above a threshold defined as (maximum (OD600)) – 0.05. The MLR corresponds to the maximal slope of any 8 or 10 consecutive time points in the time period after the lag for the 30°C and 42°C conditions, respectively. If there are less points than this number of points in the decay phase, all these points are fitted. If the decay rate was too slow to be determined, then it was replaced with the lowest measured experimental rate. The MLR is calculated using linear regression from the logarithmically transformed values. The LT corresponds to the intersection point of the lines defined by the MLR and the maximum (OD600) – 0.05 (Figure S8).

### **Calculation of the differential temperature Codon Stabilization Coefficient (dtCSC)**

The relative difference of the RNA half-lives measured at 20°C and 42°C (Data S1) was used to calculate the dtCSC for each codon.

$$d_r t_{1/2} = \frac{\frac{t_{1/2} 20^\circ C - t_{1/2} 42^\circ C}{t_{1/2} 20^\circ C + t_{1/2} 42^\circ C}}{2}$$

The dtCSC is equal to the Pearson rho correlation between the frequency of a specific codon in the mRNAs and the relative difference of the respective half-lives,  $d_r t_{1/2}$ , unless otherwise indicated. The frequency of the codon was calculated with the Biostrings package in R from Saccharomyces Genome Database (SGD) sequences (29). The number of mRNAs included in the calculation ( $N = 95$ ) encompassed the set of representative mRNAs and the set of stable and unstable mRNAs.

The number of synonymous mutations among all codons is less than 1% in the multiplexed gene dataset, and consequently, it has minimal impact on the dtCSC values (Figure S6A, B): the dtCSC calculated with and without the synonymous mutations, which differentiate the controlled genes from the endogenous genes, are highly correlated (0.99).

The  $\sum \text{dtCSC}$  is the scalar product of the codon frequency and the corresponding dtCSC. To clone genes with extreme  $\sum \text{dtCSC}$  values, the dtCSC was calculated from a smaller set of genes ( $N = 81$ ).

Genes were ranked according to the  $\sum \text{dtCSC}$  values to select the genes with extreme  $\sum \text{dtCSC}$  values. The following genes were eliminated from this list: genes that have uncharacterized ORF, unknown function and mitochondrial genes encoded by the mitochondrial genome. Genes enriched in both Tyr and Asn/Ser codons (above the 95 percentile in the codon frequency distribution) were also eliminated because of the dominance of codons that do not have significant dtCSCs. The remaining genes with extreme  $\sum \text{dtCSC}$  values were cloned (Figure S6C, D).

## RESULTS

### Temperature dependence of mRNA turnover

To examine the temperature dependence of mRNA turnover, we measured the half-life of a representative set of mRNAs in the eukaryotic model organism budding yeast. Cells were grown in the trisaccharide raffinose at low (20°C), intermediate (30°C) and high (42°C) temperatures. For the high temperature growth, the cells were subjected to heat shock: we first cultured the cells at 30°C and measured the mRNA half-life 30 min after raising the temperature to 42°C. We used the gene control method to determine the half-lives (see Materials and Methods) since the applied doxycycline introduces minimal stress (30). Thus, it is well suited to study mRNA turnover in different environmental conditions, including heat-stress. The median mRNA half-life shortens as the temperature increases ( $t_{1/2} = 3.4$  min at 20°C, 2.0 min at 30°C and 1.5 min at 42°C) (Figure 1A, B).

mRNAs are degraded 5'→3' by Xrn1 and 3'→5' by the exosome but the overall degradation rate is also influenced by the preceding molecular steps, such as the removal of polyA tail and decapping (31). In order to examine the temperature dependence of degradation per se, we monitored RNA degradation in vitro by adding the purified yeast exonuclease Xrn1 to total RNA (Text S1). Xrn1 is a major determinant of differential mRNA

stability (19,20,31). We fitted the half-life of the 18S RNA, because it is not 5'-capped and thus, Xrn1 can bind to the RNA without pretreatment (32). The half-life of the 18S RNA decreased with increasing temperature between 20°C and 42°C (Figure S1).

The relatively large correlation between the half-lives (Figure 1C) indicates that mRNA turnover responds coherently and gradually to temperature. To examine the coupling of mRNA turnover to cellular metabolism, we measured the growth rate. The cells grew faster at 30°C than at 20°C but raising the temperature further to 42°C did not increase the growth rate in spite of the faster RNA turnover (Figure 1B). After the temperature shift from 30 to 42°C, the growth rate declined considerably with longer cultivation: the cells grew initially exponentially but after one day of culturing, the growth came to a halt (Figure S2). These results indicate that central processes of gene expression, including RNA degradation and translation, persist for a sufficiently long period and permit cells to undergo a few, around three cell divisions before they enter a quiescent state.

Cell growth, RNA nucleocytoplasmic export and degradation stop ultimately upon heat shock; the exact temperature and time at which this ensues varies with growth conditions (33-35). Typically, slower growth results in superior thermotolerance. Heat shock is often studied in cells cultured in glucose, resulting in high-flux fermentation and ethanol accumulation, which can cause further stress (36). These factors may explain why growth in raffinose permits a few cell divisions at 42 °C before cells enter cellular quiescence.

In contrast to our results, a mild heat shock (37°C) has been reported to increase mRNA half-lives in two studies using metabolic labelling (cDTA) and genomic run-on (GRO) (20,37). The two datasets (cDTA, GRO) did not correlate with each other (Figure 1D). The 30°C dataset of the metabolic labelling study (cDTA) did correlate highly with our multiplexed gene control (MGC) dataset (19) implying a high inter-method reliability. On the other hand, the heat-shock cDTA dataset did not correlate with the 30°C cDTA dataset and with our MGC datasets (Figure 1D), which suggests that our data reflect the physiologically unperturbed and gradual response of the mRNA turnover to temperature changes, allowing cells to grow and divide.

### **Analysis of translation-dependence of mRNA degradation with no-AUG mRNAs.**

Next, we analyzed the translation-dependence of mRNA decay in different conditions, including heat-shock. Translation inhibitors perturb cell physiology and mRNA decoding (31). To circumvent the use of inhibitors, we created mutant genes devoid of start codons

(Figure 1E). Genes encoding mRNAs with extreme half-lives, i.e. a set of stable and unstable mRNAs was selected for the mutation. At 20°C, the mRNAs assumed relatively uniform half-lives, when translation was diminished or abrogated. We calculated the interdecile ratio to assess the dispersion, which equals the ratio of 90<sup>th</sup> to 10<sup>th</sup> percentile of the half-life distribution. Indeed, the no-AUG mRNAs spanned a much narrower range of half-lives (interdecile ratio: 2.3) in comparison to their WT counterpart (interdecile ratio: 11.4) (Figure 1E).

We quantified the degree of translational stabilization by dividing the half-lives of the mRNAs by that of the no-AUG mRNAs. There is a very strong correlation between mRNA half-life and translational stabilization (Pearson correlation coefficient  $\rho = 0.88$ , Spearman rank correlation  $r_s = 0.90$ , Figure 1F). This finding confirms that translation is a major determinant of mRNA stability.

### **Comparison of the molecular and kinetic properties of no-AUG mRNAs to their AUG counterparts**

Before analyzing the temperature response of no-AUG mRNAs, we tested whether they preserve the main features of mRNA processing and degradation.

mRNAs are degraded primarily in the cytoplasm (31). Thus, we assessed first their cellular distribution. The single-molecule RNA FISH images indicate that both the WT and no-AUG mRNAs have similar distribution at 30°C as well as 30 min after shifting the temperature to 42°C (Figure 2A-C). The majority of molecules are in the cytoplasm and the nascent RNA is visible in the nucleus (Figure 2B, C, S3). The number of RNA molecules declines substantially both in the cytoplasm and nucleus after an overnight growth at 42°C (Figure 2C). This decline is consistent with the cessation of growth of cells exposed to elevated temperature over longer periods of time (Figure S2).

Second, we examined the initiation of 5'→3' degradation. The 5'cap protects the mRNA from the Xrn1 exonuclease, and decapping must precede the 5'→3' degradation. To assess the 5' capping state of the mRNAs, we performed splinted-ligation qPCR (qSL-RT-PCR, Methods). qSL-RT-PCR is typically performed with RNA isolated from  $\Delta xrn1$  cells, in which the 5'→3' exonuclease activity is absent, and the decapped mRNAs accumulate (22,38). With a minor modification of the SL-qPCR protocol, we attained a high-signal-to-noise ratio (Figure 2D) and were able to measure the percentage of the decapped mRNAs even in WT cells in which the decapped mRNAs do not accumulate because Xrn1 rapidly

degrades the decapped RNAs (Figure 2E). In  $\Delta xrn1$  cells, around 10% of the *RPL41A* mRNA (*YDL184C*) was decapped, similar to the value reported in the study using the original protocol (22), and we therefore used it as positive control. Rpl41a is a micro-protein in the large subunit of the ribosome, consisting of 25 amino acid residues (39). We also quantified the decapping of the stable (*YBR025C*, *YJL190C*) and unstable (*YLR094C*) mRNAs. In  $\Delta xrn1$  cells, the percentage of decapped mRNAs ranged from 5 to 15%. The values were considerably lower in WT cells. Importantly, the decapping percentages of normal, endogenous and MGC mRNAs (0.2%-0.6%) and their RNA counterparts without AUG (0.3%-0.6%) were in a similarly low range.

### **The neutral point defines the half-life above which mRNAs are stabilized by translation**

The above results indicate that the no-AUG mRNAs preserve key molecular characteristics of mRNA turnover, specifically the intracellular distribution and the decapping rates (Figure 2), which makes them suitable for quantifying the half-life of untranslated mRNAs. The translation stabilization quotients suggest that translation stabilizes the stable mRNAs but destabilizes the unstable mRNAs (Figure 1F). This dichotomy is interesting because most studies with translation inhibitors suggest that translation is solely stabilizing (31). To characterize this dichotomy in more detail, we calculated the average half-life of the no-AUG mRNAs, which we termed the neutral point. The neutral point of the no-AUG mRNAs marks the neutral half-life of the normal (AUG containing) mRNAs. Translation stabilizes mRNAs above the neutral half-life, but destabilizes them below this (Figure 3A).

We calculated the neutral point for different conditions. In cells grown in raffinose at 30°C, the neutral point is 3.3 min. The equivalent neutral half-life divides the representative set of mRNAs into two subpopulations, with around 22% of the mRNAs being stabilized by translation (Figure 3A). Interestingly, the percentage of mRNAs stabilized by translation was similar (20-25%) for all carbon sources at 30°C despite the considerably slower growth in glycerol in comparison to glucose (Figures 1C, 3B). That is, even nutrient limitation due to growth on a suboptimal carbon source, glycerol, does not alter this proportion. Only the high-temperature condition (42°C in raffinose) lead to a substantial change; in this case, a very small fraction of the mRNAs was stabilized by translation (5%, Figure 3A, B). This strong destabilizing effect of mRNA translation may contribute to the cessation of growth upon multiple rounds of cell division at 42°C.

### **Upf1 promotes the stability of no-AUG mRNAs after heat shock**

To confirm that the neutral point is an unbiased estimate of the neutral half-life, we wanted to examine if residual translation affects the decay of no-AUG mRNAs. Translation is normally initiated at AUG codons but some mRNAs can initiate non-canonical translation at degenerate start codons at a very low rate (40,41). In certain sequence contexts, this rate can reach around one-tenth of the canonical initiation (42). Furthermore, non-canonical translation can become more widespread under specific conditions in yeast, for example, during meiosis, which occurs during sporulation (43). Any such translation would terminate at an early stop codon as we mutated AUGs to UAG codons, resulting in a large the number of stop codons in all reading frames. Such premature translational termination is expected to induce nonsense-mediated decay (NMD). Since NMD is mediated by Upf1, the deletion of *UPF1* stabilizes the mRNAs subject to premature translational termination and thereby increases their abundance (43-45). Using *upf1Δ* cells, we tested whether non-canonically initiated translation gains in importance at low and high temperatures and whether it influences RNA degradation.

No significant difference was observed between the half-lives in WT and *upf1Δ* cells at 20°C (P-value = 0.42, sign test). Only one of the no-AUG mRNAs was stabilized more than two times in *upf1Δ* cells (Figure 4A). This frequency of NMD targets, around 5%, is in good agreement with the previous finding that 5% of ribosome footprints are due to non-canonical translation in vegetative cells (46). In wild-type cell background, the half-lives of the no-AUG mRNAs are strongly correlated at lower temperatures ( $r_s = 0.87$  between 20 and 30°C, P-value =  $2.6 \cdot 10^{-8}$ ), but they change their behavior in response to heat shock as evidenced by the loss of correlation between 30°C and 42°C ( $r_s = 0.16$ , P-value = 0.46). It turned out that this change was *UPF1*-dependent: we observed a significant difference between the mean mRNA half-lives in WT and *upf1Δ* cells at 42°C (P-value = 0.0015, sign test). Contrary to expectations, most of the no-AUG mRNAs were destabilized –and not stabilized - in the *upf1Δ* cells (Figure 4B). Typically, the RNAs with the longest half-lives underwent the strongest stabilization, as evidenced by the large correlation ( $\rho = 0.82$ ) between the half-lives measured in WT and the stabilization ratio due to Upf1. Accordingly, the half-lives became more uniform in *upf1Δ* cells (interdecile ratio = 1.8). These findings suggest that the Upf1 promotes the stability of some no-AUG mRNAs, directly or indirectly. The 20-to-42°C ratio of average mRNA half-life calculated from the set of stable and unstable mRNAs is 2.39. The ratio decreases to 1.37 when translational initiation is eliminated but returns to near the original number in the *upf1Δ* cells (2.26). These findings suggest that Upf1 is a major determinant of the stabilization of no-AUG mRNAs at 42°C, a function not classically associated with NMD.

## Temperature dependence of mRNA degradation by Upf1

Since the stabilization of no-AUG mRNAs by Upf1 shifts the neutral point, we examined the direct effect of Upf1 on mRNA turnover. We measured the half-life of the set of stable and unstable mRNAs in *upf1Δ* cells (Figures 4C-E). At 30°C, there was no significant difference between the WT and *upf1Δ* cells (P-value = 0.21, sign-test). Only one of the 23 mRNAs was stabilized more than two times (Figure 4E). In contrast, Upf1 had a specific effect on the decay at 20 and 42°C. At 20°C, the mRNAs were slightly but significantly destabilized by *UPF1* (P-value = 0.01, sign test), accelerating the decay across the entire range of half-lives (Figure 4C). At 42°C, the strong positive correlation between the half-life and the *UPF1* stabilization ratio (USR) indicates a preferential destabilization of unstable mRNAs by *UPF1* (Figure 4D).

To assess whether the temperature rise moderates *UPF1* activity, we calculated the USR(42°C):USR(20°C) ratio. This ratio correlates positively with the mRNA half-life at 30°C (Figure 4F). The ratios calculated for mRNAs at 42°C above the neutral point (4 min) were significantly higher than one (P-value = 0.012, signed-rank test), indicating that heat shock suspends the destabilizing activity of Upf1 against the mRNAs in the subpopulation stabilized by translation. To examine how Upf1 activity affects temperature adaptation, we calculated the correlation between the USR(42°C):USR(20°C) ratio and the relative difference of the half-life measured at 20 and 42°C ( $d_r t_{1/2}$ , Materials and Methods). A significant negative correlation ( $r_s = -0.49$ , P-value = 0.016) indicates that *UPF1* contributes to temperature compensation of mRNA degradation.

## Few specific codons are associated with the temperature compensation in mRNA degradation

After identifying the extrinsic determinants, the translation and *UPF1*-dependence of the temperature control of mRNA degradation, we turned to the intrinsic determinants, the codon composition. Codons explain a large proportion of variation in the mRNA half-lives under standard conditions, and mRNAs enriched in certain codons have longer half-lives (8,16). The codon stability coefficient (CSC) indicates how strongly a codon contributes to mRNA stability, and is calculated exactly as the correlation coefficient between the codon frequency and half-life (15,16). Codons with positive CSC stabilize mRNAs whereas those with negative values destabilize them. The CSC is a consistent measure, confirmed by specific

variants of all three major methods used to measure RNA stability (15), including the multiplexed gene control (19), the method employed in this study.

The most stabilizing and destabilizing codons that we identified at 20°C and at 42°C (Figure S5) correspond to the stabilizing and destabilizing codons previously identified at the standard growth temperature (30°C) (15,16), which indicates that the degradation code in general withstands temperature variations. In order to identify codons that respond to a temperature shift, we defined a related measure, the differential temperature CSC (dtCSC), which is the correlation coefficient between the codon frequency and the relative difference in the half-lives measured at two different temperatures (Figure S6A, B). Unlike CSC, which implies a single condition, the dtCSC always refers to two conditions. The dtCSC values indicate that only few codons contribute significantly to the differential stability at 20°C to 42°C (Figure 5A). Some codons for asparagine and serine dampen the response of mRNA degradation to the temperature shift, and thus promote temperature compensation (negative dtCSC). Conversely, a codon for tyrosine was associated with sensitizing RNA degradation rates to the temperature shift (positive dtCSC).

We tested the above correlations by creating synthetic minigenes containing Asn and Ser codons with the most negative dtCSC. As a control, we used codons with positive dtCSC. Upon the shift of temperature from 20°C to 42°C, the half-life of the control mRNA was halved (Figure 5B). Conversely, the half-life of mRNA composed of codons for Asn and Ser remained essentially unchanged. This reveals that a complete temperature compensation in RNA degradation can be attained with appropriate codons. We also studied coding sequences with homogeneous codon composition containing 15 identical codons. Barcoded primers were used to detect these repetitive sequences in the RT-qPCR (see Materials and Methods). The half-lives of mRNAs consisting of Asn (AAC) and Ser (UCA) codons were in agreement with the previous findings on the temperature compensation, whereas that of the Tyr (UAU) codon was in agreement with the temperature sensitization in mRNA degradation (Figure 5C). The Ser (UCC) and the Leu (CUU) codons had intermediate effect.

Next, we designed longer synthetic genes that encode proteins of 100 amino acids. Long, repetitive sequences of Asn and Ser codons were avoided by adding other codons with negative dtCSC (Figure S7). Two similar Ser/Asn rich sequences were designed: SN-rich 1, 2 (Figure S7). The SN-rich 1, 2 mRNAs attenuated the temperature response better than a long control mRNA lacking codons for Asn and Ser. The same open reading frame yielded different absolute values for the half-lives in the context of two different flanking UTR



sequences (*NRG2* and *RPS22A*). At the same time, the temperature compensation was observed in both contexts (Figure 5D). The SN-rich 1 mRNA displays a 1.73fold temperature compensation relative to the control mRNA.

### **The role of temperature degradation code in the turnover of mRNAs encoding key cell membrane and cell wall proteins**

Since there are only few codons with compensating or sensitizing effect, the enrichment of mRNAs in these codons is expected to promote temperature adaptation in specific cellular processes. Ser-rich proteins are overrepresented in cell-wall and other cell membrane related components (47). Stress granules and P bodies are enriched in Asn-rich or Gln-rich proteins or protein domains, and a weaker positive association is found also for Ser (47), (Data S3). Asn and Ser also act as acceptor sites for glycosylation: Asn for N-glycosylation and Ser for O-glycosylation, and strongly glycosylated proteins reach the cell membrane and cell wall via the secretory pathway. The cell wall integrity signaling has been long known to be involved in the adaptation to growth at elevated temperature (48).

We summed up the dtCSCs for each mRNA and ranked them according the  $\sum dtCSC$ . mRNAs with the most negative  $\sum dtCSC$  often encoded cell membrane and cell wall proteins (Figure S6C, D). Among the mRNAs with the most positive  $\sum dtCSC$ , there was a large number of mitochondrial proteins encoded by nuclear genes. We analyzed them in more detail (Figure 6A, B).

The mRNAs encoding Ser/Asn-rich membrane or membrane-associated proteins (*OST4*, *ECM33*, *MTL1* and *PST1*, Figure 6B) displayed temperature compensation.

To confirm the role of the relevant codons in the context of a typically long mRNA, we created mRNA mutant sequences of the *MTL1* gene. The *MTL1* coding sequence is 1656 bp long. The Mtl1 is serine-rich, heavily glycosylated membrane protein and act as stress sensor in the cell integrity pathway (49). To design the mutant sequence, we analyzed the significance of the differences between dtCSCs (Text S2, Tables S6 and S7), which is determined by the covariance of the frequency of the two codons to be compared and their dtCSC (50). The synonymous Tyr codons have positive dtCSC, whereas all but one Asn and Ser codons have negative dtCSC. Thus, the Asn and Ser codons generally promote temperature compensation, whereas Tyr codons promote temperature sensitization, but to an extent and significance that varies with the specific codon. Both Asn codons and four out of the six Ser codons differ significantly (at a significance level of  $\alpha=0.01$ ) from the Leu(CTT)

and Tyr(TAT) codons (Table S6). There are numerical but no significant differences between the synonymous codon of Asn, Ser or Tyr (Table S7). This suggests that mRNA must be enriched in codons of specific amino acids to display temperature compensation or sensitization. We mutated the sequence so that the substituted codons have a significant difference in dtCSC. Specifically, the TAT (Tyr) codons were converted to AAC (Asn) in the SN-rich version. Since these mRNAs are already Asn/Ser rich, this change results in a small change relative to the WT gene. In order to create the Tyr-rich version, the opposite change was performed (Figure 6A). Furthermore, Ser (TCT) was changed to a Val(GTT) to avoid long segments of TAT (Tyr) codons; the GTT (Val) has a numerically positive dtCSC value with a significant difference in this mutation (Table S7). The above changes affected nearly half of the *MTL1* sequence. Serine-rich proteins in the cell membrane and cell wall are targeted to their cellular location through the secretory pathway, and many of them have signal peptides, including the *MTL1*, which target them to the ER (49). Therefore, we created a second variant of the Tyr-rich sequence that lacked the signal peptide. The temperature compensation of the *MTL1* mRNA was significant with respect to both Tyr-rich sequences, with and without the signal peptide sequence (Figure 6A).

The physiological response of the cell is determined by the abundance and activity of the proteins translated from the mRNAs. The stability coefficients of the codons (CSC) positively correlate with their translation efficiency at standard temperature (15). It can be hypothesized that there is a similar relation for dtCSC, as well. On the other hand, a strong translation at high temperature can be unfavorable because aggregation and degradation of proteins become prominent (51). Since the nascent proteins are in unfolded state, their high concentration at the ribosomes associated with a strongly translated mRNA can lead to aggregation at high temperatures (52,53). In the light of these conflicting expectations, we measured mRNA and protein levels upon heat shock to assess translation efficiency. For most proteins in this group, peptides were identified for the mass-spectrometric measurement using selective reaction monitoring (Materials and Methods) and their level was assessed 3 hours after the shift to 42°C. Among the examined proteins, the abundance of Pst1 and Mtl1 proteins increased while the level of the other proteins decreased or remained unchanged (Figure 6C). Interestingly, the mRNA expressed from the *PST1* and *MTL1* genes declined in the period from 30 to 90 min after the heat shock but starting from a high level, indicating a pulse of transcription after the temperature shift. For all other genes, including *ECM33*, the mRNA levels increased after the initial decline in transcription. A comparison of the changes in protein and mRNA levels (Figure 6C) suggests that translation of most proteins is

unchanged or decreased, which is consistent with the observed decline in translation of most proteins upon heat-shock (54,55).

To analyze the activity of a process in which proteins encoded with extreme  $\Sigma dtCSC$  play a major role in glycosylation and cell integrity, we measured the resistance of cells to a mixture of glucanases (zymolyase). An accelerated degradation of the cell wall by glucanases indicates a deficient cell wall resistance in cells in which a particular gene is deleted (Figure 6D). At 30°C, none of the gene deletions resulted in deficient cell wall resistance when compared to cells containing control deletions ( $\Delta gal2$  or  $\Delta gal3$ ). The cell wall sensitivity of the control cells changed from a ZRI of 10 at 30°C to  $10^{-1}$  at 42°C. Thus, the control cells became significantly more resistant against the glucanases when the growth temperature was shifted from 30°C to 42°C, indicating an enhanced cell surface glycosylation in response to heat. The  $\Delta ost4$  and  $\Delta ecm33$  cells had deficient cell wall resistance at 42°C, showing that genes with temperature-compensating codons can promote cellular integrity. Ost4 (oligosaccharyltransferase 4) is a 36-amino acid residue microprotein involved in the N-glycosylation in the endoplasmic reticulum (56,57), while Ecm33 is a GPI-anchored protein anchored at the cell surface and may regulate glycosylation, as well (58). Its homologue in *Candida albicans* is involved in cell-host interaction (59). Even though we expected the mitochondrial genes to act simply as control genes, their deletion resulted in an increased cell wall resistance. For  $\Delta pet100$  (chaperone of cytochrome c oxidase) and  $\Delta cox14$  (cytochrome c oxidase), this effect was evident at 30°C while for  $\Delta qcr6$  (cytochrome-c reductase 6) at 42°C. The deletion of other genes did not have significant effect. These results (Figure 6C, D) suggest that the increase in the activity of or in the physiological response associated with the relevant proteins, such as Ecm33, rather than their abundance promotes cell integrity upon heat shock.

## DISCUSSION

The measurement of half-lives under stressful conditions, such as heat shock, is challenging due to the interaction of stress and the perturbations introduced by the specific methods of measuring half-lives. In the first part of our work, we showed that mRNA turnover can be measured reliably with the multiplexed gene control (MGC) method even under stressful conditions, as evidenced by the highly correlated half-lives measured over a wide temperature range (Figure 1B). This gradual change with temperature is in contradiction

to the massive, abrupt changes reported by other studies which otherwise use methods that are consistent with one another at standard temperature (Figure 1D). There may be several reasons why the short-pulse metabolic labelling (cDTA) detects dramatic changes in mRNA stability upon a mild heat shock (37°C). Cell density twice as high was used in the cDTA study, and the cells may be more prone to enter the stationary state. Furthermore, the 4-thiouracil used for the metabolic labelling of RNA in the cDTA induces the formation of P-bodies (30), as does heat stress. Thus, together, they can enhance the sequestration of mRNAs in the P-bodies, which would explain the slower decay rate in the 37°C cDTA dataset. Perturbations induced by other methods, such as the transcriptional inhibition and the cell wall digestion in the runoff experiments, imitate heat shock (17), which may explain why the genetic run-on (GRO) and the cDTA datasets do not correlate even under standard conditions. At very high temperatures (46-47°C), the proteins start to denature and aggregate, which is likely to lead to slower degradation (51,60).

Our MGC measurements revealed that mRNA turnover is fast in all examined conditions, and short median half-life (2.9 min) was observed even in glycerol, in which cell growth is slow, indicating that the rates of mRNA turnover and cell growth can be decoupled. The strong correlations indicate that the overall RNA degradation program is robust to changes in growth conditions.

Capitalizing on the reliability of the MGC, we examined in the second part of our work how translation affects the mRNA degradation at different temperatures by mutating all the start codons of the mRNA. In this way, we obviated the perturbations introduced by translation inhibitors or mutations that affect cell physiology. Much of the debate so far has centered on the question as to whether translation stabilizes or destabilizes mRNAs (31). mRNAs with optimal codons have long half-lives, while mRNAs with non-optimal codons have short half-lives due to the lower translational efficiency. By linear extrapolation of this relationship, it is expected that a further decrease in translation by eliminating translational initiation will result in very short half-lives. Intriguingly, the half-life of no-AUG mRNAs exceeded that of the unstable mRNAs, but ranked below the stable mRNAs. Accordingly, future studies have to identify molecular mechanisms that are consistent with this more general, nonlinear model, which does not view translation exclusively as either an mRNA stabilizing or a destabilizing process.

By calculating the average half-life of the no-AUG mRNAs, we obtained the neutral point (Figure 3), which divides the mRNA population into two subpopulations. 20-25% of

mRNAs are stabilized by translation, which is in good agreement with the analyses showing that one third of mRNAs of the genome are enriched in optimal codons (15). The proportion of translationally stabilized mRNAs remains relatively constant at 30°C despite the wide variations in the growth rate of cells cultured in different carbon sources (Figure 1). Heat shock was the only one under the conditions tested that changed substantially this proportion (Figure 3B): translation stabilizes a mere 5% of mRNAs at 42°C. At the same time, this subpopulation differed more strongly from the rest of the population (Figure 3A), which is also evidenced by the small standard error of the estimated subpopulation size (Figure 3B).

In principle, the proportion of translationally stabilized mRNAs can be changed directly by (de)stabilizing mRNAs or indirectly by shifting the neutral half-life. Our results suggest that Upf1 contributes to both of these modes. Upf1 is one of the up-frameshift (UPF) factors that target mRNAs with premature stop codons to nonsense mediated decay. The prototypical example of the Upf targets are the pre-mRNAs leaked into the cytoplasm, which contain premature stop codons in the retained introns. However, the majority of genes that increase their expression in response to the deletion of the *UPF* genes do not contain premature stop codons (44). It has been suggested that some of these mRNAs undergo poor start codon scanning during translation initiation, and the NMD is activated due to the start of translation in a nonsense frame. Furthermore, many of these mRNAs are enriched in non-optimal codons (61), which usually also destabilize mRNAs. Recently, non-classical functions of Upf1 have been described in mammalian cells that do not even require translational termination (62). For example, Upf1 can recognize highly structured mRNAs, typically in the noncoding regions (UTR).

Under the standard conditions (30°C), only one out of the 23 mRNAs that comprised the set of stable and unstable mRNAs underwent a more than twofold stabilization in *upf1Δ* cells (Figure 4D): the *YML107C* (*PML39*). Pml39 is required for the nuclear retention of unspliced pre-mRNAs (63). In a high-throughput study, the deletion of the *UPF* genes tripled the expression of *YML107C* (*PML39*) (44,61), and this was the only mRNA among the 23 mRNAs whose expression more than doubled. This agreement is surprisingly good since a direct comparison between half-lives and steady-state expression levels is limited by the buffering effect of feedback loops that are activated when genes involved in RNA degradation and processing are deleted (20). *PML39* is an intronless gene, and the targeting of the *PML39* mRNA by Upf1 to degradation may represent a feedback loop that prevents the NMD pathway from becoming saturated by retaining unspliced mRNAs in the nucleus.

Interestingly, the Upf1 has a stronger effect on mRNA turnover at both low (20°C) and high (42°C) temperatures than at 30°C (Figure 4C-E). The involvement of Upf1 in temperature adaptation is mediated by two different mechanisms. Due to a non-classical function, Upf1 stabilizes untranslated mRNAs upon heat-shock, which reduces the proportion translationally stabilized mRNAs indirectly. Many mRNAs in this subpopulation are more likely to be destabilized at lower temperatures by Upf1. In this way, Upf1 provides a mechanism for temperature compensation by acting directly on mRNAs (Figures 4F, 7A). By the combination of these indirect and direct effects, the translationally stabilized mRNA subpopulation becomes more distinct from the rest of the population (Figure 3B). Thus, Upf1 is an extrinsic determinant of temperature adaptation of mRNA turnover.

In the third part of our work, we investigated how temperature affects mRNA stability through an intrinsic factor, the codon composition of the mRNA. While a large number of codons are stabilizing or destabilizing (16), only few codons contribute to temperature compensation or sensitization (Figure 5A). mRNA degradation can be fully or partially temperature compensated when the mRNA is enriched in specific codons (Asn and Ser). Conversely, a Tyr codon sensitizes mRNA degradation in response to temperature (Figure 7B).

mRNAs encoding Ser-rich cell surface proteins that are subject to temperature compensation display various expression patterns. The *MTL1* expression increases in a pulse-like manner upon heat shock, while *ECM33* expression declines. Heat shock evokes a succession of phases before cells enter the quiescent state. The abundance of mRNA and proteins varies over this period (Figure 6C) (51), which makes it difficult to quantify translation efficiency. Our data suggest that translation remains unchanged or declines for most of the mRNAs examined (Figure 6C). A reduction in translation upon heat shock has been observed in several studies (54,64). A counterintuitive benefit of diminished translation is demonstrated by the observations that translation inhibitors can improve the survival of cells exposed to high temperatures (52), presumably due to the alleviation of proteotoxicity (53). Accordingly, the activity of a protein or associated physiological response can gain in importance despite reduced translation, as evidenced by our observation that the resistance to glucanases is enhanced after a heat shock (Figure 6D). Whereas the *ECM33* does not contribute to cell wall resistance at 30°C, it does so at 42°C despite the reduced *ECM33* transcription and/or translation.

We will discuss two hypothetical mechanisms, the activity of the decoding tRNAs and the targeting of mRNAs to specific cell organelles or aggregates, which can explain temperature compensation of mRNAs enriched in these codons.

The stability coefficients of the mRNA codons correlate well with the abundance and translational adaption index tAi of the tRNA that decode them ( $r = 0.6$  to  $0.7$ ). Temperature shift alters the abundance, covalent modifications or confirmation of tRNAs (65,66), which may underlie the codon-dependence of thermal adaptation. In principle, these mechanisms can destabilize mRNAs more at lower temperatures than at high temperatures, providing an alternative temperature compensation mechanism. The sequence context of the codons can also influence mRNA decay. The translation of repetitive sequences, often encoding identical amino acids, has been shown alter the elongation rate (67,68), which can indirectly influence mRNA stability (16). This may lead to nonlinear relationships between the translation efficiency of individual codons and mRNA stability. Analogously, the degradation of mRNAs enriched in temperature-compensating or -sensitizing codons may be influenced by the local density of the codons and the nature of encoded amino acids.

Localization can play a similarly important role. Ser-rich proteins are targeted via the endoplasmic reticulum (ER) and the secretory pathway to the cell membrane and cell wall (47), which is preceded by the association of the corresponding mRNA with the ER. The induction of secretory pathway components in yeast can increase mRNA stability (69). Glycosylation of the proteins in the ER facilitates protein folding in general, and promotes cellular integrity at higher temperatures (70,71).

In addition to targeting to organelles, aggregation can also promote localization. P-bodies and stress granules are enriched in Asn-containing low complexity domains (47). Asn-richness promotes assembly of self-templating amyloids (72), which may contribute to the formation of ribonucleoprotein aggregates. The ratio of Ser to Tyr plays is an important determinant of aggresome formation in vitro (73). Interestingly, the C-terminal domain of the Lsm4 protein, which is responsible for the formation of P-bodies and aggregates into amyloids (72), is highly enriched in asparagine (N, 36%) and moderately enriched in serine (S, 17%), and the gene lacks the Tyr(TAT) codon (74). This composition is similar to the synthetic sequences encoding Asn/Ser-rich proteins analyzed in our study. The C-terminal domain of Lsm4p is the P-body component that is most highly enriched in asparagine (Data S3).

While P-bodies and stress granules share important similarities, there are stress-specific differences in composition and assembly (75,76). Typically, they are viewed as storage sites of translationally repressed mRNAs. However, translation has been observed in these granules, suggesting that repression is partial and not complete (77). Temperature compensation would then simply result from the storage and stabilization of these mRNAs in ribonucleoprotein aggregates, in which translation is reduced. Since more and more proteins aggregate with increasing temperature (51), it remains to be clarified whether and which form of ribonucleoprotein aggregates are relevant for temperature compensation. Interestingly, Upf1p can target both nonsense and normal mRNAs to P-bodies, without promoting the degradation of normal mRNA (78). Similarly, Upf1 promotes the formation of aggresomes, which accumulate misfolded proteins during heat stress (51,79). Such a non-classical function of Upf1 can explain the stabilization of untranslated no-AUGs upon heat shock. The physiological relevance of the involvement of Upf1 in temperature adaptation is underlined by a study showing that Upf1 mutant cells have increased heat sensitivity (80). Thus, both the extrinsic and intrinsic determinants of temperature adaptation overlap with P-body components. Whereas the extrinsic determinant, Upf1 may target mRNAs to P-bodies directly, the formation of aggregates containing mRNAs enriched in compensating codons may be co-translational since Asn-rich proteins are prone to aggregate, a process that can particularly affect nascent proteins at high temperature. Interestingly, the two Asn/Ser-rich cellular compartments interact, since the cell wall integrity pathway controls P-body assembly upon cell wall stress (10).

Our results with consistent half-lives over a broad range of temperatures provide insight into the temperature adaptation under physiological conditions and into the early phase of heat shock response when cells still divide. This facilitated the identification of the regulators and the sequence specific determinants of the temperature adaptation of mRNA degradation.

## **DATA AVAILABILITY**

Data are available as supplementary data.

## **SUPPLEMENTARY DATA**

Supplementary data (Text S1-S2, Figures S1-S8, Tables S1-S7 and Data S1-S3) are available at NAR Online.



## FUNDING

This work was supported in part by the StoNets RTD from SystemsX.ch.

## AUTHOR CONTRIBUTIONS

A. B. designed the experiments and wrote the manuscript. V.J., D. T. and A.B. analyzed the data. S.W., S.V., V.J. and E.C.V performed the experiments.

## ACKNOWLEDGMENTS

We thank David Sommer, Melissa Langlois, Patrick Romann, Vinciane Fluhler, Phillippe Demougin, Mara Julseth, Sayanur Rahman and Chandraday Prodhan for the experimental help, Alexander Schmidt (Proteomics Core Facility) for the proteomics measurements, Stephen N. Floor for helpful discussion, and Ertugrul Ozbudak for comments on the manuscript.

## DECLARATION OF INTERESTS

The authors declare that they have no competing interests.

## REFERENCES

1. Alster, C.J., von Fischer, J.C., Allison, S.D. and Treseder, K.K. (2020) Embracing a new paradigm for temperature sensitivity of soil microbes. *Glob Chang Biol*, **26**, 3221-3229.
2. Kortmann, J. and Narberhaus, F. (2012) Bacterial RNA thermometers: molecular zippers and switches. *Nat Rev Microbiol*, **10**, 255-265.
3. Tomita, J., Nakajima, M., Kondo, T. and Iwasaki, H. (2005) No transcription-translation feedback in circadian rhythm of KaiC phosphorylation. *Science*, **307**, 251-254.
4. Robertson, R.M. and Money, T.G. (2012) Temperature and neuronal circuit function: compensation, tuning and tolerance. *Curr Opin Neurobiol*, **22**, 724-734.
5. Irvine, S.Q. (2020) Embryonic canalization and its limits-A view from temperature. *J Exp Zool B Mol Dev Evol*, **334**, 128-144.
6. Zinani, O.Q.H., Keseroglu, K., Ay, A. and Ozbudak, E.M. (2021) Pairing of segmentation clock genes drives robust pattern formation. *Nature*, **589**, 431-436.
7. Chen, Y.H. and Collier, J. (2016) A Universal Code for mRNA Stability? *Trends Genet*, **32**, 687-688.
8. Bazzini, A.A., Del Viso, F., Moreno-Mateos, M.A., Johnstone, T.G., Vejnar, C.E., Qin, Y., Yao, J., Khokha, M.K. and Giraldez, A.J. (2016) Codon identity regulates mRNA stability and translation efficiency during the maternal-to-zygotic transition. *EMBO J*, **35**, 2087-2103.
9. Mishima, Y. and Tomari, Y. (2016) Codon Usage and 3' UTR Length Determine Maternal mRNA Stability in Zebrafish. *Mol Cell*, **61**, 874-885.
10. Garcia, R., Pulido, V., Orellana-Munoz, S., Nombela, C., Vazquez de Aldana, C.R., Rodriguez-Pena, J.M. and Arroyo, J. (2019) Signalling through the yeast MAPK Cell Wall Integrity pathway controls P-body assembly upon cell wall stress. *Sci Rep*, **9**, 3186.

11. Luo, Y., Na, Z. and Slavoff, S.A. (2018) P-Bodies: Composition, Properties, and Functions. *Biochemistry*, **57**, 2424-2431.
12. Balagopal, V. and Parker, R. (2009) Polysomes, P bodies and stress granules: states and fates of eukaryotic mRNAs. *Curr Opin Cell Biol*, **21**, 403-408.
13. Herrick, D., Parker, R. and Jacobson, A. (1990) Identification and comparison of stable and unstable mRNAs in *Saccharomyces cerevisiae*. *Mol Cell Biol*, **10**, 2269-2284.
14. Wada, T. and Becskei, A. (2017) Impact of Methods on the Measurement of mRNA Turnover. *Int J Mol Sci*, **18**.
15. Carneiro, R.L., Requião, R.D., Rossetto, S., Domitrovic, T. and Palhano, F.L. (2019) Codon stabilization coefficient as a metric to gain insights into mRNA stability and codon bias and their relationships with translation. *Nucleic Acids Res*, **47**, 2216-2228.
16. Presnyak, V., Alhusaini, N., Chen, Y.H., Martin, S., Morris, N., Kline, N., Olson, S., Weinberg, D., Baker, K.E., Graveley, B.R. *et al.* (2015) Codon optimality is a major determinant of mRNA stability. *Cell*, **160**, 1111-1124.
17. Adams, C.C. and Gross, D.S. (1991) The yeast heat shock response is induced by conversion of cells to spheroplasts and by potent transcriptional inhibitors. *J Bacteriol*, **173**, 7429-7435.
18. Malik, I., Qiu, C., Snively, T. and Kaplan, C.D. (2017) Wide-ranging and unexpected consequences of altered Pol II catalytic activity in vivo. *Nucleic Acids Res*, **45**, 4431-4451.
19. Baudrimont, A., Voegeli, S., Vilorio, E.C., Stritt, F., Lenon, M., Wada, T., Jaquet, V. and Becskei, A. (2017) Multiplexed gene control reveals rapid mRNA turnover. *Sci Adv*, **3**, e1700006.
20. Sun, M., Schwalb, B., Schulz, D., Pirkl, N., Etzold, S., Lariviere, L., Maier, K.C., Seizl, M., Tresch, A. and Cramer, P. (2012) Comparative dynamic transcriptome analysis (cDTA) reveals mutual feedback between mRNA synthesis and degradation. *Genome Res*, **22**, 1350-1359.
21. Reimann, C., Filzmoser, P. and Garrett, R.G. (2005) Background and threshold: critical comparison of methods of determination. *Sci Total Environ*, **346**, 1-16.
22. Blewett, N., Collier, J. and Goldstrohm, A. (2011) A quantitative assay for measuring mRNA decapping by splinted ligation reverse transcription polymerase chain reaction: qSL-RT-PCR. *RNA*, **17**, 535-543.
23. Pelechano, V., Wei, W. and Steinmetz, L.M. (2013) Extensive transcriptional heterogeneity revealed by isoform profiling. *Nature*, **497**, 127-131.
24. Raj, A. and Tyagi, S. (2010) Detection of individual endogenous RNA transcripts in situ using multiple singly labeled probes. *Methods Enzymol*, **472**, 365-386.
25. Baudrimont, A., Jaquet, V., Wallerich, S., Voegeli, S. and Becskei, A. (2019) Contribution of RNA Degradation to Intrinsic and Extrinsic Noise in Gene Expression. *Cell Rep*, **26**, 3752-3761 e3755.
26. Gencoglu, M., Schmidt, A. and Becskei, A. (2017) Measurement of In Vivo Protein Binding Affinities in a Signaling Network with Mass Spectrometry. *ACS Synth Biol*, **6**, 1305-1314.
27. Stringer, C., Wang, T., Michaelos, M. and Pachitariu, M. (2020) Cellpose: a generalist algorithm for cellular segmentation. 2020.2002.2002.931238.
28. Ovalle, R., Lim, S.T., Holder, B., Jue, C.K., Moore, C.W. and Lipke, P.N. (1998) A spheroplast rate assay for determination of cell wall integrity in yeast. *Yeast*, **14**, 1159-1166.
29. Cherry, J.M., Hong, E.L., Amundsen, C., Balakrishnan, R., Binkley, G., Chan, E.T., Christie, K.R., Costanzo, M.C., Dwight, S.S., Engel, S.R. *et al.* (2012) *Saccharomyces Genome Database: the genomics resource of budding yeast*. *Nucleic Acids Res*, **40**, D700-705.
30. Eshleman, N., Luo, X., Capaldi, A. and Buchan, J.R. (2020) Alterations of signaling pathways in response to chemical perturbations used to measure mRNA decay rates in yeast. *RNA*, **26**, 10-18.
31. Huch, S. and Nissan, T. (2014) Interrelations between translation and general mRNA degradation in yeast. *Wiley Interdiscip Rev RNA*, **5**, 747-763.

32. Fleischmann, J., Rocha, M.A., Hauser, P.V., Gowda, B.S. and Pilapil, M.G.D. (2020) Exonuclease resistant 18S and 25S ribosomal RNA components in yeast are possibly newly transcribed by RNA polymerase II. *BMC Mol Cell Biol*, **21**, 59.
33. Gibney, P.A., Lu, C., Caudy, A.A., Hess, D.C. and Botstein, D. (2013) Yeast metabolic and signaling genes are required for heat-shock survival and have little overlap with the heat-induced genes. *Proc Natl Acad Sci U S A*, **110**, E4393-4402.
34. Zakrzewska, A., van Eikenhorst, G., Burggraaff, J.E., Vis, D.J., Hoefsloot, H., Delneri, D., Oliver, S.G., Brul, S. and Smits, G.J. (2011) Genome-wide analysis of yeast stress survival and tolerance acquisition to analyze the central trade-off between growth rate and cellular robustness. *Mol Biol Cell*, **22**, 4435-4446.
35. Garcia-Martinez, J., Delgado-Ramos, L., Ayala, G., Pelechano, V., Medina, D.A., Carrasco, F., Gonzalez, R., Andres-Leon, E., Steinmetz, L., Warringer, J. *et al.* (2016) The cellular growth rate controls overall mRNA turnover, and modulates either transcription or degradation rates of particular gene regulons. *Nucleic Acids Res*, **44**, 3643-3658.
36. Izawa, S., Kita, T., Ikeda, K. and Inoue, Y. (2008) Heat shock and ethanol stress provoke distinctly different responses in 3'-processing and nuclear export of HSP mRNA in *Saccharomyces cerevisiae*. *Biochem J*, **414**, 111-119.
37. Castells-Roca, L., Garcia-Martinez, J., Moreno, J., Herrero, E., Belli, G. and Perez-Ortin, J.E. (2011) Heat shock response in yeast involves changes in both transcription rates and mRNA stabilities. *PLoS One*, **6**, e17272.
38. Luo, Y., Schofield, J.A., Simon, M.D. and Slavoff, S.A. (2020) Global Profiling of Cellular Substrates of Human Dcp2. *Biochemistry*.
39. Yu, X. and Warner, J.R. (2001) Expression of a micro-protein. *J Biol Chem*, **276**, 33821-33825.
40. Kearse, M.G. and Wilusz, J.E. (2017) Non-AUG translation: a new start for protein synthesis in eukaryotes. *Genes Dev*, **31**, 1717-1731.
41. Chang, K.J. and Wang, C.C. (2004) Translation initiation from a naturally occurring non-AUG codon in *Saccharomyces cerevisiae*. *J Biol Chem*, **279**, 13778-13785.
42. Chen, S.J., Lin, G., Chang, K.J., Yeh, L.S. and Wang, C.C. (2008) Translational efficiency of a non-AUG initiation codon is significantly affected by its sequence context in yeast. *J Biol Chem*, **283**, 3173-3180.
43. Eisenberg, A.R., Higdon, A.L., Hollerer, I., Fields, A.P., Jungreis, I., Diamond, P.D., Kellis, M., Jovanovic, M. and Brar, G.A. (2020) Translation Initiation Site Profiling Reveals Widespread Synthesis of Non-AUG-Initiated Protein Isoforms in Yeast. *Cell Syst*, **11**, 145-160 e145.
44. He, F., Li, X., Spatrick, P., Casillo, R., Dong, S. and Jacobson, A. (2003) Genome-wide analysis of mRNAs regulated by the nonsense-mediated and 5' to 3' mRNA decay pathways in yeast. *Mol Cell*, **12**, 1439-1452.
45. Bonde, M.M., Voegeli, S., Baudrimont, A., Seraphin, B. and Becskei, A. (2014) Quantification of pre-mRNA escape rate and synergy in splicing. *Nucleic Acids Res*, **42**, 12847-12860.
46. Brar, G.A., Yassour, M., Friedman, N., Regev, A., Ingolia, N.T. and Weissman, J.S. (2012) High-resolution view of the yeast meiotic program revealed by ribosome profiling. *Science*, **335**, 552-557.
47. Cascarina, S.M. and Ross, E.D. (2018) Proteome-scale relationships between local amino acid composition and protein fates and functions. *PLoS Comput Biol*, **14**, e1006256.
48. Levin, D.E. (2011) Regulation of cell wall biogenesis in *Saccharomyces cerevisiae*: the cell wall integrity signaling pathway. *Genetics*, **189**, 1145-1175.
49. Petkova, M.I., Pujol-Carrion, N. and de la Torre-Ruiz, M.A. (2012) Mtl1 O-mannosylation mediated by both Pmt1 and Pmt2 is important for cell survival under oxidative conditions and TOR blockade. *Fungal Genet Biol*, **49**, 903-914.
50. Steiger, J.H. (1980) Tests for Comparing Elements of a Correlation Matrix. *Psychol Bull*, **87**, 245-251.
51. Muhlhofer, M., Berchtold, E., Stratil, C.G., Csaba, G., Kunold, E., Bach, N.C., Sieber, S.A., Haslbeck, M., Zimmer, R. and Buchner, J. (2019) The Heat Shock Response in Yeast Maintains

- Protein Homeostasis by Chaperoning and Replenishing Proteins. *Cell Rep*, **29**, 4593-4607 e4598.
52. Jarolim, S., Ayer, A., Pillay, B., Gee, A.C., Phrakaysone, A., Perrone, G.G., Breitenbach, M. and Dawes, I.W. (2013) *Saccharomyces cerevisiae* genes involved in survival of heat shock. *G3 (Bethesda)*, **3**, 2321-2333.
  53. Tye, B.W. and Churchman, L.S. (2021) Hsf1 activation by proteotoxic stress requires concurrent protein synthesis. *Mol Biol Cell*, **32**, 1800-1806.
  54. Miller, M.J., Xuong, N.H. and Geiduschek, E.P. (1979) A response of protein synthesis to temperature shift in the yeast *Saccharomyces cerevisiae*. *Proc Natl Acad Sci U S A*, **76**, 5222-5225.
  55. Neef, D.W. and Thiele, D.J. (2009) Enhancer of decapping proteins 1 and 2 are important for translation during heat stress in *Saccharomyces cerevisiae*. *Mol Microbiol*, **73**, 1032-1042.
  56. Shrimal, S. and Gilmore, R. (2019) Oligosaccharyltransferase structures provide novel insight into the mechanism of asparagine-linked glycosylation in prokaryotic and eukaryotic cells. *Glycobiology*, **29**, 288-297.
  57. Chi, J.H., Roos, J. and Dean, N. (1996) The OST4 gene of *Saccharomyces cerevisiae* encodes an unusually small protein required for normal levels of oligosaccharyltransferase activity. *J Biol Chem*, **271**, 3132-3140.
  58. Pardo, M., Monteoliva, L., Vazquez, P., Martinez, R., Molero, G., Nombela, C. and Gil, C. (2004) PST1 and ECM33 encode two yeast cell surface GPI proteins important for cell wall integrity. *Microbiology*, **150**, 4157-4170.
  59. Gil-Bona, A., Reales-Calderon, J.A., Parra-Giraldo, C.M., Martinez-Lopez, R., Monteoliva, L. and Gil, C. (2016) The Cell Wall Protein Ecm33 of *Candida albicans* is Involved in Chronological Life Span, Morphogenesis, Cell Wall Regeneration, Stress Tolerance, and Host-Cell Interaction. *Front Microbiol*, **7**, 64.
  60. Hilgers, V., Teixeira, D. and Parker, R. (2006) Translation-independent inhibition of mRNA deadenylation during stress in *Saccharomyces cerevisiae*. *RNA*, **12**, 1835-1845.
  61. Celik, A., Baker, R., He, F. and Jacobson, A. (2017) High-resolution profiling of NMD targets in yeast reveals translational fidelity as a basis for substrate selection. *RNA*, **23**, 735-748.
  62. Lavysh, D. and Neu-Yilik, G. (2020) UPF1-Mediated RNA Decay-Danse Macabre in a Cloud. *Biomolecules*, **10**.
  63. Palancade, B., Zuccolo, M., Loeillet, S., Nicolas, A. and Doye, V. (2005) Pml39, a novel protein of the nuclear periphery required for nuclear retention of improper messenger ribonucleoparticles. *Mol Biol Cell*, **16**, 5258-5268.
  64. Dever, T.E., Kinzy, T.G. and Pavitt, G.D. (2016) Mechanism and Regulation of Protein Synthesis in *Saccharomyces cerevisiae*. *Genetics*, **203**, 65-107.
  65. Torrent, M., Chalancon, G., de Groot, N.S., Wuster, A. and Madan Babu, M. (2018) Cells alter their tRNA abundance to selectively regulate protein synthesis during stress conditions. *Sci Signal*, **11**.
  66. Lorenz, C., Lunse, C.E. and Morl, M. (2017) tRNA Modifications: Impact on Structure and Thermal Adaptation. *Biomolecules*, **7**.
  67. Tesina, P., Lessen, L.N., Buschauer, R., Cheng, J., Wu, C.C., Berninghausen, O., Buskirk, A.R., Becker, T., Beckmann, R. and Green, R. (2020) Molecular mechanism of translational stalling by inhibitory codon combinations and poly(A) tracts. *EMBO J*, **39**, e103365.
  68. Chandrasekaran, V., Juszkievicz, S., Choi, J., Puglisi, J.D., Brown, A., Shao, S., Ramakrishnan, V. and Hegde, R.S. (2019) Mechanism of ribosome stalling during translation of a poly(A) tail. *Nat Struct Mol Biol*, **26**, 1132-1140.
  69. Hyde, M., Block-Alper, L., Felix, J., Webster, P. and Meyer, D.I. (2002) Induction of secretory pathway components in yeast is associated with increased stability of their mRNA. *J Cell Biol*, **156**, 993-1001.
  70. Lehrman, M.A. (2006) Stimulation of N-linked glycosylation and lipid-linked oligosaccharide synthesis by stress responses in metazoan cells. *Crit Rev Biochem Mol Biol*, **41**, 51-75.

71. Cherepanova, N., Shrima, S. and Gilmore, R. (2016) N-linked glycosylation and homeostasis of the endoplasmic reticulum. *Curr Opin Cell Biol*, **41**, 57-65.
72. Halfmann, R., Alberti, S., Krishnan, R., Lyle, N., O'Donnell, C.W., King, O.D., Berger, B., Pappu, R.V. and Lindquist, S. (2011) Opposing effects of glutamine and asparagine govern prion formation by intrinsically disordered proteins. *Mol Cell*, **43**, 72-84.
73. Kato, M., Han, T.W., Xie, S., Shi, K., Du, X., Wu, L.C., Mirzaei, H., Goldsmith, E.J., Longgood, J., Pei, J. *et al.* (2012) Cell-free formation of RNA granules: low complexity sequence domains form dynamic fibers within hydrogels. *Cell*, **149**, 753-767.
74. Reijns, M.A., Alexander, R.D., Spiller, M.P. and Beggs, J.D. (2008) A role for Q/N-rich aggregation-prone regions in P-body localization. *J Cell Sci*, **121**, 2463-2472.
75. Escalante, L.E. and Gasch, A.P. (2021) The role of stress-activated RNA-protein granules in surviving adversity. *RNA*.
76. Tishinov, K. and Spang, A. (2021) The mRNA decapping complex is buffered by nuclear localization. *J Cell Sci*, **134**.
77. Lui, J., Castelli, L.M., Pizzinga, M., Simpson, C.E., Hoyle, N.P., Bailey, K.L., Campbell, S.G. and Ashe, M.P. (2014) Granules harboring translationally active mRNAs provide a platform for P-body formation following stress. *Cell Rep*, **9**, 944-954.
78. Sheth, U. and Parker, R. (2006) Targeting of aberrant mRNAs to cytoplasmic processing bodies. *Cell*, **125**, 1095-1109.
79. Park, Y., Park, J., Hwang, H.J., Kim, B., Jeong, K., Chang, J., Lee, J.B. and Kim, Y.K. (2020) Nonsense-mediated mRNA decay factor UPF1 promotes aggresome formation. *Nat Commun*, **11**, 3106.
80. Sinha, H., David, L., Pascon, R.C., Clauder-Munster, S., Krishnakumar, S., Nguyen, M., Shi, G., Dean, J., Davis, R.W., Oefner, P.J. *et al.* (2008) Sequential elimination of major-effect contributors identifies additional quantitative trait loci conditioning high-temperature growth in yeast. *Genetics*, **180**, 1661-1670.

**Figure 1. Dependence of mRNA half-lives on temperature, carbon source and translation.**

(A, B) The cells were grown in 2% raffinose at 20°C ( $N = 75$ ), 30°C ( $N = 78$ ) or 42°C ( $N = 75$ ), or in 2% glucose ( $N = 67$ ), and 3% glycerol ( $n = 69$ ) at 30°C. The representative set of mRNAs are encoded by genes in the II (YBR) and XIII (YML) chromosomes (Materials and Methods). The distribution of half-lives (A). The half-lives plotted against cell doubling time (mean and standard error from three replicate measurements of the BY4743 strain); the time series of culture density measured over 6 hours was used to fit the doubling time by linear regression (B).

(C) The Spearman's rank correlation between the half-lives of the mRNAs in different culturing conditions (data as in A).

(D) The Spearman correlation between the half-lives of mRNAs present in all datasets ( $N = 82$ ). The median half-lives ( $N = 82$ ) are 23.1 min (GRO, 25°C), 27.7 min (GRO, 37°C), 13.3 min (cDTA, 30°C) and 20.6 min (37°C). The GRO 37°C half-lives were calculated from the mRNA amounts and transcription rates measured 40 min after the heat shock.

(E) The no-ATG genes were constructed by converting all ATG triplets into TAG within the ORF and UTRs (diagram). The half-lives of the set of stable and unstable mRNAs and their no-AUG counterparts in cells grown at 20°C. The dashed lines indicate the position of the lowest and highest deciles (1.5 and 17.1 min for the set of stable and unstable mRNAs and 3.5 and 8.2 min for the no-AUG counterparts).

(F) The translational stabilization is the ratio of the half-lives of normal (AUG) to that of no-AUG mRNAs. The domains of stabilization (ratio > 1) and destabilization (ratio < 1) are separated by a thick gray line (ratio = 1, no effect of translation). Data identical to those shown in (E).

**Figure 2. Cellular distribution and the decapping of AUG and no-AUG RNAs.**

(A) smFISH images showing the cellular distribution of the *TSI1* mRNA with and without AUG in cells grown at 30°C. Scale bar, 5  $\mu$ m.

(B) Cells grown at 42°C; in addition to the RNA molecules (red) and DAPI stained nuclear and mitochondrial DNA (blue), the background fluorescence is shown (green). The intense background fluorescence (green) indicates dead cells.

(C) Number of RNA molecules in the cytoplasm and nucleus at 30°C, 42 °C after 30 min or overnight (ON) incubation. The data for each condition are combined from two or three biological replicates. The boxes and whiskers denote the 25 to 75 and the 10 to 90 percentiles, respectively. The  $\Delta tsI1$  cells hybridized to the *TSI1* (AUG) and no-AUG *TSI1* probes serve as negative controls. The distribution of number of RNA molecules was obtained from  $N$

cells:  $N(\Delta tsl1, \text{AUG probe}) = 87$ ,  $N(\Delta tsl1, \text{noAUG probe}) = 254$ ,  $N(\text{AUG}, 30^\circ\text{C}) = 558$ ,  $N(\text{AUG}, 42^\circ\text{C } 30 \text{ min}) = 472$ ,  $N(\text{AUG}, 42^\circ\text{C ON}) = 343$ ,  $N(\text{noAUG}, 30^\circ\text{C}) = 239$ ,  $N(\text{noAUG}, 42^\circ\text{C}, 30 \text{ min}) = 777$ ,  $N(\text{noAUG}, 42^\circ\text{C ON}) = 270$ .

(D) The signal-to-noise ratio of the SL-qPCR assay (see Materials and Methods for the definition). Endo: endogenous genes,  $\Delta xrn1$ : endogenous mRNAs in  $\Delta xrn1$  cells, WT(MGC): 4 silent mutations in ORF, same construct as the one used to determine decay rate.

(E) Percentage of decayed mRNA measured with the SL-qPCR assay. Error bars: standard error ( $n = 3$ ).

### Figure 3. Global effect of temperature on the turnover of translated mRNAs

(A) The half-life of the mRNA with and without AUG codons in cells grown in raffinose at  $30^\circ\text{C}$  or  $42^\circ\text{C}$ . The neutral point denotes the mean no-AUG half-life (horizontal line in the left panel). The right panels indicate the probability density functions fitted to the half-lives of the representative mRNA set.

(B) The percentage of stabilized mRNAs and the location of the neutral point in different growth conditions (5.5, 3.3 and 4.0 min for raffinose at  $20^\circ$ ,  $30^\circ\text{C}$  and  $42^\circ\text{C}$ ; 3.9 and 4.2 min for glucose and glycerol, respectively). The error bars represent the standard error obtained by bootstrapping.

### Figure 4. The half-lives of mRNAs and their no-AUG counterparts in *upf1Δ* cells.

The half-life ( $t_{1/2}$ ) of the set of stable and unstable mRNAs and their no-AUG counterparts was measured in WT and *upf1Δ* cells. The Upf1 stabilization ratio ( $USR = t_{1/2}[\text{WT}] / t_{1/2}[\text{upf1}\Delta]$ ) reflects how the deletion of *UPF1* affects the half-life. A *USR* larger and less than one indicates stabilization and destabilization by *UPF1*, respectively. The gray band denotes a neutral ratio,  $USR=1$  and the orange lines denote twofold stabilization and destabilization by *UPF1*. The black dashed line is obtained with linear regression, which appears curved in the logarithmic plots.  $GM(USR)$  is the geometric mean of the USRs. The Spearman rank correlation  $r_s$  and the P-value (P) is calculated for the two displayed variables.

(A) no-AUG mRNAs at  $20^\circ\text{C}$ .  $GM(USR) = 0.92$  ( $N = 25$ );  $r_s = -0.09$ , ( $P = 0.67$ )

(B) no-AUG mRNAs at  $42^\circ\text{C}$ .  $GM(USR) = 1.48$  ( $N = 24$ );  $r_s = 0.82$  ( $P = 4.6 \cdot 10^{-7}$ ).

(C) mRNAs at  $20^\circ\text{C}$ .  $GM(USR) = 0.66$  ( $N = 23$ );  $r_s = 0.09$  ( $P = 0.69$ ).

(D) mRNAs at  $42^\circ\text{C}$ .  $GM(USR) = 0.74$  ( $N = 23$ );  $r_s = 0.73$  ( $P = 7.9 \cdot 10^{-5}$ ). The interdecile ratio is reduced from 12 in WT cells to 4.9 in *upf1Δ* cells.

(E) mRNAs at  $30^\circ\text{C}$ .  $GM(USR) = 0.90$  ( $N = 23$ );  $r_s = 0.50$  ( $P = 0.014$ ).

(F) The  $USR(42^\circ\text{C}) : USR(20^\circ\text{C})$  ratio calculated for mRNAs.  $r_s = 0.77$  ( $P = 3.8 \cdot 10^{-5}$ ).

### Figure 5. Codon-dependence of temperature adaptation in RNA degradation

(A) The dtCSC values calculated based on the representative and stable-unstable mRNA sets ( $N = 95$ ). P-values are given for the corresponding Spearman rank correlation due to the deviation from normality: Asn(AAC) 0.0003; Tyr(TAT) 0.006; Leu(CTT) 0.010; Ser(TCC) 0.014, Ser(TCT) 0.016 and Ser(TCA) 0.038. Associations having p-values less than 0.01 are indicated by thick edges.

(B) The half-lives of the mRNAs expressed from synthetic genes comprise 15 amino acids between the start and stop codons. The bar plots show the composition of the two Ser/Asn-rich genes, consisting of three (C3) and four (C4) different codons. The control gene (cyan stars) contains three copies of each of the following codons, with the dtCSC given in parenthesis: GAA (Glu, 0.03), GCA (Ala, 0.19 ); GGA, GGC and GGT (Gly; 0.15, 0.1 and 0.07). The error bars indicate standard errors ( $n = 3$  independent experiments). The temperature compensation of the SN-rich C3 mRNAs relative to the control (ratio of the slopes of the pink and cyan lines) is 1.87 (yellow arrow).

(C) The half-lives of the mRNAs expressed from synthetic genes encode 14 identical amino acids and a methionine (start codon). The error bars indicate standard errors ( $n = 3$  independent experiments).

(D) The half-lives of mRNAs expressed from synthetic genes encoding 100 amino acids long proteins were inserted between the *NRG2* or *RPS22A* UTRs. The error bars indicate standard errors ( $n = 3$ ). The regression lines (dashed lines) are calculated for the most differing constructs.

### Figure 6. Functional relevance of enrichment of mRNAs in Asn and Ser codons.

(A) The role of Asn, Ser and Tyr codons in the temperature compensation of the *MTLI* mRNA degradation. The codon composition of the Asn/Ser-rich (NS), WT and Tyr-rich (Y) sequences are shown in the pie charts. The NoSP denotes the construct with no signal peptide sequence. The error bars denote standard errors calculated from three biological replicates. The P-values were calculated for the log ratios of the half-life measured at 20°C to that at 42°C for the t-test:  $P = 0.028$  for *MTLI*(NS) versus (Y) and  $P = 0.013$  for *MTLI*(NS) vs (Y, No SP). Using Mann-Whitney yields  $P = 0.029$  for both pairs.

(B) The ratio of half-lives measured at 20 °C and 42°C (standard error,  $n = 3$ ) for the mRNAs enriched in temperature-compensating or temperature-sensitizing codons. The mRNAs are marked with multiple stop codons. The temperature-compensating mRNAs encoding genes responsible for the resistance against zymolyase are shown in dark blue.

(C) Fold change of protein and mRNA levels measured at 20 versus 42°C ( $n = 3$  replicates). Proteins were measured 3 hours after shifting the temperature to 42°C, whereas the corresponding mRNAs were measured at 30 (empty symbols) and 90 (full symbols) min after the shift. Each gene is denoted by an empty and full symbol, which refer to the same protein measurement. This timing allows the typically slowly degrading proteins to integrate rapid



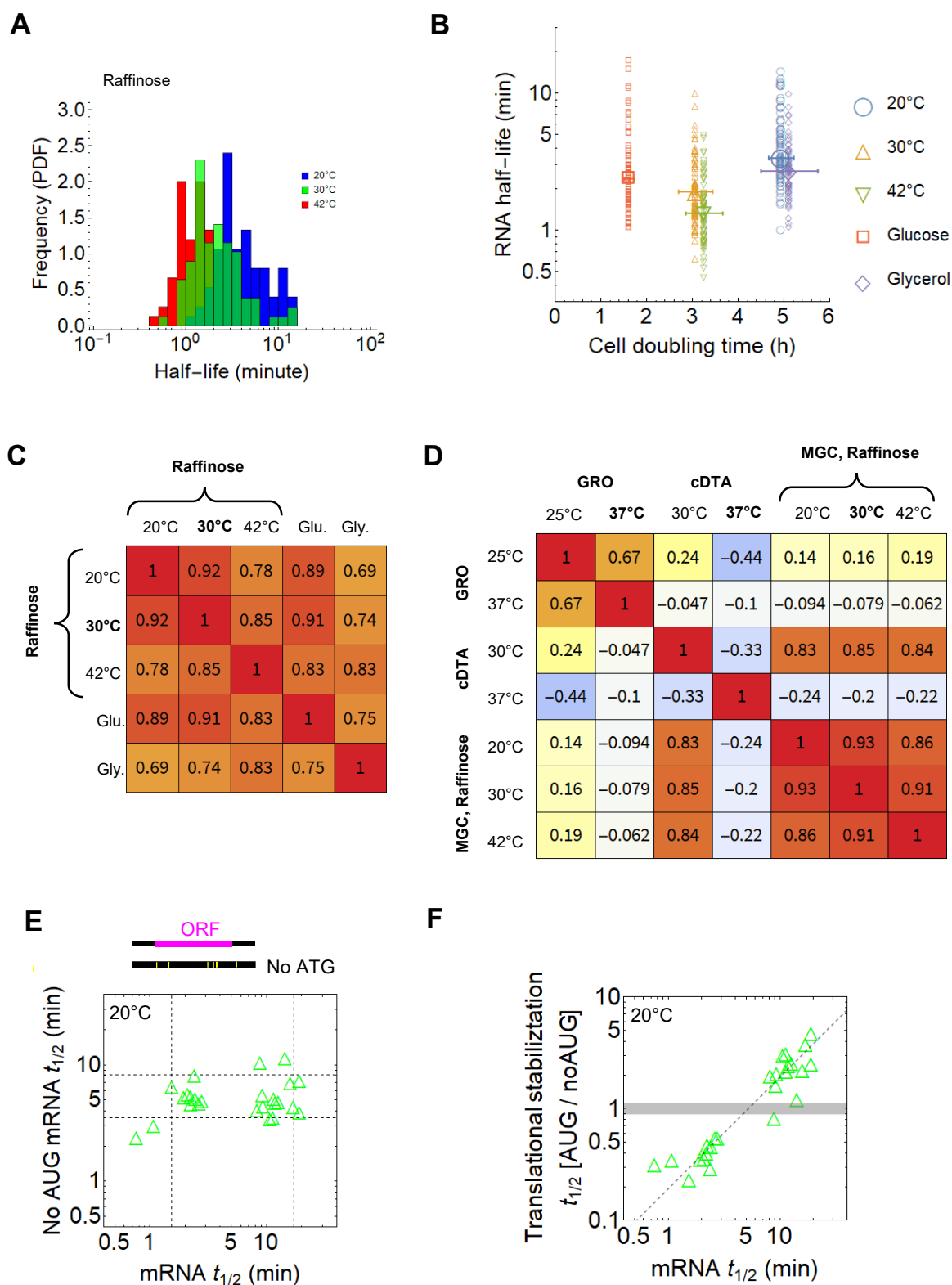
changes in the amount of mRNA over the previous period. The thick gray line denotes equal change of protein and mRNA levels, which indicates that translation remains constant provided the protein half-life and transcription does not change.

**(D)** The cell wall (CW) sensitivity against glycosidases (zymolyase rate index, ZRI) for cells in which the indicated genes are deleted. The full gray line indicates the same sensitivity at 30 and 42°C. The upper and lower gray dashed lines denote 10 times higher and lower sensitivity at 42°C, respectively. The *Δgal2* and *Δgal3* cells were used as control deletions (gray). The error bars denote the standard error from  $n = 3$  biological replicates for cells grown at 30°C, and  $n = 5$  at 42°C. Significant differences (Mann-Whitney) relative to the control cells (*Δgal2*, *Δgal3*) were found for *Δecm33* ( $P=0.006$ ,  $0.012$ ), *Δost4* ( $P=0.006$ ) and *Δqcr6* ( $P=0.012$ ) cells at 42°C. For *Δgat1*  $P=0.006$  (vs *Δgal2*) and  $0.094$  (vs *Δgal3*).

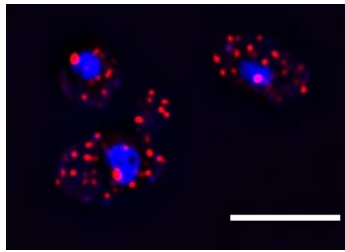
**Figure 7. Scheme of the extrinsic and intrinsic determinants of the temperature adaptation of mRNA degradation.**

**(A)** Extrinsic determinants. Translation stabilizes mRNAs with a half-life greater than the neutral half-life (cyan area) but below that destabilizes them (orange area). The arrows indicate processes associated with a shift from low to high temperature. Heat shock reduces the proportion of translationally stabilized mRNAs indirectly because Upf1 increases the neutral half-life. At the same time, the increase in temperature buffers the destabilizing activity of Upf1 against some of the translationally stabilized mRNAs (cross). Consequently, the degradation of mRNAs is partially temperature compensated.

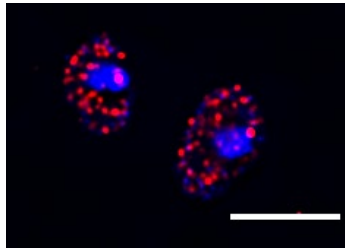
**(B)** Codons are the intrinsic determinants of mRNAs temperature adaptation. Most codons do not change their stabilizing effect significantly upon temperature shift (gray arrows). However, specific Asn and Ser codons buffer the increase in the mRNA degradation rate as the temperature rises (compensation, yellow arrow). On the other hand, Tyr codons amplify the temperature-induced change in mRNA stability (sensitization, green arrow).



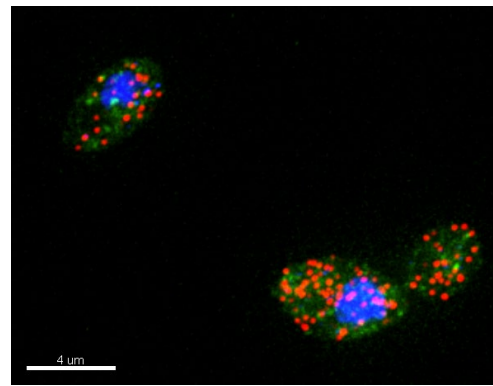
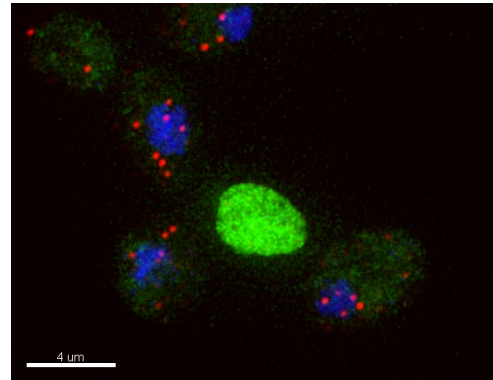
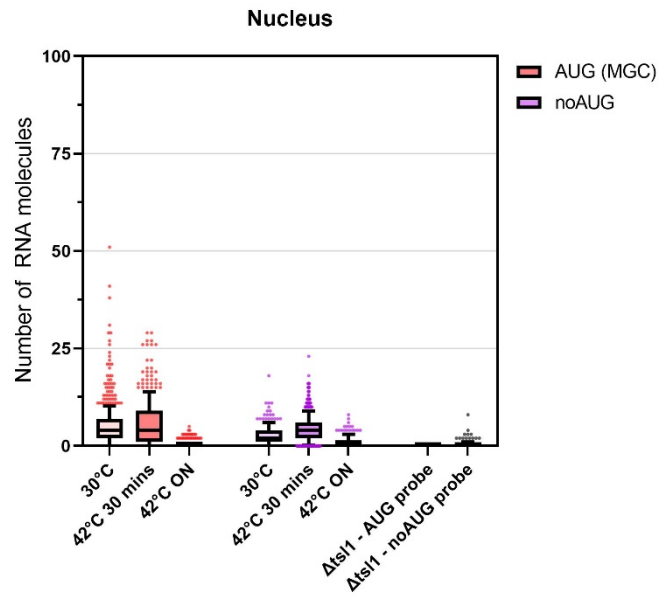
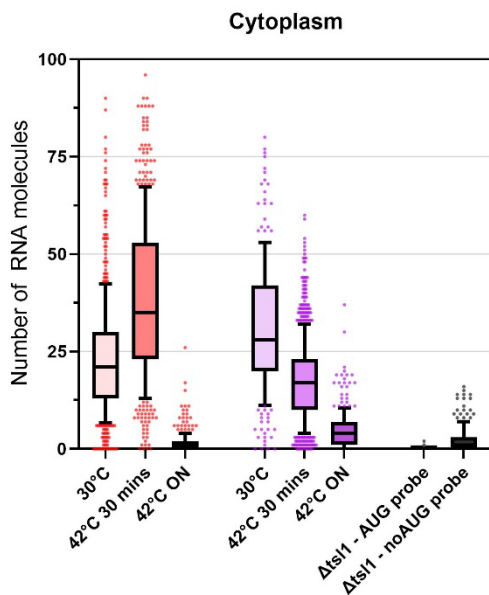
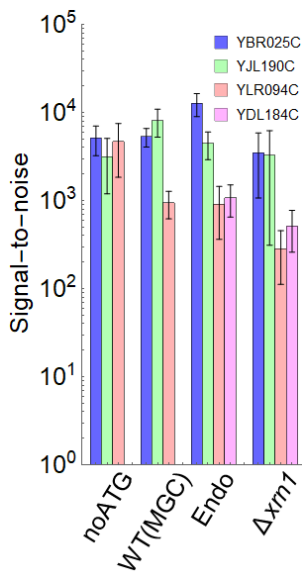
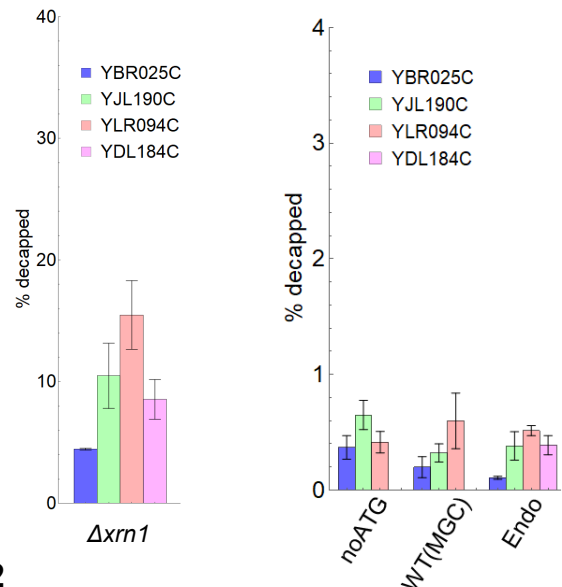
**Fig. 1**

**A**

30°C TSL1 (noAUG)



30°C TSL1 (AUG)

**B**TSL1 (AUG)  
42°C 30 minTSL1 (AUG)  
42°C Overnight**C****D****E****Fig. 2**

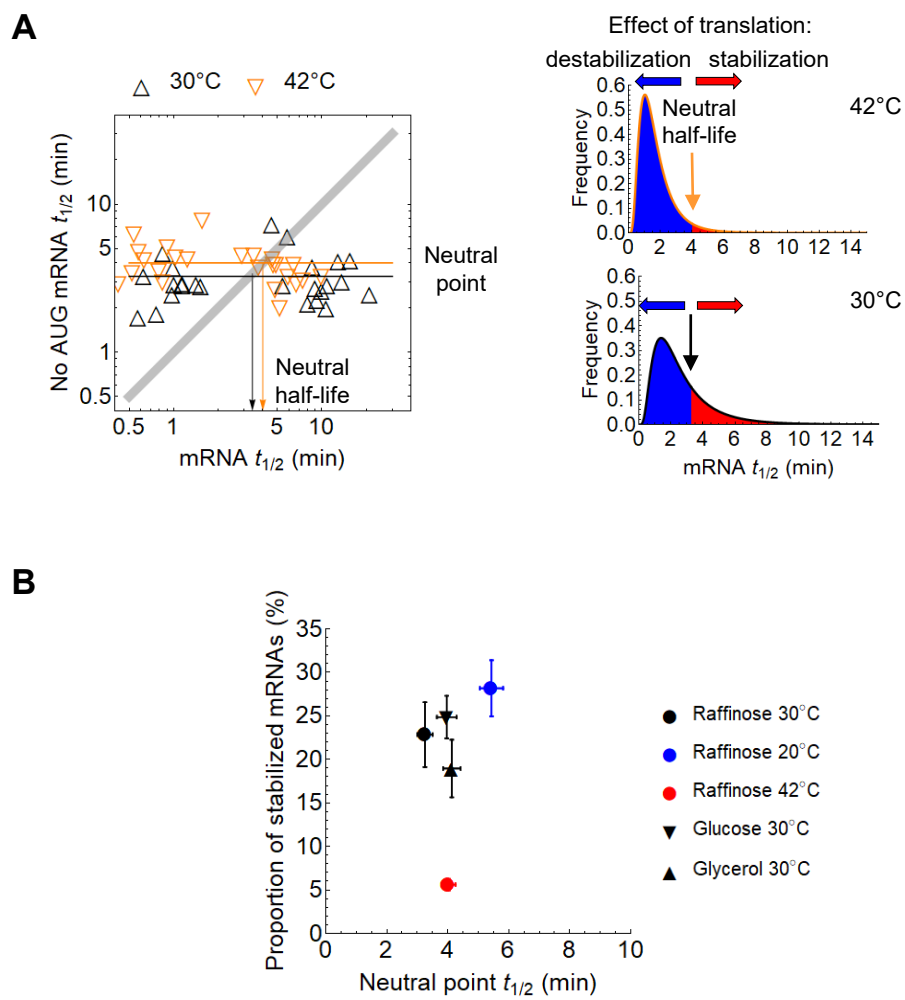


**Fig. 3**

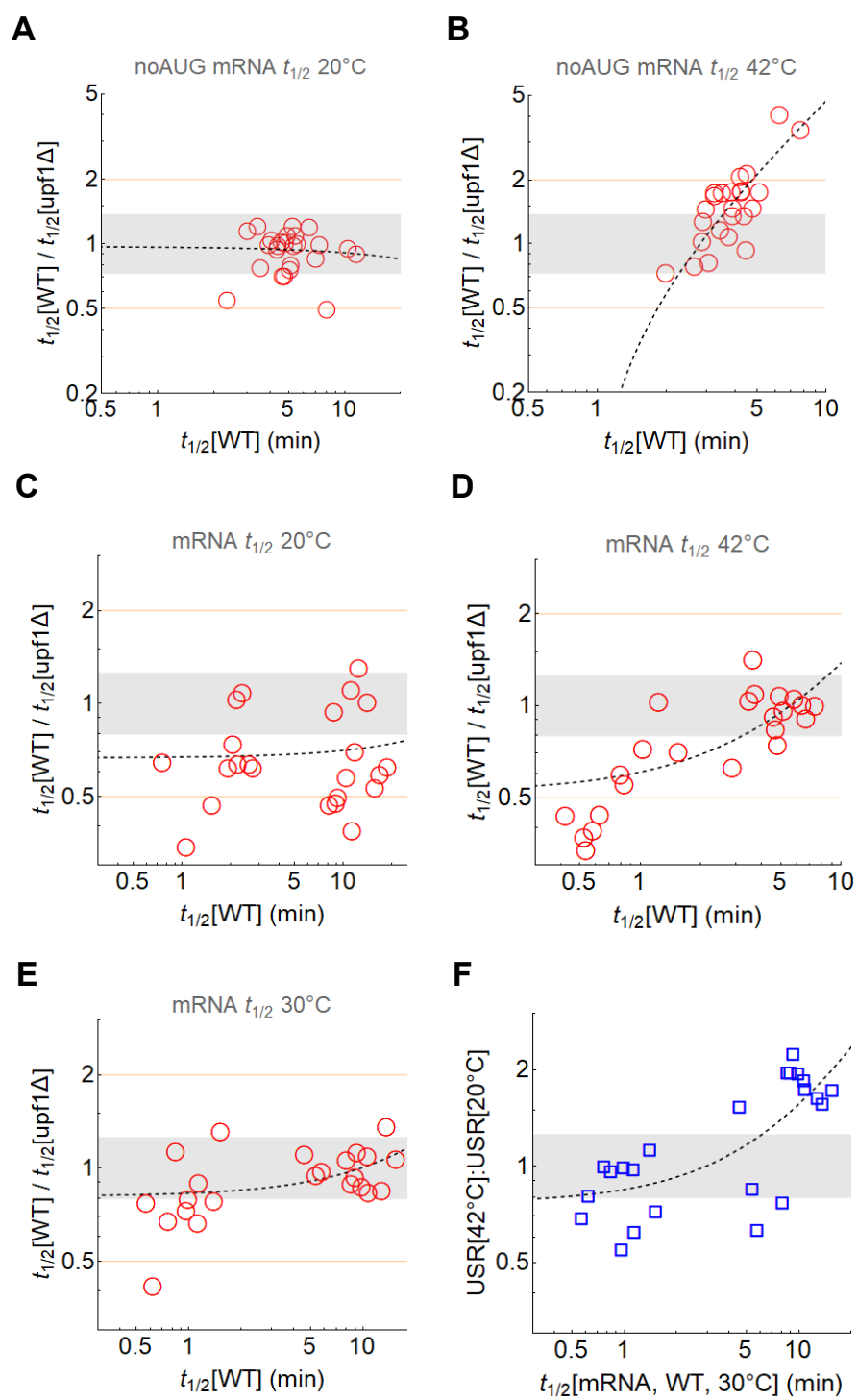


**Fig. 4**

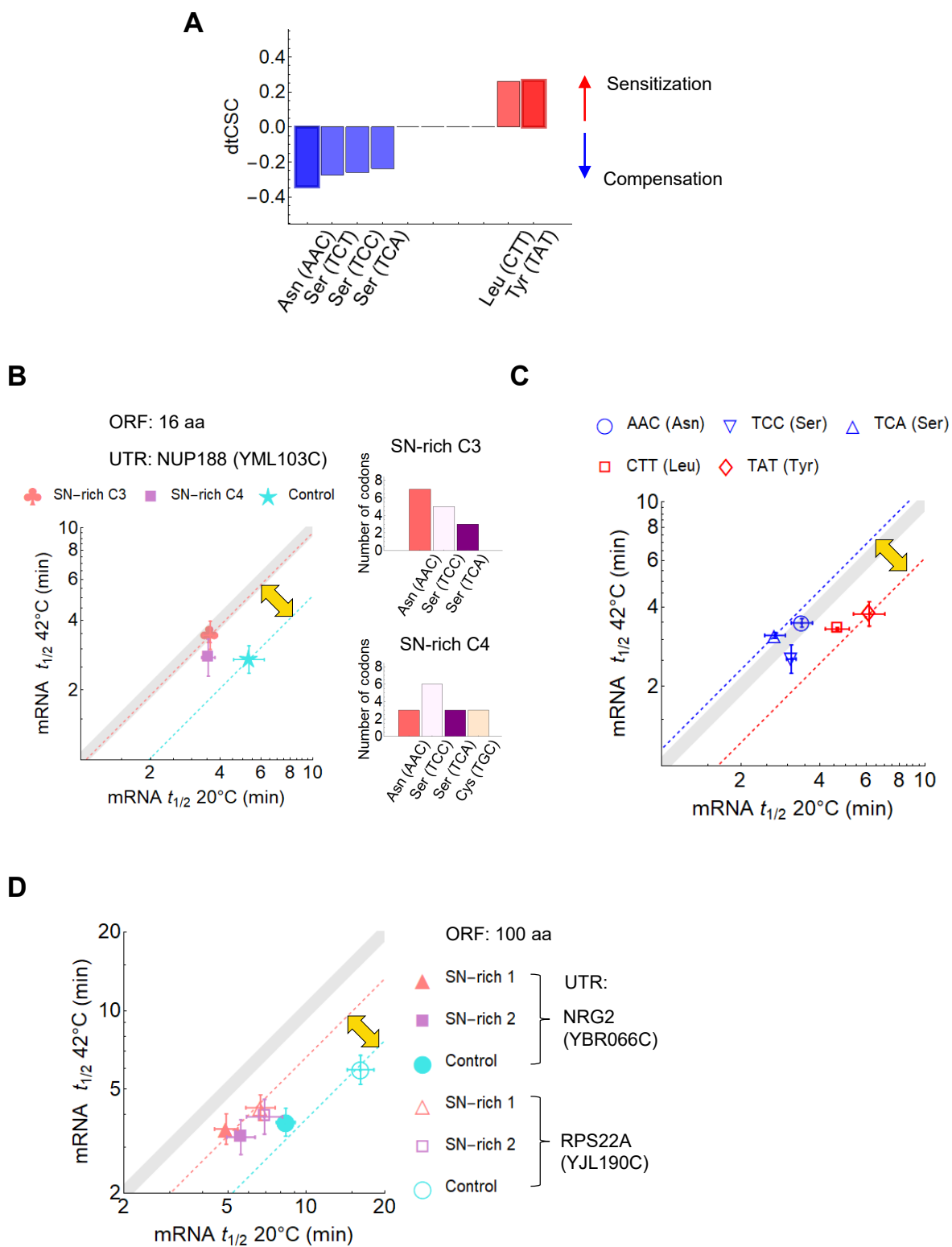


**Fig. 5**

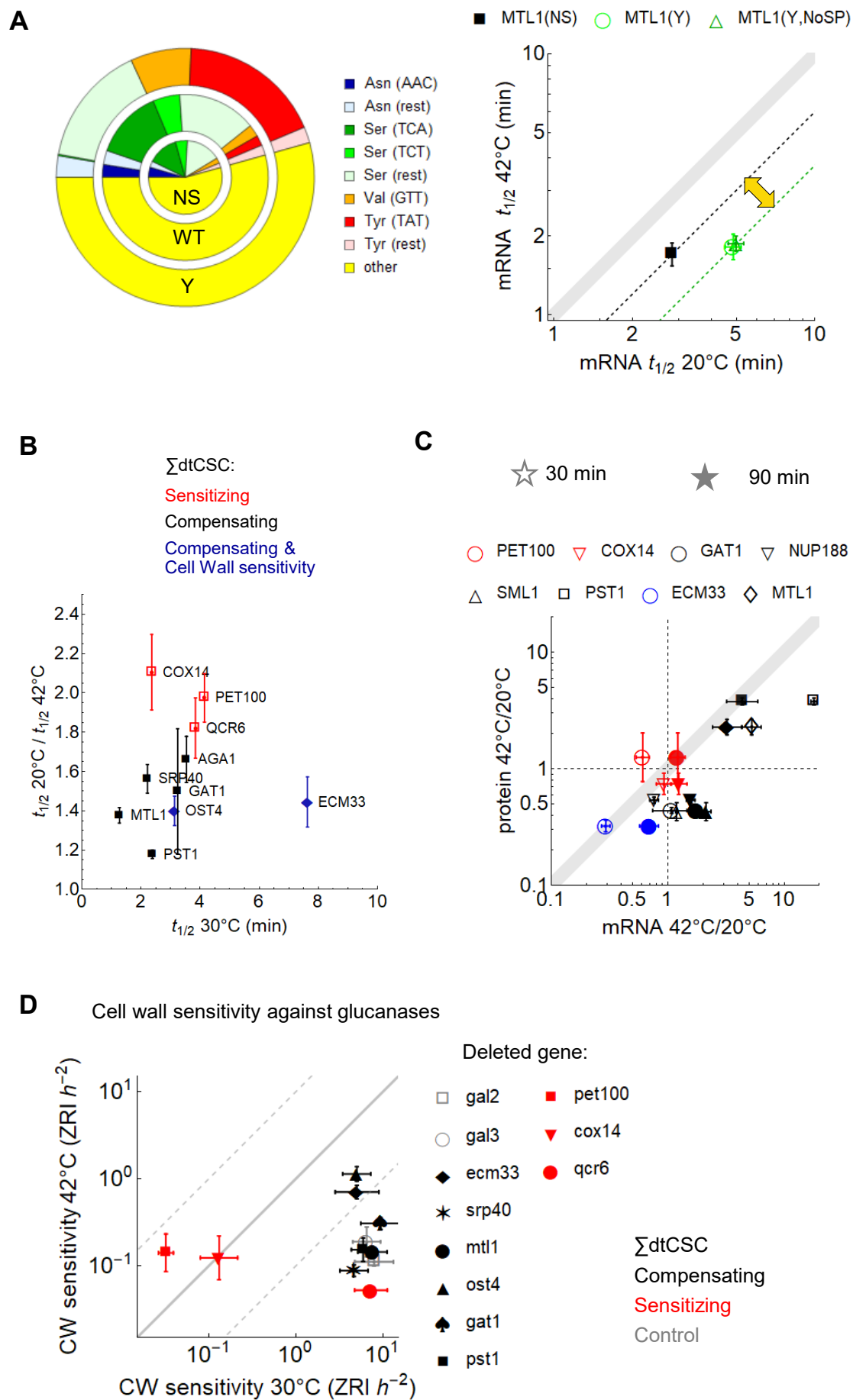


**Fig. 6**

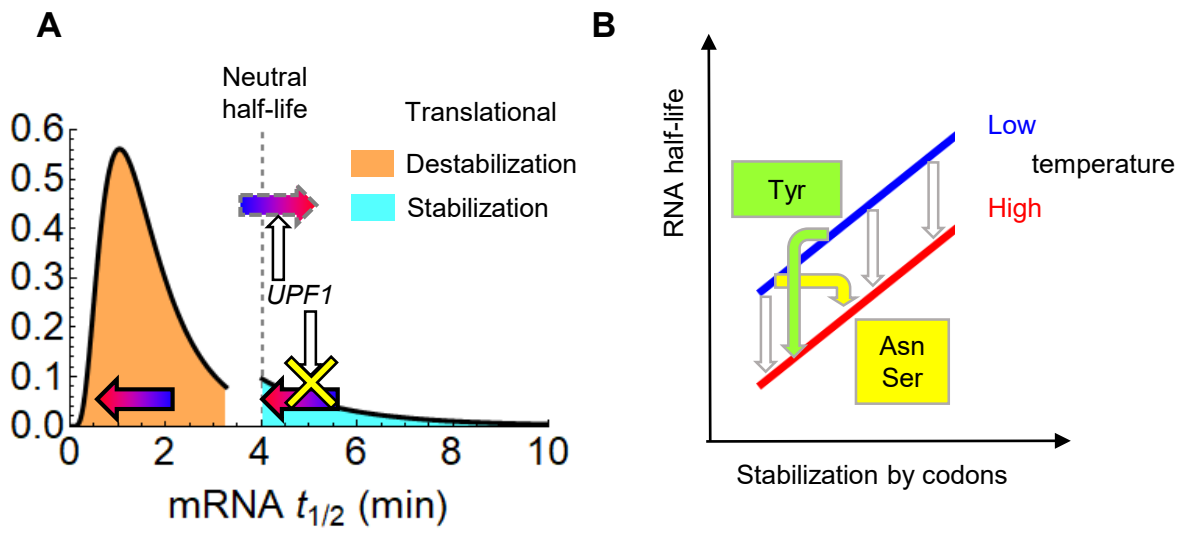


**Fig. 7**



# Determinants of the temperature adaptation of mRNA degradation

Vincent Jaquet, Sandrine Wallerich, Sylvia Voegeli, Demeter Túrós, Eduardo Calero Vilorio and Attila Becskei

## Contents

Supplementary Texts .....	3
Supplementary Materials and Methods .....	3
Text S1. Measurement of in vitro Xrn1 activity.....	3
Text S2. Calculation of the significance of difference between the dtCSCs of two codons .....	3
Supplementary Figures.....	4
Figure S1. The in vitro decay of 18S rRNA at different temperatures upon the addition of the Xrn1 protein to total RNA. ....	4
Figure S2. Cellular growth upon heat shock. ....	5
Figure S3. Negative controls for smFISH imaging. ....	6
Figure S4. The design of the primers for the detection of decapped mRNA. ....	7
Figure S5. The most stabilizing and destabilizing codons. ....	8
Figure S6. Calculation of dtCSC and its variants.....	9
Figure S7. Codon composition of the synthetic genes encoding 100 amino acids.....	10
Figure S8. Example of the degradation of the cell wall with zymolyase. ....	11
Supplementary Tables .....	12
Table S1. Plasmid list.....	12
Table S2. Strain list. ....	18
Table S3. qPCR primers. ....	23
Table S4. Oligos used in the splinted ligation reverse transcription polymerase chain reaction (SLqPCR) assay. ....	31
Table S5. Sequences of smFISH probes binding TSL1 (5' to 3').....	32
Table S6. Significance of difference between dtCSC values. ....	33
Table S7. Significance of difference between dtCSC values of synonymous codons. ....	34
Supplementary Data .....	35
Data S1. Half-lives of mRNAs.....	35
Data S2. Mass-spectrometry measurements.....	35
Data S3. Enrichment of codons in P-body components. ....	35

Supplementary References .....	35
--------------------------------	----

## Supplementary Texts

### Supplementary Materials and Methods

#### **Text S1. Measurement of in vitro Xrn1 activity**

The in vitro RNA degradation was initiated by adding Xrn1 (New England Biolabs) to a final concentration of 40 Units/ml to a 5 mM MgCl<sub>2</sub>, 50 mM KCl, 0.5 mM dithiothreitol and 25 mM Tris-HCl (pH = 7.9) solution containing total RNA (60 µg/ml) at a temperature corresponding to the reaction temperature (20, 30 or 42°C). The reaction was incubated further at the same temperature in a thermo-shaker (ThermoMixer, Eppendorf). At the indicated time points, 5 µl samples were removed from the reaction and transferred to 95 µl ice-cold water, to which 350 µl RLT solution (Qiagen) was added in order to stop the reaction. The Xrn1 was removed with the subsequent application of the RNA Cleanup kit (Qiagen, RNeasy MinElute), which contains the chaotropic denaturant guanidine-isothiocyanate. The purified RNA was quantitated by RT-qPCR as described above. The amount of the 18S rRNA was normalized by the geometric mean of the UBC6 and TFC1.

#### **Text S2. Calculation of the significance of difference between the dtCSCs of two codons**

For the comparison of the dtCSCs of two codons, we used the test for the difference between two dependent correlations with one variable in common (1), which is the codon frequency.

Thus, the two correlations (dtCSC) are corrected by the correlation between the frequencies of the two relevant codons in the mRNAs. We used a stringent significance level ( $\alpha = 0.01$ ) because the applied test is parametric and elsewhere we use non-parametric tests. For example, the dtCSC(AAC, Asn) defined as the parametric Pearson correlation coefficient yields  $\rho = -0.34$  (P-value = 0.00069), whereas the corresponding nonparametric Spearman rank correlation  $r_s = -0.29$  (P-value = 0.0038). This approximately 5fold change in the P-value is the largest of all codons.

The P-values (two-tailed) were calculated at Lee, I. A., & Preacher, K. J. (2013, September, <http://quantpsy.org/corrttest/corrttest2.htm>) based on (1).

## Supplementary Figures

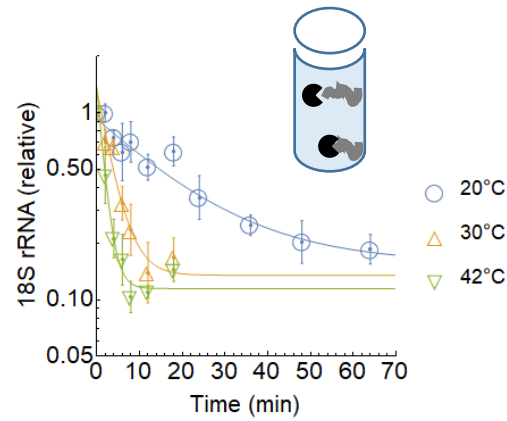


**Figure S1. The in vitro decay of 18S rRNA at different temperatures upon the addition of the Xrn1 protein to total RNA.**

The 18S rRNA amount is normalized to the *TFC1* and *UBC6* mRNAs; the means and standard errors are shown from  $n = 4$  independent experiments. The following half-lives were fitted:  $t_{1/2}$  (20°C) = 12.4,  $t_{1/2}$  (30°C) = 2.2 and  $t_{1/2}$  (42°C) = 1.1 min.

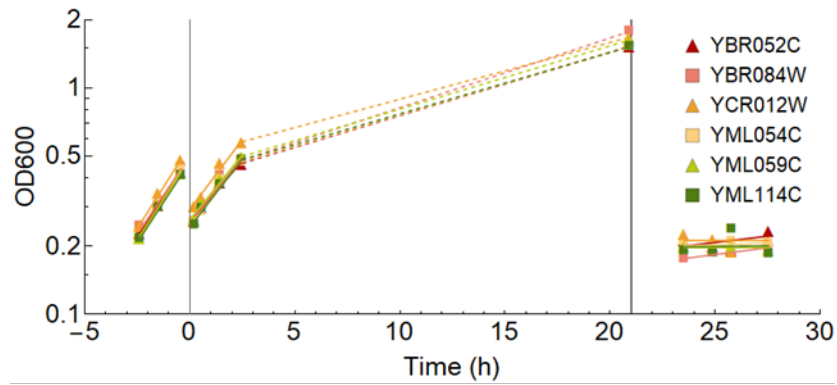


**Figure S2. Cellular growth upon heat shock.**

The growth of cells expressing the genes indicated in the legend under the control of TET promoters. The cells were pre-grown at 30°C until time 0 (left vertical line). The cells were then pelleted and re-suspended in a 42°C medium and cellular growth was monitored. After the overnight growth (dashed lines), the cells were refreshed again (second vertical bar). The following doubling times were fitted (mean  $\pm$  standard deviation calculated from the six strains):  $2.09 \pm 0.03$  at 30°C;  $2.60 \pm 0.06$  at 42°C after the temperature shift. After the overnight growth at 42°C, the cell doubling was very slow ( $>10^2$  h).

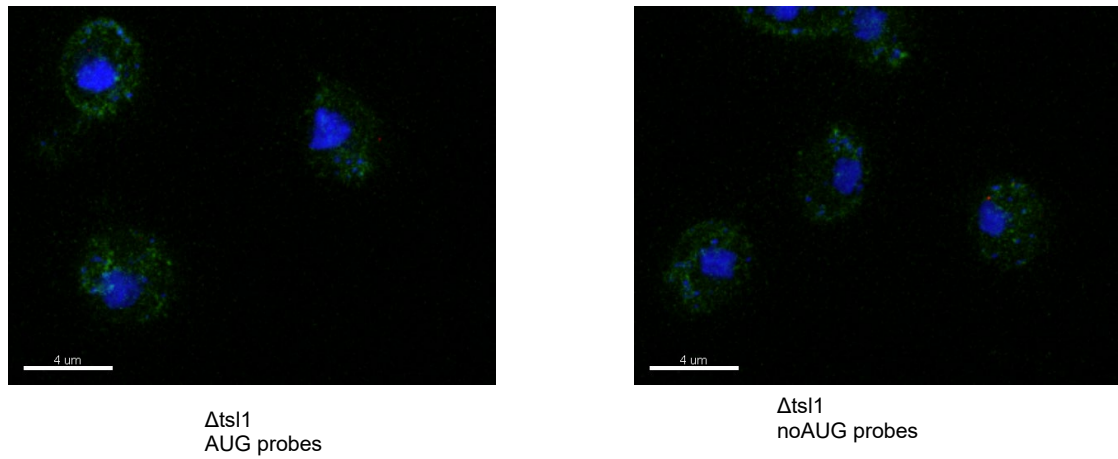


**Figure S3. Negative controls for smFISH imaging.**

Cells lacking *TSL1* gene ( $\Delta ts11$ ) were used as negative controls. Probes for the *TSL1* and no-AUG *TSL1* mRNAs were used for hybridization.

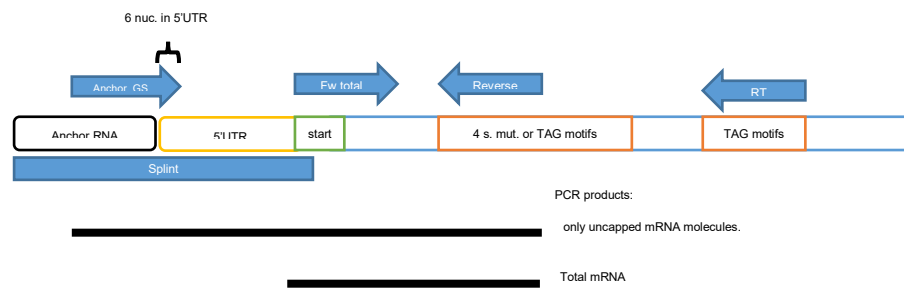


**Figure S4. The design of the primers for the detection of decapped mRNA.**

The forward anchor primer extends to beyond the anchor RNA and overlaps with the 5'UTR. See Materials and Methods for details of the modified SL-RT-qPCR.

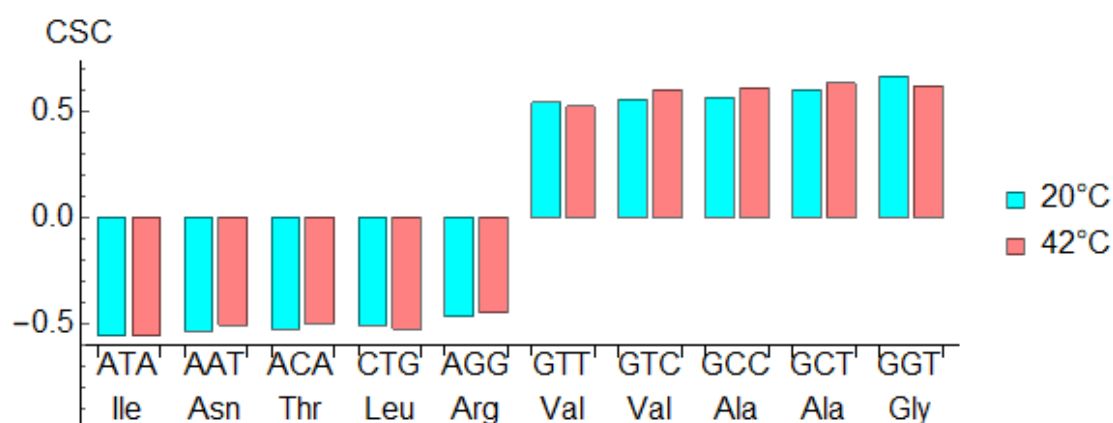


**Figure S5. The most stabilizing and destabilizing codons.**

The CSCs (defined with the Person correlation) were calculated from the mRNA half-lives of the representative mRNA set. The 5 most stabilizing and destabilizing codons at 20°C are shown. The CSC were calculated for these codons also from the 42°C dataset.



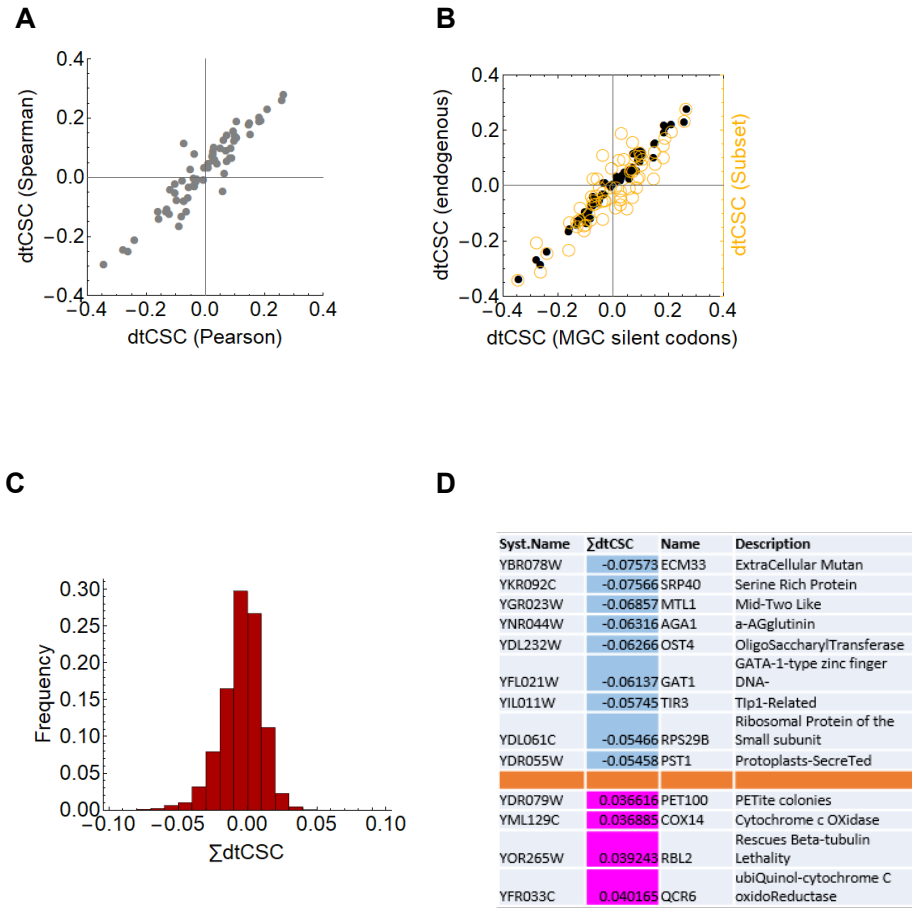


**Figure S6. Calculation of dtCSC and its variants.**

(A) The relation between dtCSC and the dtCSC (Spearman) for each codon. The latter is calculated in the same way as the dtCSC but the Spearman rank correlation coefficient was used instead of the Pearson correlation coefficient.

(B) Values of dtCSC calculated using the codon frequencies of the endogenous (WT) genes and those of the multiplexed gene control (MGC) genes including the synonymous codons (black filled circles). They are highly correlated (Spearman rank correlation coefficient = 0.99). The right axis shows the dtCSC that was used to obtain the extreme values of  $\Sigma dtCSC$ . The dtCSC calculated based on a smaller subset of genes missing the YBR025C, YCR012W, YGR159C, YIL162W, YKL109W, YLR367W, YML053C, YML068W, YML078W, YML094W, YML098W, YML108W, YPL081W, YPR008W genes from the list of 95 genes (yellow empty circles).

(C) The distribution of the  $\Sigma dtCSC$  values calculated for all genes in the yeast genome.

(D) The list of genes with greatest and least  $\Sigma dtCSC$  values using the dtCSC values shown in (B).

AA	codon	SN-	SN-	Control
Asn	AAC	23	22	0
Ser	TCC	18	18	0
Ser	TCA	13	13	0
Cys	TGC	11	11	0
Ser	TCT	10	10	0
Arg	CGC	6	6	0
Leu	TTG	5	5	0
Leu	CTC	5	4	0
Phe	TTC	4	4	0
Met	ATG	2	1	1
Ser	AGC	2	2	0
STOP	TAA	1	1	1
Asp	GAC	1	1	0
Gly	GGT	0	0	20
Tyr	TAT	0	0	15
Glu	GAA	0	0	15
Leu	CTT	0	0	11
Val	GTA	0	0	7
Gly	GGG	0	0	7
Gly	GGC	0	0	5
Ala	GCA	0	0	5
Lys	AAG	0	0	4
Gly	GGA	0	0	4
Phe	TTT	0	0	2
Asp	GAT	0	0	1
Leu	TTA	0	0	1
Leu	CTG	0	0	1
Thr	ACG	0	0	1

**Figure S7. Codon composition of the synthetic genes encoding 100 amino acids.**  
The two Ser/Asn rich gene variants and the control genes are shown.

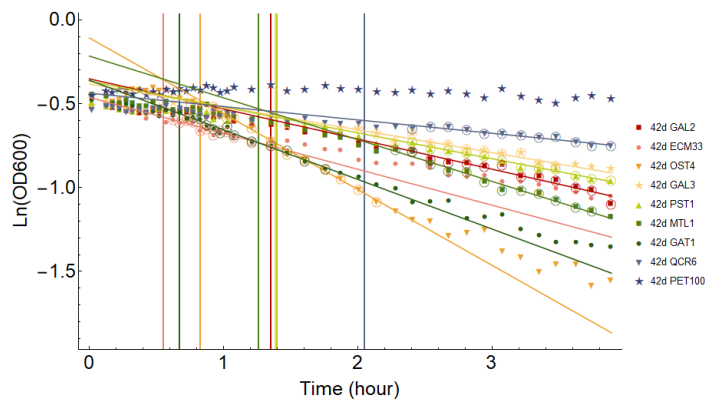


**Figure S8. Example of the degradation of the cell wall with zymolyase.**

The vertical lines denote the lag time (LT). The circles around the symbols indicate the time points that were used to determine the maximal lysis rate (MLR). The indicated genes are deleted in the respective strains.

## Supplementary Tables

**Table S1. Plasmid list.**

The lengths of sequences upstream (and downstream) of the coding regions that include the 5' (and 3') UTR.

Plasmid number	Systematic name	Plasmid description	5' UT R (bp)	3' UT R (bp)
pSV597	16 aa SN-rich C3	pRS303-ApaI-Fig1-XhoI-Tgal7-AvrII-[tetO2]4inPgal1-SphI-5'UTR NUP188_16 aa SN-rich C3_3'UTR+100bp NUP188_XmaI-Ter-NotI	100	149
pSV598	16 aa SN-rich C4	pRS303-ApaI-Fig1-XhoI-Tgal7-AvrII-[tetO2]4inPgal1-SphI-5'UTR NUP188_16 aa SN-rich C4_3'UTR+100bp NUP188_XmaI-Ter-NotI	100	149
pSV601	16 aa control	pRS303-ApaI-Fig1-XhoI-Tgal7-AvrII-[tetO2]4inPgal1-SphI-5'UTR NUP188_16 aa control_3'UTR+100bp NUP188_XmaI-Ter-NotI	100	149
pSV606	100 aa SN-rich 1	pRS303-ApaI-Fig1-XhoI-Tgal7-AvrII-[tetO2]4inPgal1-SphI_noATG_YBR066C_5'UTR_BamHI-100 aa SN-rich 1-KasI_3'UTR_XmaI-Ter-MluI-mut-NotI	180	205
pSV607	100 aa SN-rich 2	pRS303-ApaI-Fig1-XhoI-Tgal7-AvrII-[tetO2]4inPgal1-SphI_noATG_YBR066C_5'UTR_BamHI-100 aa SN-rich 2-KasI_3'UTR_XmaI-Ter-MluI-mut-NotI	180	205
pSV608	100 aa control	pRS303-ApaI-Fig1-XhoI-Tgal7-AvrII-[tetO2]4inPgal1-SphI_noATG_YBR066C_5'UTR_BamHI-100 aa control-KasI_3'UTR_XmaI-Ter-MluI-mut-NotI	180	205
pSV609	100 aa SN-rich 1	pRS303-ApaI-Fig1-XhoI-Tgal7-AvrII-[tetO2]4inPgal1-SphI_noATG_YJL190C_5'UTR_BamHI-100 aa SN-rich 1-KasI_3'UTR_XmaI-Ter-MluI-mut-NotI	100	289
pSV610	100 aa SN-rich 2	pRS303-ApaI-Fig1-XhoI-Tgal7-AvrII-[tetO2]4inPgal1-SphI_noATG_YJL190C_5'UTR_BamHI-100 aa SN-rich 2-KasI_3'UTR_XmaI-Ter-MluI-mut-NotI	100	289
pSV611	100 aa control	pRS303-ApaI-Fig1-XhoI-Tgal7-AvrII-[tetO2]4inPgal1-SphI_noATG_YJL190C_5'UTR_BamHI-100 aa control-KasI_3'UTR_XmaI-Ter-MluI-mut-NotI	100	289
pSYN010_pBM01	YBR025C	pRS303-ApaI-Fig1-XhoI-Tgal7-AvrII-[tetO2]4inPgal1-SphI-5'UTR_YBR025C_woATG_3'UTR+100bp_XmaI-Ter-NotI	133	332
pSV437	YBR048W	pRS303-ApaI-Fig1-XhoI-Tgal7-AvrII-[tetO2]4inPgal1-SphI-5'UTR_YBR048W_4silmut_3'UTR+100bp_XmaI-Ter-NotI	100	343
pSYN012_pBM03	YBR052C	pRS303-ApaI-Fig1-XhoI-Tgal7-AvrII-[tetO2]4inPgal1-SphI-5'UTR_YBR052C_woATG_3'UTR+100bp_XmaI-Ter-NotI	100	165
pCP002	YBR066C	pRS306-KpnI-Fig1-XhoI-Tgal7-AvrII-[tetO2]4inPgal1-BglII-5'UTR_YBR066C_4silmut_RS_BamHI-EcoRI-Ter-NotI	142	

pSYN01 3_pBM 04	YBR066C	pRS303-ApaI-Fig1-XhoI-Tgal7-AvrII-[tetO2]4inPgal1-SphI-5'UTR_YBR066C_woATG_3'UTR+100bp_XmaI-Ter-NotI	180	205
pSV308	YBR074W	pRS306-KpnI-Fig1-XhoI-Tgal7-AvrII-[tetO2]4inPgal1-BglII-5'UTR_YBR074W_4silmut_RS_BamHI-SphI-Ter-NotI	100	
pSV629	YBR078W	pRS303-ApaI-Fig1-XhoI-Tgal7-AvrII-[tetO2]4inPgal1-SphI-5'UTR_YBR078W_plus3stopcodons_3'UTR+100bp_XmaI-Ter-NotI	163	141
pSV390	YBR221C	pRS306-KpnI-Fig1-XhoI-Tgal7-AvrII-[tetO2]4inPgal1-BglII-5'UTR_YBR221C_4silmut_RS_SpeI-EcoRI-Ter-NotI	232	
pSYN04 0_pGB0 1	YBR221C	pRS303-ApaI-Fig1-XhoI-Tgal7-AvrII-[tetO2]4inPgal1-SphI_5'UTR_YBR221C_woATG_wSM_3'UTR+100bp_XmaI-Ter-NotI	232	340
pSV392	YCL009C	pRS306-KpnI-Fig1-XhoI-Tgal7-AvrII-[tetO2]4inPgal1-BglII-5'UTR_YCL009C_4silmut_RS_SpeI-EcoRI-Ter-NotI	100	
pSYN04 1_pGB0 2	YCL009C	pRS303-ApaI-Fig1-XhoI-Tgal7-AvrII-[tetO2]4inPgal1-SphI_5'UTR_YCL009C_woATG_wSM_3'UTR+100bp_XmaI-Ter-NotI	100	254
pSYN04 2_pGB0 3	YCR012W	pRS303-ApaI-Fig1-XhoI-Tgal7-AvrII-[tetO2]4inPgal1-SphI_5'UTR_YCR012W_woATG_wSM_3'UTR+100bp_XmaI-Ter-NotI	100	258
pSV636	YDL232W	pRS303-ApaI-Fig1-XhoI-Tgal7-AvrII-[tetO2]4inPgal1-SphI-5'UTR_YDL232W_plus2stopcodons_3'UTR+100bp_XmaI-Ter-NotI	100	388
pSV443	YDR025W	pRS303-ApaI-Fig1-XhoI-Tgal7-AvrII-[tetO2]4inPgal1-SphI-5'UTR_YDR025W_4silmut_3'UTR+100bp_XmaI-Ter-NotI	100	204
pSV304	YDR032C	pRS306-KpnI-Fig1-XhoI-Tgal7-AvrII-[tetO2]4inPgal1-BamHI-5'UTR_YDR032C_4silmut_RS_SpeI-SphI-Ter-NotI	100	
pSYN04 3_pGB0 4	YDR032C	pRS303-ApaI-Fig1-XhoI-Tgal7-AvrII-[tetO2]4inPgal1-SphI_5'UTR_YDR032C_woATG_wSM_3'UTR+100bp_XmaI-Ter-NotI	100	293
pSV642	YDR055W	pRS303-ApaI-Fig1-XhoI-Tgal7-AvrII-[tetO2]4inPgal1-SphI-5'UTR_YDR055W_plus2stopcodons_3'UTR+100bp_XmaI-Ter-NotI	100	227
pSV638	YDR079W	pRS303-ApaI-Fig1-XhoI-Tgal7-AvrII-[tetO2]4inPgal1-SphI-5'UTR_YDR079W_plus2stopcodons_3'UTR+100bp_XmaI-Ter-NotI	100	311
pSV386	YER057C	pRS303-ApaI-Fig1-XhoI-Tgal7-AvrII-[tetO2]4inPgal1-SphI-5'UTR_YER057C_4silmut_3'UTR+100bp_XmaI-Ter-NotI	100	201
pSYN04 4_pGB0 5	YER057C	pRS303-ApaI-Fig1-XhoI-Tgal7-AvrII-[tetO2]4inPgal1-SphI_5'UTR_YER057C_woATG_wSM_3'UTR+100bp_XmaI-Ter-NotI	100	201
pSV637	YFL021W	pRS303-ApaI-Fig1-XhoI-Tgal7-AvrII-[tetO2]4inPgal1-SphI-5'UTR_YFL021W_plus2stopcodons_3'UTR+100bp_XmaI-Ter-NotI	100	107
pSV641	YFR033C	pRS303-ApaI-Fig1-XhoI-Tgal7-AvrII-[tetO2]4inPgal1-SphI-5'UTR_YFR033C_plus2stopcodons_3'UTR+100bp_XmaI-Ter-NotI	106	241
pSV633	YGR023W	pRS303-ApaI-Fig1-XhoI-Tgal7-AvrII-[tetO2]4inPgal1-SphI-5'UTR_YGR023W_plus2stopcodons_3'UTR+100bp_XmaI-Ter-NotI	152	399
pSV466	YGR159C	pRS303-ApaI-Fig1-XhoI-Tgal7-AvrII-[tetO2]4inPgal1-SphI-5'UTR_YGR159C_4silmut_3'UTR+100bp_XmaI-Ter-NotI	100	250

pSV399	YIL043C	pRS306-KpnI-Fig1-XhoI-Tgal7-AvrII-[tetO2]4inPgal1-BglII-5'UTR_YIL043C_4silmut_RS_SpeI-EcoRI-Ter-NotI	100	
pSYN04 5_pGB0 6	YIL043C	pRS303-ApaI-Fig1-XhoI-Tgal7-AvrII-[tetO2]4inPgal1-SphI_5'UTR_YIL043C_woATG_wSM_3'UTR+100bp_XmaI-Ter-NotI	100	222
pSV445	YIL133C	pRS303-ApaI-Fig1-XhoI-Tgal7-AvrII-[tetO2]4inPgal1-SphI-5'UTR_YIL133C_4silmut_3'UTR+100bp_XmaI-Ter-NotI	100	263
pSV438	YJL190C	pRS303-ApaI-Fig1-XhoI-Tgal7-AvrII-[tetO2]4inPgal1-SphI-5'UTR_YJL190C_4silmut_3'UTR+100bp_XmaI-Ter-NotI	100	289
pSYN01 4_pBM 05	YJL190C	pRS303-ApaI-Fig1-XhoI-Tgal7-AvrII-[tetO2]4inPgal1-SphI-5'UTR_YJL190C_woATG_3'UTR+100bp_XmaI-Ter-NotI	100	289
pSYN04 6_pGB0 7	YJL190C	pRS303-ApaI-Fig1-XhoI-Tgal7-AvrII-[tetO2]4inPgal1-SphI_5'UTR_YJL190C_woATG_wSM_3'UTR+100bp_XmaI-Ter-NotI	100	289
pSV303	YJR139C	pRS306-KpnI-Fig1-XhoI-Tgal7-AvrII-[tetO2]4inPgal1-BglII-5'UTR_YJR139C_4silmut_RS_BamHI-EcoRI-Ter-NotI	100	
pSYN04 7_pGB0 8	YJR139C	pRS303-ApaI-Fig1-XhoI-Tgal7-AvrII-[tetO2]4inPgal1-SphI_5'UTR_YJR139C_woATG_wSM_3'UTR+100bp_XmaI-Ter-NotI	112	198
pSV420	YKL109W	pRS306-KpnI-Fig1-XhoI-Tgal7-AvrII-[tetO2]4inPgal1-BamHI-5'UTR_YKL109W_4silmut_RS_SpeI-SphI-Ter-NotI	281	
pSV630	YKR092C	pRS303-ApaI-Fig1-XhoI-Tgal7-AvrII-[tetO2]4inPgal1-SphI-5'UTR_YKR092C_plus3stopcodons_3'UTR+100bp_XmaI-Ter-NotI	100	347
pSV421	YLR094C	pRS306-KpnI-Fig1-XhoI-Tgal7-AvrII-[tetO2]4inPgal1-BglII-5'UTR_YLR094C_4silmut_RS_SphI-EcoRI-Ter-NotI	100	
pSYN01 5_pBM 06	YLR094C	pRS303-ApaI-Fig1-XhoI-Tgal7-AvrII-[tetO2]4inPgal1-SphI-5'UTR_YLR094C_woATG_3'UTR+100bp_XmaI-Ter-NotI	100	219
pSYN04 8_pGB0 9	YLR094C	pRS303-ApaI-Fig1-XhoI-Tgal7-AvrII-[tetO2]4inPgal1-SphI_5'UTR_YLR094C_woATG_wSM_3'UTR+100bp_XmaI-Ter-NotI	100	219
pSV444	YLR367W	pRS303-ApaI-Fig1-XhoI-Tgal7-AvrII-[tetO2]4inPgal1-SphI-5'UTR_YLR367W_4silmut_3'UTR+100bp_XmaI-Ter-NotI	664	171
pSV355	YML030W	pRS303-ApaI-Fig1-XhoI-Tgal7-AvrII-[tetO2]4inPgal1-SphI-5'UTR_YML030W_4silmut_3'UTR+100bp_XmaI-Ter-NotI	100	313
pSV357	YML036W	pRS303-ApaI-Fig1-XhoI-Tgal7-AvrII-[tetO2]4inPgal1-SphI-5'UTR_YML036W_4silmut_3'UTR+100bp_XmaI-Ter-NotI	100	350
pSV309	YML038C	pRS306-KpnI-Fig1-XhoI-Tgal7-AvrII-[tetO2]4inPgal1-BglII-5'UTR_YML038C_4silmut_RS_SpeI-EcoRI-Ter-NotI	169	
pSV314	YML042W	pRS306-KpnI-Fig1-XhoI-Tgal7-AvrII-[tetO2]4inPgal1-BglII-5'UTR_YML042W_4silmut_RS_SpeI-EcoRI-Ter-NotI	100	
pSYN01 6_pBM 07	YML043C	pRS303-ApaI-Fig1-XhoI-Tgal7-AvrII-[tetO2]4inPgal1-SphI-5'UTR_YML043C_woATG_3'UTR+100bp_XmaI-Ter-NotI	164	262
pSYN01 7_pBM 08	YML051W	pRS303-ApaI-Fig1-XhoI-Tgal7-AvrII-[tetO2]4inPgal1-SphI-5'UTR_YML051W_woATG_3'UTR+100bp_XmaI-Ter-NotI	100	243
pSV315	YML052W	pRS306-KpnI-Fig1-XhoI-Tgal7-AvrII-[tetO2]4inPgal1-BglII-5'UTR_YML052W_4silmut_RS_SpeI-EcoRI-Ter-NotI	100	
pSV316	YML053C	pRS306-KpnI-Fig1-XhoI-Tgal7-AvrII-[tetO2]4inPgal1-BglII-5'UTR_YML053C_4silmut_RS_SpeI-EcoRI-Ter-NotI	100	

pSV358	YML055W	pRS303-ApaI-Fig1-XhoI-Tgal7-AvrII-[tetO2]4inPgal1-SphI-5'UTR_YML055W_4silmut_3'UTR+100bp_XmaI-Ter-NotI	100	145
pSV359	YML056C	pRS303-ApaI-Fig1-XhoI-Tgal7-AvrII-[tetO2]4inPgal1-SphI-5'UTR_YML056C_4silmut_3'UTR+100bp_XmaI-Ter-NotI	100	151
pSV360	YML058W	pRS303-ApaI-Fig1-XhoI-Tgal7-AvrII-[tetO2]4inPgal1-SphI-5'UTR_YML058W_4silmut_3'UTR+100bp_XmaI-Ter-NotI	100	341
pSYN049_pGB10	YML062C	pRS303-ApaI-Fig1-XhoI-Tgal7-AvrII-[tetO2]4inPgal1-SphI_5'UTR_YML062C_woATG_wSM_3'UTR+100bp_XmaI-Ter-NotI	100	235
pSV317	YML064C	pRS306-KpnI-Fig1-XhoI-Tgal7-AvrII-[tetO2]4inPgal1-BamHI-5'UTR_YML064C_4silmut_RS_SpeI-SphI-Ter-NotI	100	
pSYN019_pBM10	YML064C	pRS303-ApaI-Fig1-XhoI-Tgal7-AvrII-[tetO2]4inPgal1-SphI-5'UTR_YML064C_woATG_3'UTR+100bp_XmaI-Ter-NotI	108	378
pSV318	YML068W	pRS306-KpnI-Fig1-XhoI-Tgal7-AvrII-[tetO2]4inPgal1-BamHI-5'UTR_YML068W_4silmut_RS_SpeI-SphI-Ter-NotI	100	
pSV319	YML069W	pRS306-KpnI-Fig1-XhoI-Tgal7-AvrII-[tetO2]4inPgal1-BamHI-5'UTR_YML069W_4silmut_RS_SpeI-SphI-Ter-NotI	100	
pSYN020_pBM11	YML070W	pRS303-ApaI-Fig1-XhoI-Tgal7-AvrII-[tetO2]4inPgal1-SphI-5'UTR_YML070W_woATG_3'UTR+100bp_XmaI-Ter-NotI	108	170
pSV320	YML074C	pRS306-KpnI-Fig1-XhoI-Tgal7-AvrII-[tetO2]4inPgal1-BamHI-5'UTR_YML074C_4silmut_RS_SpeI-SphI-Ter-NotI	100	
pSYN021_pBM12	YML074C	pRS303-ApaI-Fig1-XhoI-Tgal7-AvrII-[tetO2]4inPgal1-SphI-5'UTR_YML074C_woATG_3'UTR+100bp_XmaI-Ter-NotI	100	201
pSV362	YML078W	pRS303-ApaI-Fig1-XhoI-Tgal7-AvrII-[tetO2]4inPgal1-SphI-5'UTR_YML078W_4silmut_3'UTR+100bp_XmaI-Ter-NotI	100	250
pSV321	YML079W	pRS306-KpnI-Fig1-XhoI-Tgal7-AvrII-[tetO2]4inPgal1-BamHI-5'UTR_YML079W_4silmut_RS_SpeI-SphI-Ter-NotI	100	
pSV322	YML082W	pRS306-KpnI-Fig1-XhoI-Tgal7-AvrII-[tetO2]4inPgal1-BglIII-5'UTR_YML082W_4silmut_RS_SpeI-EcoRI-Ter-NotI	100	
pSYN050_pGB11	YML082W	pRS303-ApaI-Fig1-XhoI-Tgal7-AvrII-[tetO2]4inPgal1-SphI_5'UTR_YML082W_woATG_wSM_3'UTR+100bp_XmaI-Ter-NotI	120	248
pSV323	YML092C	pRS306-KpnI-Fig1-XhoI-Tgal7-AvrII-[tetO2]4inPgal1-BglIII-5'UTR_YML092C_4silmut_RS_SphI-EcoRI-Ter-NotI	100	
pSV363	YML094W	pRS303-ApaI-Fig1-XhoI-Tgal7-AvrII-[tetO2]4inPgal1-SphI-5'UTR_YML094W_4silmut_3'UTR+100bp_XmaI-Ter-NotI	100	196
pSV324	YML095C	pRS306-KpnI-Fig1-XhoI-Tgal7-AvrII-[tetO2]4inPgal1-BglIII-5'UTR_YML095C_4silmut_RS_SpeI-EcoRI-Ter-NotI	100	
pSYN022_pBM13	YML095C	pRS303-ApaI-Fig1-XhoI-Tgal7-AvrII-[tetO2]4inPgal1-SphI-5'UTR_YML095C_woATG_3'UTR+100bp_XmaI-Ter-NotI	100	799
pSV364	YML098W	pRS303-ApaI-Fig1-XhoI-Tgal7-AvrII-[tetO2]4inPgal1-SphI-5'UTR_YML098W_4silmut_3'UTR+100bp_XmaI-Ter-NotI	100	280
pSV644	YML100W	pRS303-ApaI-Fig1-XhoI-Tgal7-AvrII-[tetO2]4inPgal1-SphI-TSL1_scrambled_noATG_SpeI_XbaI_XmaI-Ter-NotI	100	223
pSV365	YML101C	pRS303-ApaI-Fig1-XhoI-Tgal7-AvrII-[tetO2]4inPgal1-SphI-5'UTR_YML101C_4silmut_3'UTR+100bp_XmaI-Ter-NotI	101	156
pSV325	YML104C	pRS306-KpnI-Fig1-XhoI-Tgal7-AvrII-[tetO2]4inPgal1-BglIII-5'UTR_YML104C_4silmut_RS_SpeI-EcoRI-Ter-NotI	100	
pSYN023_pBM14	YML107C	pRS303-ApaI-Fig1-XhoI-Tgal7-AvrII-[tetO2]4inPgal1-SphI-5'UTR_YML107C_woATG_3'UTR+100bp_XmaI-Ter-NotI	100	148

pSV367	YML108W	pRS303-ApaI-Fig1-XhoI-Tgal7-AvrII-[tetO2]4inPgal1-SphI-5'UTR_YML108W_4silmut_3'UTR+100bp_XmaI-Ter-NotI	100	301
pSV328	YML109W	pRS306-KpnI-Fig1-XhoI-Tgal7-AvrII-[tetO2]4inPgal1-BamHI-5'UTR_YML109W_4silmut_RS_SpeI-SphI-Ter-NotI	100	
pSV330	YML111W	pRS306-KpnI-Fig1-XhoI-Tgal7-AvrII-[tetO2]4inPgal1-BamHI-5'UTR_YML111W_4silmut_RS_SpeI-SphI-Ter-NotI	177	
pSV331	YML112W	pRS306-KpnI-Fig1-XhoI-Tgal7-AvrII-[tetO2]4inPgal1-BamHI-5'UTR_YML112W_4silmut_RS_BglII-SphI-Ter-NotI	306	
pSV332	YML113W	pRS306-KpnI-Fig1-XhoI-Tgal7-AvrII-[tetO2]4inPgal1-BglII-5'UTR_YML113W_4silmut_RS_SphI-EcoRI-Ter-NotI	100	
pSYN02 4_pBM 15	YML113W	pRS303-ApaI-Fig1-XhoI-Tgal7-AvrII-[tetO2]4inPgal1-SphI-5'UTR_YML113W_woATG_3'UTR+100bp_XmaI-Ter-NotI	100	244
pSYN05 2_pGB1 3	YML116W	pRS303-ApaI-Fig1-XhoI-Tgal7-AvrII-[tetO2]4inPgal1-SphI_5'UTR_YML116W_woATG_wSM_3'UTR+100bp_XmaI-Ter-NotI	112	253
pSV369	YML129C	pRS303-ApaI-Fig1-XhoI-Tgal7-AvrII-[tetO2]4inPgal1-SphI-5'UTR_YML129C_4silmut_3'UTR+100bp_XmaI-Ter-NotI	100	270
pSV639	YML129C	pRS303-ApaI-Fig1-XhoI-Tgal7-AvrII-[tetO2]4inPgal1-SphI-5'UTR_YML129C_plus2stopcodons_3'UTR+100bp_XmaI-Ter-NotI	100	296
pSV632	YMR173W	pRS303-ApaI-Fig1-XhoI-Tgal7-AvrII-[tetO2]4inPgal1-SphI-5'UTR_YMR173W_plus2stopcodons_3'UTR+100bp_XmaI-Ter-NotI	100	171
pSV521	YMR205C	pRS306-KpnI-Fig1-XhoI-Tgal7-AvrII-[tetO2]4inPgal1-BamHI-5'UTR_YMR205C_4silmut_RS_ClaI-SphI-Ter-NotI	100	
pSV423	YNR039C	pRS306-KpnI-Fig1-XhoI-Tgal7-AvrII-[tetO2]4inPgal1-BglII-5'UTR_YNR039C_4silmut_RS_SphI-EcoRI-Ter-NotI	100	
pSYN05 3_pGB1 4	YNR039C	pRS303-ApaI-Fig1-XhoI-Tgal7-AvrII-[tetO2]4inPgal1-SphI_5'UTR_YNR039C_woATG_wSM_3'UTR+100bp_XmaI-Ter-NotI	100	
pSV635	YNR044W	pRS303-ApaI-Fig1-XhoI-Tgal7-AvrII-[tetO2]4inPgal1-SphI-5'UTR_YNR044W_plus2stopcodons_3'UTR+100bp_XmaI-Ter-NotI	100	171
pSV403	YPL048W	pRS306-KpnI-Fig1-XhoI-Tgal7-AvrII-[tetO2]4inPgal1-BglII-5'UTR_YPL048W_4silmut_RS_SpeI-EcoRI-Ter-NotI	117	169
pSYN05 4_pGB1 5	YPL048W	pRS303-ApaI-Fig1-XhoI-Tgal7-AvrII-[tetO2]4inPgal1-SphI_5'UTR_YPL048W_woATG_wSM_3'UTR+100bp_XmaI-Ter-NotI	100	
pSV467	YPL081W	pRS303-ApaI-Fig1-XhoI-Tgal7-AvrII-[tetO2]4inPgal1-SphI-5'UTR_YPL081W_4silmut_3'UTR+100bp_XmaI-Ter-NotI	120	245
pSV761	MTL1 asn-rich	pRS303-ApaI-Fig1-XhoI-Tgal7-AvrII-[tetO2]4inPgal1-SphI-MTL1 asn-rich-XmaI-Ter-NotI	152	399
pSV762	MTL1 tyr-rich	pRS303-ApaI-Fig1-XhoI-Tgal7-AvrII-[tetO2]4inPgal1-SphI-MTL1 tyr-rich-XmaI-Ter-NotI	152	399
pSV763	MTL1 tyr-rich No SP	pRS303-ApaI-Fig1-XhoI-Tgal7-AvrII-[tetO2]4inPgal1-SphI-MTL1 tyr-rich No Signal Peptide-XmaI-Ter-NotI	152	399
pSV647	[AUG-[AAC(Asn)]15-STOP]inYML103C_UTR	pRS303-ApaI-Fig1-XhoI-Tgal7-AvrII-[tetO2]4inPgal1-SphI-5'UTR_YML103C_Asn-15AA_3'UTR+100bp_YML103C_XmaI-Ter-NotI	100	149



pSV648	[AUG- [TCC(Ser)] 15- STOP]inY ML103C_ UTR	pRS303-ApaI-Fig1-XhoI-Tgal7-AvrII-[tetO2]4inPgal1-SphI- 5'UTR YML103C_Ser1-15AA_3'UTR+100bp YML103C_XmaI-Ter-NotI	100	149
pSV649	[AUG- [TCA(Ser)] 15- STOP]inY ML103C_ UTR	pRS303-ApaI-Fig1-XhoI-Tgal7-AvrII-[tetO2]4inPgal1-SphI- 5'UTR YML103C_Ser2-15AA_3'UTR+100bp YML103C_XmaI-Ter-NotI	100	149
pSV651	[AUG- [CTT(Leu)] 15- STOP]inY ML103C_ UTR	pRS303-ApaI-Fig1-XhoI-Tgal7-AvrII-[tetO2]4inPgal1-SphI- 5'UTR YML103C_Leu-15AA_3'UTR+100bp YML103C_XmaI-Ter-NotI	100	149
pSV652	[AUG- [TAT(Tyr)] 15- STOP]inY ML103C_ UTR	pRS303-ApaI-Fig1-XhoI-Tgal7-AvrII-[tetO2]4inPgal1-SphI- 5'UTR YML103C_Tyr-15AA_3'UTR+100bp YML103C_XmaI-Ter-NotI	100	149

**Table S2. Strain list.**

Strain number	Systematic name	silent mutati ons	ATG		Plasmid number	Marker
			WT (+) or noAT G (-)	Strain background		
YVJ616.1	16 aa SN-rich C3	-	+	BY4743*	pSV597	-LEU2, -HIS3
YVJ617.2	16 aa SN-rich C4	-	+	BY4743*	pSV598	-LEU2, -HIS3
YVJ620.1	16 aa control	-	+	BY4743*	pSV601	-LEU2, -HIS3
YVJ634.10	100 aa SN-rich 1	-	+	BY4743*	pSV606	-LEU2, -HIS3
YVJ635.10	100 aa SN-rich 2	-	+	BY4743*	pSV607	-LEU2, -HIS3
YVJ636.10	100 aa control	-	+	BY4743*	pSV608	-LEU2, -HIS3
YVJ637.4	100 aa SN-rich 1	-	+	BY4743*	pSV609	-LEU2, -HIS3
YVJ638.6	100 aa SN-rich 2	-	+	BY4743*	pSV610	-LEU2, -HIS3
YVJ639.3	100 aa control	-	+	BY4743*	pSV611	-LEU2, -HIS3
YVJ514.4	YBR025C	-	-	BY4743*	pSYN010_ pBM01	-LEU2, -HIS3
YMX356	YBR048W	+	+	BY4743*	pSV437	-LEU2, -HIS3
YVJ516.1	YBR052C	-	-	BY4743*	pSYN012_ pBM03	-LEU2, -HIS3
YVJ517.4	YBR066C	-	-	BY4743*	pSYN013_ pBM04	-LEU2, -HIS3
YMX185	YBR074W	+	+	BY4743*	pSV308	-LEU2, -URA3
YVJ649.2	YBR078W	-	+	BY4743*	pSV629	-LEU2, -HIS3
YMX290	YBR221C	+	+	BY4743*	pSV390	-LEU2, -URA3
YSW004.4	YBR221C	+	-	BY4743*	pSYN040_ pGB01	-LEU2, -HIS3
YMX312	YCL009C	+	+	BY4743*	pSV392	-LEU2, -URA3
YSW005.4	YCL009C	+	-	BY4743*	pSYN041_ pGB02	-LEU2, -HIS3
YSW006.3	YCR012W	+	-	BY4743*	pSYN042_ pGB03	-LEU2, -HIS3
YVJ651.5	YDL232W	-	+	BY4743*	pSV636	-LEU2, -HIS3
YMX362.1	YDR025W	+	+	BY4743*	pSV443	-LEU2, -HIS3
YMX189	YDR032C	+	+	BY4743*	pSV304	-LEU2, -URA3
YSW007.2	YDR032C	+	-	BY4743*	pSYN043_ pGB04	-LEU2, -HIS3
YSW034.13	YDR055W	-	+	BY4743*	pSV642	-LEU2, -HIS3
YVJ652.4	YDR079W	-	+	BY4743*	pSV638	-LEU2, -HIS3
YMX288	YER057C	+	+	BY4743*	pSV386	-LEU2, -HIS3
YSW008.3	YER057C	+	-	BY4743*	pSYN044_ pGB05	-LEU2, -HIS3
YVJ665.9	YFL021W	-	+	BY4743*	pSV637	-LEU2, -HIS3
YVJ655.3	YFR033C	-	+	BY4743*	pSV641	-LEU2, -HIS3

YSW032.13	YGR023W	-	+	BY4743*	pSV633	-LEU2, -HIS3
YMX368	YGR159C	+	+	BY4743*	pSV466	-LEU2, -HIS3
YMX304	YIL043C	+	+	BY4743*	pSV399	-LEU2, -URA3
YSW009.3	YIL043C	+	-	BY4743*	pSYN045_ pGB06	-LEU2, -HIS3
YMX366.1	YIL133C	+	+	BY4743*	pSV445	-LEU2, -HIS3
YMX358	YJL190C	+	+	BY4743*	pSV438	-LEU2, -HIS3
YVJ518.2	YJL190C	-	-	BY4743*	pSYN014_ pBM05	-LEU2, -HIS3
YSW010.4	YJL190C	+	-	BY4743*	pSYN046_ pGB07	-LEU2, -HIS3
YMX191	YJR139C	+	+	BY4743*	pSV303	-LEU2, -URA3
YSW011.4	YJR139C	+	-	BY4743*	pSYN047_ pGB08	-LEU2, -HIS3
YCP85.3	YJR139C	+	-	BY4743**	pSYN047_ pGB08	-LEU2, -HIS3
YMX318	YKL109W	+	+	BY4743*	pSV420	-LEU2, -URA3
YVJ663.1	YKR092C	-	+	BY4743*	pSV630	-LEU2, -HIS3
YMX320	YLR094C	+	+	BY4743*	pSV421	-LEU2, -URA3
YVJ519.2	YLR094C	-	-	BY4743*	pSYN015_ pBM06	-LEU2, -HIS3
YSW012.2	YLR094C	+	-	BY4743*	pSYN048_ pGB09	-LEU2, -HIS3
YMX364.1	YLR367W	+	+	BY4743*	pSV444	-LEU2, -HIS3
YMX254	YML030W	+	+	BY4743*	pSV355	-LEU2, -HIS3
YMX256	YML036W	+	+	BY4743*	pSV357	-LEU2, -HIS3
YMX193	YML038C	+	+	BY4743*	pSV309	-LEU2, -URA3
YMX195	YML042W	+	+	BY4743*	pSV314	-LEU2, -URA3
YVJ520.2	YML043C	-	-	BY4743*	pSYN016_ pBM07	-LEU2, -HIS3
YVJ521.2	YML051W	-	-	BY4743*	pSYN017_ pBM08	-LEU2, -HIS3
YMX197	YML052W	+	+	BY4743*	pSV315	-LEU2, -URA3
YMX199	YML053C	+	+	BY4743*	pSV316	-LEU2, -URA3
YMX258	YML055W	+	+	BY4743*	pSV358	-LEU2, -HIS3
YMX260	YML056C	+	+	BY4743*	pSV359	-LEU2, -HIS3
YMX262	YML058W	+	+	BY4743*	pSV360	-LEU2, -HIS3
YSW013.3	YML062C	+	-	BY4743*	pSYN049_ pGB10	-LEU2, -HIS3
YMX201	YML064C	+	+	BY4743*	pSV317	-LEU2, -URA3
YVJ523.6	YML064C	-	-	BY4743*	pSYN019_ pBM10	-LEU2, -HIS3
YMX203	YML068W	+	+	BY4743*	pSV318	-LEU2, -URA3
YMX205	YML069W	+	+	BY4743*	pSV319	-LEU2, -URA3
YVJ524.1	YML070W	-	-	BY4743*	pSYN020_ pBM11	-LEU2, -HIS3
YMX207	YML074C	+	+	BY4743*	pSV320	-LEU2, -URA3
YVJ525.2	YML074C	-	-	BY4743*	pSYN021_ pBM12	-LEU2, -HIS3
YMX264	YML078W	+	+	BY4743*	pSV362	-LEU2, -HIS3

YMX209	YML079W	+	+	BY4743*	pSV321	-LEU2, -URA3
YMX211	YML082W	+	+	BY4743*	pSV322	-LEU2, -URA3
YSW014.1	YML082W	+	-	BY4743*	pSYN050_ pGB11	-LEU2, -HIS3
YMX213	YML092C	+	+	BY4743*	pSV323	-LEU2, -URA3
YMX266	YML094W	+	+	BY4743*	pSV363	-LEU2, -HIS3
YMX215	YML095C	+	+	BY4743*	pSV324	-LEU2, -URA3
YVJ526.3	YML095C	-	-	BY4743*	pSYN022_ pBM13	-LEU2, -HIS3
YMX268	YML098W	+	+	BY4743*	pSV364	-LEU2, -HIS3
YVJ667.1	YML100W (scrambled)	-	-	BY4743*	pSV644	-LEU2, -HIS3
YMX270	YML101C	+	+	BY4743*	pSV365	-LEU2, -HIS3
YMX217	YML104C	+	+	BY4743*	pSV325	-LEU2, -URA3
YVJ527.4	YML107C	-	-	BY4743*	pSYN023_ pBM14	-LEU2, -HIS3
YMX272	YML108W	+	+	BY4743*	pSV367	-LEU2, -HIS3
YMX219	YML109W	+	+	BY4743*	pSV328	-LEU2, -URA3
YMX221	YML111W	+	+	BY4743*	pSV330	-LEU2, -URA3
YMX223	YML112W	+	+	BY4743*	pSV331	-LEU2, -URA3
YMX225	YML113W	+	+	BY4743*	pSV332	-LEU2, -URA3
YVJ528.3	YML113W	-	-	BY4743*	pSYN024_ pBM15	-LEU2, -HIS3
YSW016.5	YML116W	+	-	BY4743*	pSYN052_ pGB13	-LEU2, -HIS3
YMX276	YML129C	+	+	BY4743*	pSV369	-LEU2, -HIS3
YVJ653.5	YML129C	-	+	BY4743*	pSV639	-LEU2, -HIS3
YSW031.19	YMR173W	-	+	BY4743*	pSV632	-LEU2, -HIS3
YVJ509	YMR205C	+	+	BY4743*	pSV521	-LEU2, -URA3
YMX324	YNR039C	+	+	BY4743*	pSV423	-LEU2, -URA3
YSW017.2	YNR039C	+	-	BY4743*	pSYN053_ pGB14	-LEU2, -HIS3
YSW033.11	YNR044W	-	+	BY4743*	pSV635	-LEU2, -HIS3
YMX310	YPL048W	+	+	BY4743*	pSV403	-LEU2, -URA3
YSW018.4	YPL048W	+	-	BY4743*	pSYN054_ pGB15	-LEU2, -HIS3
YMX369	YPL081W	+	+	BY4743*	pSV467	-LEU2, -HIS3
YMX328	YPR008W	+	+	BY4743*	pSV425	-LEU2, -URA3
YSW094	MTL1 asn-rich	-	+	BY4743*	pSV_761	-LEU2, -HIS3
YSW095	MTL1 tyr-rich	-	+	BY4743*	pSV_762	-LEU2, -HIS3
YSW096	MTL1 tyr-rich No Signal Peptide	-	+	BY4743*	pSV_763	-LEU2, -HIS3
YVJ670	[AUG-[AAC(Asn)]15- STOP]inYML103C_U TR	-	+	BY4743*	pSV647	-LEU2, -HIS3
YVJ671	[AUG-[TCC(Ser)]15- STOP]inYML103C_U TR	-	+	BY4743*	pSV648	-LEU2, -HIS3

YVJ672	[AUG-[TCA(Ser)]15-STOP]inYML103C_U TR	-	+	BY4743*	pSV649	-LEU2, -HIS3
YVJ674	[AUG-[CTT(Leu)]15-STOP]inYML103C_U TR	-	+	BY4743*	pSV651	-LEU2, -HIS3
YVJ675	[AUG-[TAT(Tyr)]15-STOP]inYML103C_U TR	-	+	BY4743*	pSV652	-LEU2, -HIS3
ABY1001	YBR052C_woATG	-	-	$\Delta$ upf1	pSYN012_ pBM03	-LEU2, -HIS3
ABY1002	YML064C_woATG	-	-	$\Delta$ upf1	pSYN019_ pBM10	-LEU2, -HIS3
ABY1003	YML070W_woATG	-	-	$\Delta$ upf1	pSYN020_ pBM11	-LEU2, -HIS3
ABY1004	YML074C_woATG	-	-	$\Delta$ upf1	pSYN021_ pBM12	-LEU2, -HIS3
ABY1005	YML095C_woATG	-	-	$\Delta$ upf1	pSYN022_ pBM13	-LEU2, -HIS3
ABY1006	YML107C_woATG	-	-	$\Delta$ upf1	pSYN023_ pBM14	-LEU2, -HIS3
ABY1007	YML113W_woATG	-	-	$\Delta$ upf1	pSYN024_ pBM15	-LEU2, -HIS3
ABY1008	YML051W_woATG	-	-	$\Delta$ upf1	pSYN017_ pBM08	-LEU2, -HIS3
ABY1009	YBR221C_woATG	+	-	$\Delta$ upf1	pSYN040_ pGB01	-LEU2, -HIS3
ABY1010	YCL009C_woATG	+	-	$\Delta$ upf1	pSYN041_ pGB02	-LEU2, -HIS3
ABY1012	YDR032C_woATG	+	-	$\Delta$ upf1	pSYN043_ pGB04	-LEU2, -HIS3
ABY1017	YML062C_woATG	+	-	$\Delta$ upf1	pSYN049_ pGB10	-LEU2, -HIS3
ABY1011	YCR012W_woATG	+	-	$\Delta$ upf1	pSYN042_ pGB05	-LEU2, -HIS3
ABY1013	YER057C_woATG	+	-	$\Delta$ upf1	pSYN044_ pGB03	-LEU2, -HIS3
ABY1014	YIL043C_woATG	+	-	$\Delta$ upf1	pSYN045_ pGB06	-LEU2, -HIS3
ABY1015	YJL190C_woATG	+	-	$\Delta$ upf1	pSYN046_ pGB07	-LEU2, -HIS3
ABY1016	YJR139C_woATG	+	-	$\Delta$ upf1	pSYN047_ pGB08	-LEU2, -HIS3
ABY1018	YML082W_woATG	+	-	$\Delta$ upf1	pSYN050_ pGB11	-LEU2, -HIS3
ABY1019	YML116W_woATG	+	-	$\Delta$ upf1	pSYN052_ pGB13	-LEU2, -HIS3
ABY1020	YNR039C_woATG	+	-	$\Delta$ upf1	pSYN053_ pGB14	-LEU2, -HIS3
ABY1021	YPL048W_woATG	+	-	$\Delta$ upf1	pSYN054_ pGB15	-LEU2, -HIS3
YCP024	YBR025C woATG	-	-	$\Delta$ upf1	pSYN010_ pBM01	-LEU2, -HIS3

YCP028	YBR066C woATG	-	-	$\Delta$ upf1	pSYN013_ pBM04	-LEU2, -HIS3
YCP032	YLR094C woATG	-	-	$\Delta$ upf1	pSYN015_ pBM06	-LEU2, -HIS3
YCP036	YML043C woATG	-	-	$\Delta$ upf1	pSYN016_ pBM07	-LEU2, -HIS3
YABD1022	YML070W	+	+	$\Delta$ upf1	pSV_207	-LEU2, -URA3
YABD1023	YML062C	+	+	$\Delta$ upf1	pSV_210	-LEU2, -URA3
YABD1024	YBR025C	+	+	$\Delta$ upf1	pSV_228	-LEU2, -URA3
YABD1025	YLR094C	+	+	$\Delta$ upf1	pSV_421	-LEU2, -URA3
YSW109.1/2	YBR052C	+	+	$\Delta$ upf1	pCP001	-LEU2, -URA3
Ysw110.6	YML074C	+	+	$\Delta$ upf1	pSV_320	-LEU2, -URA3
Ysw111.5/4	YML095C	+	+	$\Delta$ upf1	pSV_324	-LEU2, -URA3
YSW112.1/2	YML107C	+	+	$\Delta$ upf1	pSV_274	-LEU2, -URA3
YSW113.1/5	YML051W	+	+	$\Delta$ upf1	pSV_267	-LEU2, -URA3
YSW115.1/2	YCL009C	+	+	$\Delta$ upf1	pSV_392	-LEU2, -URA3
YSW128	YJL190C	+	+	$\Delta$ upf1	pSV438	-LEU2, -HIS3
YSW129	YDR032C	+	+	$\Delta$ upf1	pSV304	-LEU2, -URA3
YSW130	YBR066C	+	+	$\Delta$ upf1	pCP002	-LEU2, -URA3
YSW131	YJR139C	+	+	$\Delta$ upf1	pSV303	-LEU2, -URA3
YSW132	YPL048W	+	+	$\Delta$ upf1	pSV403	-LEU2, -URA3
YSW133	YER057C	+	+	$\Delta$ upf1	pSV386	-LEU2, -HIS3
YSW134	YBR221C	+	+	$\Delta$ upf1	pSV390	-LEU2, -URA3
YSW135	YML116W	+	+	$\Delta$ upf1	pSM006	-LEU2, -URA3
YSW136	YML043C	+	+	$\Delta$ upf1	pSM002	-LEU2, -URA3
YSW149	YIL043C	+	+	$\Delta$ upf1	pSV399	-LEU2, -URA3
YSW150	YML064C	+	+	$\Delta$ upf1	pSV317	-LEU2, -URA3
YSW151	YML113W	+	+	$\Delta$ upf1	pSV332	-LEU2, -URA3
YSW152	YNR039C	+	+	$\Delta$ upf1	pSV423	-LEU2, -URA3

\* : The haploid strain containing the tTA (Ysv71.1, MatA) was mated with the strain containing the RNA expression cassettes (Mat $\alpha$ ).

**Table S3. qPCR primers.**

The amplification factor is shown for the primers, which were used to detect marked mRNAs or mRNAs expressed from synthetic genes.

Plasmid name	Systematic name	Reverse transcription primer	Forward primer (5' to 3')	Reverse primer (5' to 3')	Am. Fact.
pSV597	16 aa SN-rich C3	GCACTGTTCAT TATTATATTAT GTAGCTTTACA TA	CAAACCTCCAAC CCAACATCC	GCACTGTTCATT ATTATATTATGT AGCTTTACATA	1.57
pSV598	16 aa SN-rich C4	GCACTGTTCAT TATTATATTAT GTAGCTTTACA TA	TCCTCCAACCTCC TCATGCAAC	GCACTGTTCATT ATTATATTATGT AGCTTTACATA	1.58
pSV601	16 aa control	GCACTGTTCAT TATTATATTAT GTAGCTTTACA TA	GGAGCAGGTGA AGGCGG	GCACTGTTCATT ATTATATTATGT AGCTTTACATA	1.61
pSV606	100 aa SN-rich 1	GTTCTTGGTGA GTATTACTAAC CCGC	TTGCTCTCCCTC AACGACTC	GTTCTTGGTGAG TATTACTAACCC GC	1.89
pSV607	100 aa SN-rich 2	GTTCTTGGTGA GTATTACTAAC CCGC	CTTGTTCCACGA CCTCCACT	GTTCTTGGTGAG TATTACTAACCC GC	1.87
pSV608	100 aa control	GTTCTTGGTGA GTATTACTAAC CCGC	TCTTGGAGCAGT AGAAGGGC	GTTCTTGGTGAG TATTACTAACCC GC	1.90
pSV609	100 aa SN-rich 1	AGTAAAGTTAT GAGGCTATCTT GTGTTTATTA	TTGCTCTCCCTC AACGACTC	AGTAAAGTTATG AGGCTATCTTGT GTTTATTA	1.77
pSV610	100 aa SN-rich 2	AGTAAAGTTAT GAGGCTATCTT GTGTTTATTA	CTTGTTCCACGA CCTCCACT	AGTAAAGTTATG AGGCTATCTTGT GTTTATTA	1.78
pSV611	100 aa control	AGTAAAGTTAT GAGGCTATCTT GTGTTTATTA	TCTTGGAGCAGT AGAAGGGC	AGTAAAGTTATG AGGCTATCTTGT GTTTATTA	1.83
pSYN010_pBM01	YBR025C	TCAACGTGGAT AATTCAGCTA CTA	GGTATTGTCGGT TTGCCATA	TCAACGTGGATA ATTCAGCTACT A	1.90
pSV437	YBR048W	AGCAGAGACCT TGACGAC	AGATGGTATAAG AATGCAGGATTA GGT	TCTTCTGATGAC AATGGTACGGT	1.93
pSYN012_pBM03	YBR052C	CCCAATGGGAC TAAAATGACAC CTA	GCAAGGGTGATA CAGAATAGTGTA TCTA	CCCAATGGGACT AAAATGACACCT A	1.90
pCP002	YBR066C	TGAACCCAGTA GAGCAGATC	AGAAAGTGCGA GTTTCCCATCA	TTTCAGGCATAA GAGTTATCTGGG AGG	1.92
pSYN013_pBM04	YBR066C	GCACTTATTCA ATTTATCTTTCA AGTCTACTA	TCCCAGATAACT CTTTAGCCTGAA TA	GCACTTATTCAA TTTATCTTTCAA GTCTACTA	1.91

pSV308	YBR074W	AGTCCTGTTCG GTCTGTG	ACCGGAAAACA AATTTAAGCTTA CTACTATTAA	TGGTAGATTGAG TTTATAACGTTC ATGATC	2.00
pSV629	YBR078W	AATTGTTGCTTT AATCCTATCAC TATT	GGTGATGCCTCC AATGCTCA	AATTGTTGCTTT AATCCTATCACT ATT	1.75
pSV390	YBR221C	AAGTCCTGTGA ATGTTGAGC	CGTCGTGCCCCT ACATCATTC	CGTTCACCGAAC CTGTCCAA	1.90
pSYN04 0_pGB0 1	YBR221C	AAGTCCTGTGA ATGTTGAGC	CGTCGTGCCCCT ACATCATTC	CGTTCACCGAAC CTGTCCAA	1.91
pSV392	YCL009C	GTGGTGCAATA GTAGGTCTTC	GCTACCATGGTC CGATGTAGC	AAGGAGTGTCTA GTGTGGGCAA	2.12
pSYN04 1_pGB0 2	YCL009C	GTGGTGCAATA GTAGGTCTTC	CTACCTAGGTCC GCTGTAGC	AAGGAGTGTCTA GTGTGGGCAA	1.92
pSYN04 2_pGB0 3	YCR012W	ACCGACCTAAG AAGAGTGAG	GCGTGTCTTCAT AAGGGTCGAT	CAAGTGAGAAGC CAAGACAACG	1.92
pSV636	YDL232W	AAAACCTGAAGT TCGCTATCCAA ATGT	ACCATGTCTCCT AAGAACTAATGA TGA	AAAACCTGAAGTT CGCTATCCAAAT GT	1.76
pSV443	YDR025W	CAGCAGAGACC TTGACAAC	GGTACAAAAACG CTGGCTTG	GCCCTTCTGATG ACAATGGTA	2.03
pSV443	YDR025W (intron)	CAGCAGAGACC TTGACAAC	TGCGAATAACTT ACTAACCTTTGT ATCA	TGAATCCCAAGC CAGCGTTT	2.00
pSV304	YDR032C	CCACCGTGAAC TTCATCC	TGCCACGGCTGA AGCTGA	AACTTCTGGAGA CAACGTTTCCT	1.97
pSYN04 3_pGB0 4	YDR032C	CCACCGTGAAC TTCTACC	TGCCACGGCTGA AGCTGA	AACTTCTGGAGA CAACGTTTCCT	1.89
pSV642	YDR055W	TCGTGAATGAC AGGTACTAGTT ATCA	GGCAATCATCAT GTCTATAATGTA ATGATAG	TCGTGAATGACA GGTACTAGTTAT CA	1.90
pSV638	YDR079W	GGAAGAAAAA GTGGTCAGGTG C	TGGCTCTCAAAA AAGGATGATAGT AG	GGAAGAAAAAAG TGGTCAGGTGC	1.80
pSV386	YER057C	TTCCATGTCAA CGCCTAATG	GCTGCTGCGGCA TCTTATTCA	AGCAATGGAACC TTCAACTAACTT GTT	1.97
pSYN04 4_pGB0 5	YER057C	TTCCTAGTCAA CGCCTAATG	GCTGCTGCGGCA TCTTATTCA	AGCAATGGAACC TTCAACTAACTT GTT	1.87
pSV637	YFL021W	CGGACATGGAA AGAAGCGAG	GATTGGTTGAAT CTGAATTTATAG TGATGA	CGGACATGGAAA GAAGCGAG	1.90
pSV641	YFR033C	ACAAGACTCAG AATAAATATGA ATATAGGGA	ACCTAGATTATT TGACAAATTA GTAGTAATGA	ACAAGACTCAGA ATAAATATGAAT ATAGGGA	1.69
pSV633	YGR023W	GCTGCTTTCGC TATGATCTATC ATTAA	GTCAAGATTACA ACGACGCAGA	GCTGCTTTCGCT ATGATCTATCAT TAA	1.87



pSV466	YGR159C	TCTTCGGCGTC CTCAGATTTAC	GGCTAAGACTAC TAAAGTAAAAGG TAACA	AGCTTTTTTCTTCC TTAGCCTGC	1.98
pSV399	YIL043C	AAATTGGGAAG GCTTCATGG	CGTGGTCGTGCC ATTACTGTTT	AACCAGCGGAA ATGATTGGAAGT	1.94
pSYN04 5_pGB0 6	YIL043C	AAATTGGGAAG GCTTCTAGG	CGTGGTCGTGCC ATTACTGTTT	AACCAGCGGAA ATGATTGGAAGT	1.90
pSV445	YIL133C	ACCACGAAGAG CTTTGTAGAA	TGCTAAGCAATT ATTAAATGGACA GAAG	ACCACGAAGAGC TTTGTAGAAAG	1.83
pSV445	YIL133C (intron)	ACCACGAAGAG CTTTGTAGAA	TGAGCATCCATT CATTCATCAATA ATAATC	CTAACAACAACG ATCTTCTGTCCA	2.00
pSV438	YJL190C	TGCTTTCTTCTG GCTTCTTC	ACCAGATCTTCC GTTTTAGCTGA	CTTGACGCTTTC CTGTTTTCTCA	2.00
pSYN01 4_pBM 05	YJL190C	TCTTCTGGCTTC TTCTAGGTCCT A	CTTCCGTTTTAG CTGTAGCTTTGA TA	TCTTCTGGCTTCT TCTAGGTCCTA	1.81
pSYN04 6_pGB0 7	YJL190C	TGCTTTCTTCTG GCTTCTTC	ACCAGATCTTCC GTTTTAGCTGT	CTTGACGCTTTC CTGTTTTCTCA	1.88
pSV303	YJR139C	TTGACGTCGTT AGCTTGAC	GGTGTGTTGGT TCTGCATTTTAA	AGTCCTTGGAGA TTAAAGAACGCT	1.73
pSYN04 7_pGB0 8	YJR139C	TTGACGTCGTT AGCTTGAC	GGTGTGTTGGT TCTGCATTTTAA	AGTCCTTGGAGA TTAAAGAACGCT	1.73
pSV420	YKL109W	GTGCAGCTTTC ATCGTCC	CGCCCTCGTAGT AATCACTTCAAG	GTTTTCGAATTC CAGCGAACTATT GT	1.99
pSV630	YKR092C	TTTTATGTTTCC TATTCTTCTATC ATCATTAA	GGAACATGGGGT GAAAAGGC	TTTTATGTTTCTT ATTCTTCTATCAT CATTAA	1.72
pSV421	YLR094C	CAAGGGATGAA GTTTAGAGGAG	CTCATGTGCACG AGCACTGT	GACTTGGGATAA AATACCTTTGAT GAGTC	1.95
pSYN01 5_pBM 06	YLR094C	CTAGAGTGCAA TGCGCCTACTA	CTGCTGGACGTG AACACAAAT	CTAGAGTGCAAT GCGCCTACTA	1.86
pSYN04 8_pGB0 9	YLR094C	CAAGGGATGAA GTTTAGAGGAG	CTCTAGTGCACG AGCACTGT	GACTTGGGATAA AATACCTTTGAT GAGTC	1.91
pSV444	YLR367W	CTTTCTTCTAGC TTCCTCATGG	GGTAAGATTGTC GTGCAGCTTAAT	GTAACCGAATTG TCTGGCTGG	1.86
pSV355	YML030W	TTCGGCTCTTTT TCTCCTTG	ACGTTTCGGAGAG AGGATTATATAC CA	ACGAACATTTTG AGCAGCCAGA	2.06
pSV357	YML036W	TCTTGGGGCTT GAAATCATC	TCGATATAACCA AATATACGTCGT CGCT	TTGCTCGAATAA TGCTAGTGAAAC CT	2.04
pSV309	YML038C	TCAGATTCCTC TACTGCTGC	TTTCTGTTCAATT GCACTGTCGATA TACA	ATAAAGTAGCCT GATGGAATGTTG TCA	1.98

pSV314	YML042W	CTTACCAGGCA ATCTCGAAG	TCCGATAACCTC TAGAAGGGCAAT	TCCCCATTATTT GTCTCTACGGGA A	2.19
pSYN01 6_pBM 07	YML043C	CAAACCAATTA GGTCTATATTTT TGTTGTCTA	AGTGGTCTTGAC TTCTTACATAGG TA	CAAACCAATTAG GTCTATATTTTTG TTGTCTA	1.83
pSYN01 7_pBM 08	YML051W	AACGTTTAATG TGGAGCCCTAC TA	GGGGTTAGTAGC AGGTAAAGAAAT CTA	TTAACCTGTGTA ATATCAGAGCTA CCTA	1.81
pSV315	YML052W	ATACCCATCAT AGAGGCACC	TTTTTAGCTGGA AACACGTTGCTG	TGTTGTATTGCC CTGCACCC	2.04
pSV316	YML053C	TACCGGGTGCT TGTGATG	TGCAATTCGGGA AGTAACGCC	TGTGTGTATCAA ACTCGAAATGGT CAT	2.05
pSV358	YML055W	TTCTGAACAAG CTCAACCAG	AAAAGCACAAGT TATTGTAAGGAA AAGAGA	CTCGTCCAATGC TTGGTTCAACT	2.04
pSV359	YML056C	AACATCCAAAC CTGCTTCG	AACATTTGAAGA CATATAGCTCGA AA	CAGCAGAAGATG GGAAATTGACC	1.88
pSV360	YML058W	CGCCAGAACCA AATTTGTTG	TTCAACTGCTCA ATAATTTCCCGC T	CGATGGCGCCTG TTGTTGT	2.05
pSYN04 9_pGB1 0	YML062C	AAACTTGACCA GATCAGTGC	CACTACAGCGAG GTTGACACT	CCTGTCAGCTTG GTTACTTTTCC	1.96
pSV317	YML064C	GATGTCGATGT TGCTGGC	TACGAAATCAAG TAGAGGTACAGG TTG	ATCGTATATGTT CTGTACGTACTT CACC	2.07
pSYN01 9_pBM 10	YML064C	TCAAAAGAGGA TCGCCGATTTC TA	GAGTTAGAAGTT AGCACAGGTCTA GATA	TCAAAAGAGGAT CGCCGATTCTA	1.95
pSV318	YML068W	CATTCGCATTTT CACATGGC	ATGTACCCTGAG CTCGAGATGAA	AGTGATATCTTG AACAGTAACTTT CCGT	1.98
pSV319	YML069W	GTACATCTTCT CCTTCAGCAC	TAGCGGTAGGTT TCGAATAGCTG	AGATAATTCTGT GGCTGGTAATAA AAATGG	1.93
pSYN02 0_pBM 11	YML070W	TTAGTAATGTG ATACTGAACCC TATACCTA	GCGTTGCTGTCA TAGGTGTAGTA	CTTTAGCTGTAC CGTCTAAGCCTA	1.97
pSV320	YML074C	TTCATCCTCATC TGGGGTC	TTATACGCCCGT ACCTGCAATC	TTCTCTTCATCG ATGGCTTCCG	2.08
pSYN02 1_pBM 12	YML074C	TCGTCGCCAAT AATTTCTACCT CTA	AGAAACCCGGAC TTTGAAGTAGTA	AAAGGACGGATT CTTGGAACTCTA	1.92
pSV362	YML078W	CAACGTGTTTT CCATCCAAC	AAGGCTTGGCAA AAAAGTGTTCTT	AGCAGTTTTAGG AACCACATTATC ATATAATT	1.96
pSV321	YML079W	GGTCCCACAAG ATGTTTCAG	AGTTTTGTAAAG GTGCCAATGCC	ACCTTCTCTATG CTTGATTAATTG CCA	2.04
pSV322	YML082W	GCCATACCGCA TCTCTATG	ACACACAGCACG CCGTATCT	AACCTGGGGTAG CCAGACTTTAAA	1.93

pSYN05 0_pGB1 1	YML082W	GGGGAAGCAA AAGCACGTTT	CTGGACACACAG CACGCC	AACCTGGGGTAG CCAGACTTTAAA	1.82
pSV323	YML092C	CCTCTACCGAC TCCTTCAG	AGCGGTAAATTA GGACAGATAGAT TACG	TGTGGCAATTAC TACACCATTCGT A	2.07
pSV363	YML094W	CAAGGAATACT GGGTCTTTTCC	AGTTAAGCAACA ATTCGACCAAGA AT	TCAATACATTCT GTGAACTTGCCC T	1.97
pSV324	YML095C	CGTTTCTAGAT AAGGGCTGC	TGTGGCCAAGTT AAGGAAAGAAA AG	TCTTGATGTTTG CGGTTCTGC	2.09
pSYN02 2_pBM 13	YML095C	AAAAGTAGAGT AAATCCGTTGA ACTAATA	CACTTAAAGAGC ACCAATTGGAGA TTA	AAAAGTAGAGTA AATCCGTTGAAC TAATA	1.80
pSV364	YML098W	ATCCTCATCCT CTTCCATCTC	CAAGGATGTAAG TTCCTTACTATAT GCA	TTAGTACAAACA TCCACCAAATAT CCAGA	1.96
pSV365	YML101C	GTTCTGAGAT CTTGACG	TACCCACGCGCA CAAAAGTAA	TTGACCGTATAA ACAAACAAGCAC AC	2.03
pSV325	YML104C	AAAGGTGAGGA AGGAGCC	ACAATGGTCCGT TATAACATTTTC GC	TCGGTAAATCAG GCAAGGATTTGA	2.12
pSYN02 3_pBM 14	YML107C	GCCGTGCTATG AACCAGATCTA	CTCCATTCAAAA CTACACAAGGCT A	TCTAGGTGTAAT CGGCGACTACTA	1.92
pSV367	YML108W	TTGATATGACC TTCGTTCCG	ACTAGAAGACGA CACCAAAATTAA CAAG	AGGTATTTAATT CGTCCAGTTCGT CAA	1.85
pSV328	YML109W	CTTCTGTTCTC GACGTTAC	TGTAGAAAATAG CAGCGGAGGTAC	ACACGTCAGATT TCCTCTTCTCAA A	2.01
pSV330	YML111W	GTTTGTAGAGG ATGTAGGTTGG	TCCTTTAAAGTC TGTATCAACGGA AGA	TATTTGGATGCA GCGAATTATCTG TAGA	1.98
pSV331	YML112W	AGTCCTCTCTG TCTTGACAC	ACCTGCAGAAAA CCCTCCAC	AGAACTGTATAG GGTCATTGTTCA GC	2.08
pSV332	YML113W	TCACGTTGCTG TTAAGGTTG	CCGGTAAGGGCA AAACGTTGA	ATCTTGCTGAGA CCCGTCGG	2.04
pSYN02 4_pBM 15	YML113W	CTTGATTGCTC CCTATTATAGT AAAGTTCTA	TCTGGATTATAC CCATCAGTCATT CTA	CTTGATTGCTCC CTATTATAGTAA AGTTCTA	1.88
pSYN05 2_pGB1 3	YML116W	AACAAATGCAA TCCCTAGCC	GGTGAGTTAGAG AACGAACTGAG	GCTGTTGCTGTT AAAGATTCTCCG	1.88
pSV369	YML129C	CGGTAGGAGGT GCAGTAG	GGTGAGAACGGT TAGACGATGTAA T	TGGTGAGAGGAA GAGAACAAAAA ATAGA	2.07
pSV639	YML129C	TGCAACACTTA AAAATGTAATC TAGTACT	CACCTCCTACCG AGTAATGATGA	TGCAACACTTAA AAATGTAATCTA GTACT	1.83

pSV632	YMR173W	GAAGACATCCA AAAACATCATCA TTA	ACGATGATTCAT ACGGCTCCAG	GAAGACATCCAA AAACTCATCATT A	1.87
pSV521	YMR205C	AAGGATTGGGT GGCATGTGA	ACTGTTACTACT CCTTTTGTGAAT GG	GGCAGCTTTATA AGATTGTACTGA GTAA	1.91
pSV423	YNR039C	CTGGAATGGGA AGAGATTTGG	CAATTTGTCTCC GGAGGTAGCATT T	GTATACCGTCTA CATTCCCGACAG	2.04
pSYN05 3_pGB1 4	YNR039C	CTGGAATGGGA AGAGATTTGG	CAATTTGTCTCC GGAGGTAGCATT T	GTATACCGTCTA CTATCCCGACAG	1.90
pSV635	YNR044W	ATAAATGAATT AAATTGTTCTG ATATCATCATT	TCATCTGCTCCC TCTTCTCT	ATAAATGAATTA AATTGTTCTGAT ATCATCATT	1.82
pSV403	YPL048W	CTGGTGAAAAT CGAGGCAG	CCCAAGGGGACT CGTGAA	CATTGCCTCGGT TAGCTTGT	1.94
pSYN05 4_pGB1 5	YPL048W	CTGGTGAAAAT CGAGGCAG	CCCAAGGGGACT CGTGAA	CTATGCCTCGGT TAGCTTGT	1.93
pSV467	YPL081W	TGGAGATGTTG GAGCAAAGTCA	ATTGAAGTTGGC AGGGGAGTTT	TTGGGTCCTTTTC GTCTCTTGT	1.98
pSV761	MTL1 asn- rich	ATTTTGGTGAA AATGTTACTAC GGT	CTACAACACCAC AATAACGAAC	ATTTTGGTGAAA ATGTTACTACGG T	1.93
pSV762	MTL1 tyr- rich	AATGTATACGA AAGAGTAAGCA GATAAAC	TAACAACACTAC CGCTAAGTGTTT	AATGTATACGAA AGAGTAAGCAG ATAAAC	1.99
pSV763	MTL1 tyr- rich No SP	AATGTATACGA AAGAGTAAGCA GATAAAC	ATGGCAACTAGA CAGGAGTTG	AATGTATACGAA AGAGTAAGCAG ATAAAC	1.88
pSV647	[AUG- [AAC(Asn) ]15- STOP]inY ML103C_ UTR	GGTTACTCCAT ACTAGCCCAGA GTCCTGCAAAA TAAGTTAGTTG TTGTTGTT	AAAAGGACCCCA TCAGCCATG	GGTTACTCCATA CTAGCCCAGAGT	1.89
pSV648	[AUG- [TCC(Ser)] 15- STOP]inY ML103C_ UTR	GCCGTTTCAGTA GATGGGTCAGC AAAATAAGTTA GGAGGAGGAG GA	AAAAGGACCCCA TCAGCCATG	GCCGTTTCAGTAG ATGGGTCA	1.92
pSV649	[AUG- [TCA(Ser)] 15- STOP]inY ML103C_ UTR	TTTtagACTTC AATAACCCTAG CGCACCTGCAA AATAAGTTATG ATGATGATGA	AAAAGGACCCCA TCAGCCATG	TTTtagACTTCA ATAACCCTAGCG C	1.9
pSV651	[AUG- [CTT(Leu)] 15- STOP]inY ML103C_ UTR	CGTTCCCAAGA CGCCAAGATAA CCTGCAAAAATA AGTTAAAGAAG AAGAAG	AAAAGGACCCCA TCAGCCATG	CGTTCCCAAGAC GCCAAGAT	1.98

pSV652	[AUG- [TAT(Tyr)] 15- STOP]inY ML103C_ UTR	AGATCGACTTC TAAATTGTGGG TGGCATAACCT GCAAAATAAGT TAATAATAATA ATAAT	AAAAGGACCCCA TCAGCCATG	AGATCGACTTCT AAATTGTGGGTG G	1.86
pSYN01 2_pBM 03	YBR052C	CCCAATGGGAC TAAAATGACAC CTA	GCAAGGGTGATA CAGAATAGTGTA TCTA	CCCAATGGGACT AAAATGACACCT A	1.9
pSYN01 9_pBM 10	YML064C	TCAAAAGAGGA TCGCCGATTTC TA	GAGTTAGAAGTT AGCACAGGTCTA GATA	TCAAAAGAGGAT CGCCGATTCTA	1.95
pSYN02 0_pBM 11	YML070W	TTAGTAATGTG ATACTGAACCC TATACCTA	GCGTTGCTGTCA TAGGTGTAGTA	CTTTAGCTGTAC CGTCTAAGCCTA	1.97
pSYN02 1_pBM 12	YML074C	TCGTCGCCAAT AATTTCTACCT CTA	AGAAACCCGGAC TTTGAAGTAGTA	AAAGGACGGATT CTTGGAACCTA	1.92
pSYN02 2_pBM 13	YML095C	AAAAGTAGAGT AAATCCGTTGA ACTAATA	CACTTAAAGAGC ACCAATTGGAGA TTA	AAAAGTAGAGTA AATCCGTTGAAC TAATA	1.8
pSYN02 3_pBM 14	YML107C	GCCGTGCTATG AACCAGATCTA	CTCCATTCAAAA CTACACAAGGCT A	TCTAGGTGTAAT CGGCGACTACTA	1.92
pSYN02 4_pBM 15	YML113W	CTTGATTGCTC CCTATTATAGT AAAGTTCTA	TCTGGATTATAC CCATCAGTCATT CTA	CTTGATTGCTCC CTATTATAGTAA AGTTCTA	1.88
pSYN01 7_pBM 08	YML051W	AACGTTTAAATG TGGAGCCCTAC TA	GGGGTTAGTAGC AGGTAAAGAAAT CTA	TTAACCTGTGTA ATATCAGAGCTA CCTA	1.81
pSYN04 0_pGB0 1	YBR221C	AAGTCCTGTGA ATGTTGAGC	CGTCGTGCCCCT ACATCATTC	CGTTCACCGAAC CTGTCCAA	1.91
pSYN04 1_pGB0 2	YCL009C	GTGGTGCAATA GTAGGTCTTC	CTACCTAGGTCC GCTGTAGC	AAGGAGTGTCTA GTGTGGGCAA	1.92
pSYN04 3_pGB0 4	YDR032C	CCACCGTGAAC TTCTACC	TGCCACGGCTGA AGCTGA	AACTTCTGGAGA CAACGTTTCCT	1.89
pSYN04 9_pGB1 0	YML062C	AAACTTGACCA GATCAGTGC	CACTACAGCGAG GTTGACACT	CCTGTCAGCTTG GTTACTTTTCC	1.96
pSYN04 2_pGB0 3	YCR012W	ACCGACCTAAG AAGAGTGAG	GCGTGTCTTCAT AAGGGTCGAT	CAAGTGAGAAGC CAAGACAACG	1.92
pSYN04 4_pGB0 5	YER057C	TTCCTAGTCAA CGCCTAATG	GCTGCTGCGGCA TCTTATTCA	AGCAATGGAACC TTCAACTAACTT GTT	1.87
pSYN04 5_pGB0 6	YIL043C	AAATTGGGAAG GCTTCTAGG	CGTGGTCGTGCC ATTACTGTTT	AACCAGCGGAA ATGATTGGAAGT	1.9
pSYN04 6_pGB0 7	YJL190C	TGCTTTCTTCTG GCTTCTTC	ACCAGATCTTCC GTTTTAGCTGT	CTTGACGCTTTC CTGTTTTCTCA	1.88

pSYN04 7_pGB0 8	YJR139C	TTGACGTCGTT AGCTTGAC	GGTGTGTTGGT TCTGCATTTT	AGTCCTTGGAGA TTAAAGAACGCT	1.73
pSYN05 0_pGB1 1	YML082W	GGGGAAGCAA AAGCACGTTT	CTGGACACACAG CACGCC	AACCTGGGGTAG CCAGACTTTAAA	1.82
pSYN05 2_pGB1 3	YML116W	AACAAATGCAA TCCCTAGCC	GGTGAGTTAGAG AACGAACTGAG	GCTGTTGCTGTT AAAGATTCTCCG	1.88
pSYN05 3_pGB1 4	YNR039C	CTGGAATGGGA AGAGATTTGG	CAATTTGTCTCC GGAGGTAGCATT T	GTATACCGTCTA CTATCCCGACAG	1.9
pSYN05 4_pGB1 5	YPL048W	CTGGTGAAAT CGAGGCAG	CCCAAGGGGACT CGTGAA	CTATGCCTCGGT TAGCTTGT	1.93
pSYN01 0_pBM 01	YBR025C	TCAACGTGGAT AATTTAGCTA CTA	GGTATTGTCGGT TTGCCATA	TCAACGTGGATA ATTTAGCTACT A	1.9
pSYN01 3_pBM 04	YBR066C	GCACTTATTCA ATTTATCTTTCA AGTCTACTA	TCCCAGATAACT CTTTAGCCTGAA TA	GCACTTATTCAA TTTATCTTTCAA GTCTACTA	1.91
pSYN01 5_pBM 06	YLR094C	CTAGAGTGCAA TGCGCCTACTA	CTGCTGGACGTG AACACAAAT	CTAGAGTGCAAT GCGCCTACTA	1.86
pSYN01 6_pBM 07	YML043C	CAAACCAATTA GGTCTATATTTT TGTTGTCTA	AGTGGTCTTGAC TTCTTACATAGG TA	CAAACCAATTAG GTCTATATTTTG TTGTCTA	1.83

**Table S4. Oligos used in the splinted ligation reverse transcription polymerase chain reaction (SLqPCR) assay.**

Sequence type:	Gene	Reverse primer:	Reverse transcription primer:	Forward anchor (gene-specific):	Forward total:	Splint:
ENDO	YBR025C	AAAAGGTA GACTTACC AACATTGG C	CTCAACGTG GATAATTTCA GCATCAT	CGTTTGCTG GCTTTGATG AAAAAC	AAAACAATCAA ATAAATAGCAC TGTAACAATG	GGAGGCATGTTTTACAGTGCTA TTTATTTGATTGTTTTCATCAA AGCCAGCAAACGCAGTGTTTCAT TCATCGCCATCAGC
ENDO	YJL190C	GATTAAAA CTTGACGC TTACCGGT CTT	TCTTCTGGC TTCTTCATG GTCCAT	CGTTTGCTG GCTTTGATG AACATAC	CTTCCGTTTTA GCTGATGCTTT GAAT	ACGGAAGATCTGGTCACTCTTGG ATATGTATGTTTCATCAAAGCCA GCAAACGCAGTGTTTCATTCATC GCCATCAGC
ENDO	YLR094C	GCTTTTGA TGAGGCAA TGTTCA	CATGAGTGC AATGCGCCA TCAT	CGTTTGCTG GCTTTGATG ATACAG	ACGTGAACAC AAATCACACAC TAAT	GCAGCATCTCTATAAATTATGTCTT GTTGAAAGTGTTCTGTATCATC AAAGCCAGCAAACGCAGTGTTTC ATTCATCGCCATCAGC
ENDO	RPL41A			CGTTTGCTG GCTTTGATG AGACC		
WT (MGC)	YBR025C	CGACAATA CCGGCTTT TAAATTGT T	CTCAACGTG GATAATTTCA GCATCAT	CGTTTGCTG GCTTTGATG AAAAAC	AAAACAATCAA ATAAATAGCAC TGTAACAATG	GGAGGCATGTTTTACAGTGCTA TTTATTTGATTGTTTTCATCAA AGCCAGCAAACGCAGTGTTTCAT TCATCGCCATCAGC
WT (MGC)	YJL190C	GATTAAAA CTTGACGC TTTCCIGT ITTC	TCTTCTGGC TTCTTCATG GTCCAT	CGTTTGCTG GCTTTGATG AACATAC	CTTCCGTTTTA GCTGATGCTTT GAAT	ACGGAAGATCTGGTCACTCTTGG ATATGTATGTTTCATCAAAGCCA GCAAACGCAGTGTTTCATTCATC GCCATCAGC
WT (MGC)	YLR094C	GCTTTTGA TGAGACAG TGCTCG	CATGAGTGC AATGCGCCA TCAT	CGTTTGCTG GCTTTGATG ATACAG	ACGTGAACAC AAATCACACAC TAAT	GCAGCATCTCTATAAATTATGTCTT GTTGAAAGTGTTCTGTATCATC AAAGCCAGCAAACGCAGTGTTTC ATTCATCGCCATCAGC
No-ATG	YBR025C	AAAAGGTA GACTTACC AACTATGG G	CTCAACGTG GATAATTTCA GCTACTA	CGTTTGCTG GCTTTGATG AAAAAC	AAAACAATCAA ATAAATAGCAC TGTAACAATG	GGAGGCATGTTTTACAGTGCTA TTTATTTGATTGTTTTCATCAA AGCCAGCAAACGCAGTGTTTCAT TCATCGCCATCAGC
No-ATG	YJL190C	GATTAAAA CTTGACGC TTTCCIGT ITTC	TCTTCTGGC TTCTTCATG GTCCTA	CGTTTGCTG GCTTTGATG AACATAC	CTTCCGTTTTA GCTGATGCTTT GATA	ACGGAAGATCTGGTCACTCTTGG ATATGTATGTTTCATCAAAGCCA GCAAACGCAGTGTTTCATTCATC GCCATCAGC
No-ATG	YLR094C	GCTTTTGA TGAGACAG TGCTCG	CATGAGTGC AATGCGCCT ACTA	CGTTTGCTG GCTTTGATG ATACAG	ACGTGAACAC AAATCACACAC TATA	GCAGCATCTCTATAAATTATGTCTT GTTGAAAGTGTTCTGTATCATC AAAGCCAGCAAACGCAGTGTTTC ATTCATCGCCATCAGC

**Table S5. Sequences of smFISH probes binding TSL1 (5' to 3').**

Endogenous	noATG
TGTGTTGATCTTGCGTTGC	TGTGTTGATCTTGCGTTGC
GATGCCACGATGAGAGCC	GCAGAGATCACAGCGAGC
TGGTTGGTAGGGCAAAAACA	TTGGTATTGCAAGGGCAAAA
GAGAGGTGTCAAGCTCGAAT	GGGTAGAAAGGTCGA ACTCT
CACCTGCGAGTTCTCAGG	GTCCGACTGCTCGTTGAG
TGGATGTTACGAGAGATGAG	CGTTGATGAGCACTGAAGAC
CTGTTGGTCATTGGCCATAG	GCTGATTGTCCTAGGCCTG
GTTAGAAAGCGCACGTTGT	TTAAGAGAACGCGCTTGTTG
GACCAATGATTCTGTGAGATG	CTGACA ACTGTTTCGATTGAGT
CCTTGTTCTGGTGCTGGC	ACCTGGTTCTGGTGCGAC
TTGAGATTGCTGGGGGGA	ATTGATGGTGCGACGGGT
GGGTGACCTGGTG GCACT	TCCTTGAGGCGGTCTAC
GAGGCGCGGTTGAAAGCA	CGAGTTGCGAGCGAAGGG
AAAGTGGCAGTATTTGTCGTAG	TAAAGTGGCTGTATTAGACGTG
TGTCCGAAGAGACAAGATCAT	TATAGACGAAAGGACTACTACA
CGCAGTCAAGTTTTCCATGAA	TATCAAAGTTTCGTTGAAGTCC
GCGTATGTGAGGTAGTTGCA	TGCGTG GTTGATGCAGTC
GTTTAAGCATAGTCTTGCTTGT	AGTTTAGTCTAGCTCTTTGGTG
CCACGGAACCATTTTTCCG	TCACCGGATTATTGGGCC
GGAAGAAGGGGAGAAGAATCG	AGGAGAGAAGGATCGGAACA
GATGCGATCCGTGGGAATA	GGATCGTATCAATGGGGGAA
TCATGCTGGATTGGCGAT	CTGATGTGGGATTGCCGA
AATTCTCGAACCGGAGTCAT	ATACCCGAGTCGGACTCT
TGCTGTTGGATTGGCGAA	GCTGTGGGATAGCCGATC
TGGTCGTGGGGTCCTGCT	GGGCGTCTGGTCTTGCTG
ACTTGTTGACGTTCTTTAATAA	GACGTTCTTGTTAATAAGGTG
TCAACAGTGAGTGCACTAACAA	GACAGCACGTGCAATAACTTT
TAGGCTAGTTTGTGAGGTGTT	GCTTGATTGGTTGGTCAAGT
AATGTGGTTGTTGGGTCCT	TGTTGTTTCCGGGTAGTTCA
GCCCTCGATTTTCGGGGTA	ACCTCGGTTTAACGGTGTG
CCGAAGTAGGCCTGTTGC	AGGAGTGTTCTCGCGCC
TCCTATTA ACTAAAGAAGTAGC	AACTATAGATAAAGCAGTCGAC
GGAGGCCGAACCTTGTTT	GGAACCCGATTTTTGCCTG
CAGAAGACCCAGAAGATCCA	CCCCAGAAGAAGAAGATCCG
TAATCCTTTTAATGGAAGGTGG	TTTCCTGGAAATTGGAGGAGA
GTGACGTATCTAGCTCGAAT (This probe binds to the 4 silent mutations in the MGC version of the gene and corresponds to the 4 <sup>th</sup> probes from the endogenous sequence)	



**Table S6. Significance of difference between dtCSC values.**

Selected codons with positive (second column) and negative (second row) values are compared. P-values (green area) less than 0.01 are indicated in bold black fonts. Values between 0.01 and 0.05 are denoted in gray bold whereas those above 0.05 in regular gray fonts. The correlation between the codon frequencies is shown in the lower part of the table.

			P-value					
Amino acid			Lys	Tyr	Val	Val	Leu	Tyr
	Codon (DNA)		aag	tac	ggt	gta	ctt	tat
		dtCSC	0.0248	0.0665	0.0977	0.1910	<b>0.2607</b>	<b>0.2675</b>
Asn	aac	<b>-0.3418</b>	<b>1.57E-02</b>	<b>3.16E-03</b>	<b>3.56E-03</b>	<b>1.27E-03</b>	<b>5.00E-05</b>	<b>4.10E-05</b>
Ser	tct	<b>-0.2763</b>	<b>2.75E-02</b>	<b>2.51E-02</b>	<b>6.79E-03</b>	<b>4.84E-03</b>	<b>1.22E-03</b>	<b>5.73E-04</b>
Ser	tcc	<b>-0.2609</b>	<b>3.15E-02</b>	<b>1.36E-02</b>	<b>3.25E-03</b>	<b>6.90E-03</b>	<b>1.88E-03</b>	<b>1.59E-03</b>
Ser	tca	<b>-0.2383</b>	1.33E-01	7.58E-02	5.29E-02	<b>1.08E-03</b>	<b>2.90E-05</b>	<b>5.40E-05</b>
Ser	agc	-0.1564	2.77E-01	1.85E-01	1.48E-01	<b>1.64E-02</b>	<b>7.76E-04</b>	<b>4.71E-03</b>
Asn	aat	-0.1163	4.26E-01	2.79E-01	2.29E-01	<b>1.50E-02</b>	<b>1.17E-03</b>	<b>1.05E-03</b>
Ser	tcg	-0.0272	7.69E-01	5.57E-01	4.75E-01	<b>4.50E-02</b>	<b>2.80E-02</b>	<b>2.59E-02</b>
Ser	agt	0.0291	9.80E-01	8.26E-01	4.68E-01	1.92E-01	<b>4.48E-02</b>	5.71E-02
			Correlation between codon frequencies					
	aac		-0.14915	0.045562	-0.13335	-0.36611	-0.12955	-0.13251
	tct		0.095017	-0.13344	0.072158	-0.34251	-0.36491	-0.24262
	tcc		0.14865	0.150699	0.2805	-0.3583	-0.38758	-0.38279
	tca		-0.46672	-0.40495	-0.43733	0.159312	0.2892	0.216614
	agc		-0.29557	-0.3224	-0.44189	0.00081	0.24754	-0.09473
	aat		-0.45849	-0.32238	-0.47003	0.241065	0.344898	0.332321
	tcg		-0.4406	-0.17251	-0.41487	0.441212	0.172742	0.155011
	agt		-0.4168	-0.34125	-0.3726	0.273128	0.357612	0.240631

**Table S7. Significance of difference between dtCSC values of synonymous codons.**  
Synonymous codons of serine with the largest difference in dtCSC were compared. Further notations as in Table S6.

			P-value			
amino acid			Asn	Ser	Ser	Tyr
	codon (DNA)		aat	tcg	agt	tac
		dtCSC	-0.1163	-0.0272	0.0291	0.0665
Asn	aac	<b>-0.3418</b>	5.03E-02			
Ser	tct	<b>-0.2763</b>		1.02E-01	5.27E-02	
Ser	tcc	<b>-0.2609</b>		1.20E-01	8.85E-02	
Ser	tca	<b>-0.2383</b>		9.79E-02	<b>2.44E-02</b>	
Ser	agc	-0.1564		3.30E-01	1.33E-01	
Tyr	tat	<b>0.2675</b>				1.65E-01
			Correlation between codon frequencies			
			0.33038	0.049106	0.216099	0.045562
			-0.15826	-0.12576	-0.20313	-0.13344
			-0.32041	-0.09046	-0.39359	0.150699
			0.430506	0.221172	0.324312	-0.40495
			0.300676	0.177581	0.284952	-0.3224
			0.332321	0.155011	0.240631	-0.02004
						n=95

## Supplementary Data

### Data S1. Half-lives of mRNAs

The half-lives measured at 20°C and 42°C in raffinose were used as input to calculate the dtCSC. The data highlighted in gray (raffinose, 30°C) were reproduced from Baudrimont et al (2). The following abbreviations were used: Raff: raffinose, Glu: glucose, Gly: glycerol.

### Data S2. Mass-spectrometry measurements

The averages were calculated from three biological replicates.

### Data S3. Enrichment of codons in P-body components.

The list of P-body components was obtained from Reijns et al. The relative enrichment of codons is the ratio of the codon frequency in the given gene to the genome-wide codon frequency of the same codon (3). The latter codon usage data were obtained from <https://www.kazusa.or.jp/codon/>

## Supplementary References

1. Steiger, J.H. (1980) Tests for Comparing Elements of a Correlation Matrix. *Psychol Bull*, **87**, 245-251.
2. Baudrimont, A., Voegeli, S., Vilorio, E.C., Stritt, F., Lenon, M., Wada, T., Jaquet, V. and Becskei, A. (2017) Multiplexed gene control reveals rapid mRNA turnover. *Sci Adv*, **3**, e1700006.
3. Reijns, M.A., Alexander, R.D., Spiller, M.P. and Beggs, J.D. (2008) A role for Q/N-rich aggregation-prone regions in P-body localization. *J Cell Sci*, **121**, 2463-2472.